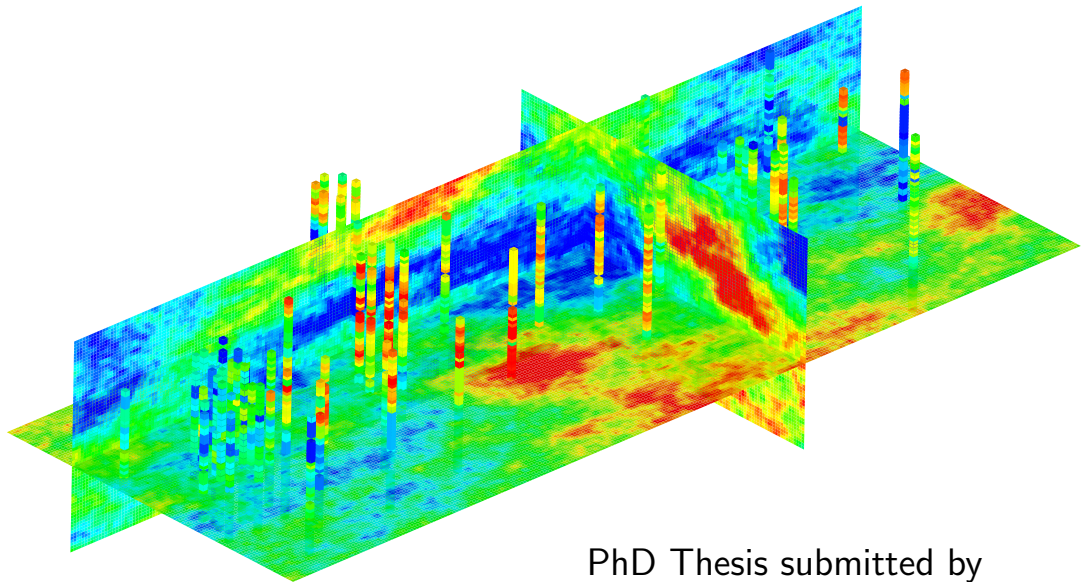


On modeling contaminant transport in complex porous media using random walk particle tracking



PhD Thesis submitted by
Peter Salamon

Advisors:
J. Jaime Gómez-Hernández
Daniel Fernàndez-Garcia

September 2006



Instituto de Ingeniería del
Agua y Medio Ambiente



On modeling contaminant transport in complex porous media using random walk particle tracking

PhD Thesis submitted by
Peter Salamon

Advisors:
J. Jaime Gómez-Hernández
Daniel Fernández-García

PhD Program:
Ingeniería Hidráulica y Medio Ambiente

Department:
Ingeniería Hidráulica y Medio Ambiente

Instituto de Ingeniería del Agua y Medio Ambiente
Universidad Politécnica de Valencia

PhD Grant:
REN2002-02428
Ministerio de Educación y Ciencia

September 2006

Cover illustration: Various slices of a three-dimensional realization of a hydraulic conductivity field conditioned to flowmeter measurements at the Macrodispersion Experiment site, Columbus Air Force Base, Mississippi, USA, generated using sequential Gaussian simulation. Columns represent the borehole locations where flowmeter measurements were performed.

To Alicia

Abstract

The need to quantify and/or reduce uncertainty associated with transport model predictions as well as the ongoing research on solute transport up-scaling require a numerical method for simulating transport which is highly computational efficient even for models with millions of grid cells and which is not prone to numerical errors. One valuable alternative tool for this purpose is the random walk particle tracking method. This thesis attempts to examine its fundamental concepts, extend its capacities, and illustrate its applicability to field problems.

The first paper reviews and assesses the basic mathematical concepts of the random walk methodology as well as its limitations and advantages. Different numerical implementation methods to overcome the problem of local solute mass conservation are examined using a simple two-layer case as well as synthetic heterogeneous two-dimensional conductivity fields and it is demonstrated that the interpolation method using a hybrid scheme, i.e., linear interpolation for velocities and tri/bilinear interpolation for the dispersion tensor field, provides a local as well as global divergence-free velocity field and that it approximates well mass balance at grid interfaces of adjacent cells with contrasting hydraulic conductivities.

The second paper presents a new approach to include multirate mass transfer processes into random walk particle tracking. Performing a Bernoulli trial on the appropriate phase transition probabilities, derived using the normalized zeroth spatial moments of the multirate transport equations, the particle distribution between the mobile domain and any immobile domain can be determined. Examples for the first-order mass transfer and the multirate mass transfer are illustrated and compared satisfactorily with analytical and semi-analytical solutions. Various implementation criteria are investigated to assure a proper simulation of the mass transfer processes. The applicability of this method is furthermore demonstrated using a synthetic example of the effects of a heterogeneous intraparticle pore diffusion distribution. The major advantages of this newly developed approach are its flexibility in the sense that it does not impose any restrictive assumptions on the spatial variability of advection, dispersion, and mass transfer, its low computational cost even for highly discretized models, and the capacity to describe a multiplicity of different mass transfer processes.

The third paper presents the simulation of tracer transport using the random walk methodology at the Macrodispersion Experiment (MADE) site, where the strong aquifer heterogeneity requires a highly discretized model grid. A geostatistical analysis of the flowmeter data is performed and results demonstrate the existence of a hole effect structure indicating an increased occurrence of clustered lenses or facies in the aquifer. Indicator variogra-

phy did not show an increased connectivity of extreme conductivity values. Tracer transport is modeled in three kriged fields as well as for three sequential simulations all of them using a high grid-resolution with a grid block size similar to the flowmeter measurement support scale. The kriged fields were not able to reproduce the anomalous tracer spreading based on an insufficient representation of the variance of $\ln K$. The sequential Gaussian simulations generally demonstrated a better tailing than the sequential Indicator simulation indicating that a multiGaussian distribution of $\ln K$ approximates well the field conditions. Using the hole effect structure for the spatial model of the Gaussian simulations resulted in an increased tailing of the tracer, caused by the enhanced occurrence of lenses/facies, and a good reproduction of the non-Gaussian plume shape for various realizations. Thus, when small-scale variability of hydraulic conductivity is correctly modeled at the flowmeter measurement support scale, the advection-dispersion equation is capable of reproducing the anomalous tracer spreading. It furthermore suggests that the heterogeneity at the flowmeter measurement scale is the main contributor to the non-Gaussian plume behavior and that mass transfer effects, claimed to be responsible for the anomalous transport at the MADE site, are principally the consequence of the use of an inadequate model grid block scale.

vi

Resumen

Example.

Resum

Example.

Acknowledgements

I wish to thank my advisor J. Jaime Gómez-Hernández for providing me the opportunity to start a PhD at his research group in Valencia. I enormously appreciate his faith in me as he never doubted to provide me with the moral, professional, and financial support necessary during this PhD. Although being very busy he always found the time for a discussion of the results of this work and to offer me his valuable advice.

I would furthermore like to thank my co-advisor Daniel Fernández-García for his time and his efforts in helping me to solve the day-to-day problems throughout the three years of this PhD. Without him I wouldn't have been able to publish three papers in such a short time.

This research was supported principally by the Spanish Ministry of Education and Science through the PhD grant number REN2002-02428. Further financial support was provided by the European Union (FUN-MIG, FP6-516514), the Spanish Ministry of Education and Science (Project Ref. CGL2004-02008), and the Generalitat Valenciana (Ref. GRUPOS04/062).

I furthermore would like to thank especially Eduardo Cassiraga, who introduced me in the world of \LaTeX , and who was always there to help me with his excellent knowledge of geostatistics. Without his valuable advice the editing of this thesis would have taken much longer. Special thanks also to Prof. J.E. Capilla-Romá for providing the MADE database.

I would like to extend my thanks to the rest of my colleagues from the hydrogeology research group (Andrés, Gero, Salvador, Jianlin, Rafa) and the IIAMA (Carlos, Manolo, David) for having a such good time during my stay here in Valencia.

I would also like to specially thank my parents for always encouraging me no matter what. Finally, I would like to thank Alicia for her unconditional love. I would not have made it without her.

Contents

1	General Context	1
1.1	Motivation and Objectives	1
1.2	Thesis Organization	2
2	A review and numerical assessment of the random walk particle tracking method (<i>Journal of Contaminant Hydrology, in press</i>)	5
	Abstract	5
2.1	Introduction	6
2.2	Basic Concepts of Random Walk Particle Tracking	8
2.2.1	Mathematical Formulation	8
2.2.2	Advantages	11
2.2.3	Limitations	12
2.2.4	Comparison with Other Approaches	13
2.3	Implementation Methods for the Local Solute Mass Conservation	14
2.3.1	The Interpolation Method	14
2.3.2	The Reflection Method	17
2.3.3	Generalized Stochastic Differential Equations	19
2.4	Method of Moments	20
2.5	Numerical Evaluation	21
2.5.1	Solute Transport in a Two-Layer Stratified Aquifer	22
2.5.2	Solute Transport in a Heterogeneous Aquifer	29
2.6	Conclusions	38
	Bibliography	41
3	Modeling Mass Transfer Processes Using Random Walk Particle Tracking (<i>Water Resources Research, in press</i>)	47
	Abstract	47
3.1	Introduction	48
3.2	Mathematical Framework	51
3.2.1	The Multirate Model	51
3.2.2	Development of Phase Transition Probabilities	52
3.3	Numerical Implementation Details	63

3.3.1	Random Walk Particle Tracking	63
3.3.2	Choice of Time Step Size	64
3.3.3	An Approximation Criteria for the Exponential Matrix	66
3.3.4	Truncation of the Multirate Series	67
3.4	The Effect of a Heterogeneous Intraparticle Pore Diffusion Distribution - An Example	69
3.5	Conclusions	73
	Bibliography	75
4	Modeling tracer transport at the Macrodispersion Experiment (MADE) site: Only a problem of scales? <i>(submitted to Water Resources Research)</i>	81
	Abstract	81
4.1	Introduction	82
4.2	Geostatistical Analysis	86
4.3	Modeling Approach	94
4.4	Simulation Results	96
4.4.1	Kriging	96
4.4.2	Sequential Simulation	97
4.5	Discussion	100
4.5.1	Support Scale of the Transport Model	103
4.5.2	Connectivity	105
4.6	Conclusions	106
	Bibliography	109
5	General Conclusions	115
5.1	Summary	115
5.2	Recommendations for Future Research	117
	Appendix	119
A	RW3D - A three-dimensional object-oriented solute transport model based on random walk particle tracking	119

List of Figures

2.1	Velocity interpolation for a finite-difference flow scheme (LaBolle et al., 1996). Velocities at the particle position can be calculated according to Table 2.1.	15
2.2	A two-layer system with a discontinuous diffusion coefficient across the interface (Uffink, 1990)	17
2.3	Schematic illustration of the two-step process of a random walk simulation in a composite porous media (LaBolle et al., 2000)	20
2.4	Schematic representation of the two-layer aquifer system	22
2.5	Behavior of the average velocity with increasing heterogeneity. (u_{x2} is kept constant and u_{x1} is decreased)	25
2.6	Behavior of the longitudinal macrodispersion with increasing heterogeneity. (u_{x2} is kept constant and u_{x1} is decreased)	26
2.7	Location of the centre of mass with respect to the y -axis using the interpolation method in combination with Itô’s interpretation of a stochastic integral. ($u_{x2} > u_{x1}$)	27
2.8	Location of the centre of mass with respect to the y -axis using the interpolation method in combination with Stratonovich’s interpretation of a stochastic integral. ($u_{x2} > u_{x1}$)	27
2.9	Location of the centre of mass with respect to the y -axis using the generalized stochastic differential equations approach. ($u_{x2} > u_{x1}$)	28
2.10	Location of the centre of mass with respect to the y -axis using the reflection method. ($u_{x2} > u_{x1}$)	28
2.11	The four models generated using Sequential Gaussian and Indicator Simulation with different spatial correlation. Circles in Models B and D denote observation well locations.	29
2.12	Normalized mass flux breakthrough curve, average velocity, and longitudinal macrodispersivity using Model A with $\sigma_{\ln K}^2 = 2.0$ and $\sigma_{\ln K}^2 = 4.0$	32
2.13	Normalized mass flux breakthrough curve, average velocity, and longitudinal macrodispersivity using Model B with $\sigma_{\ln K}^2 = 2.0$ and $\sigma_{\ln K}^2 = 4.0$	33

2.14	Normalized mass flux breakthrough curve, average velocity, and longitudinal macrodispersivity using Model C with $\sigma_{\ln K}^2 = 2.0$ and $\sigma_{\ln K}^2 = 4.0$	35
2.15	Normalized mass flux breakthrough curve, average velocity, and longitudinal macrodispersivity using Model D with $\sigma_{\ln K}^2 = 0.5$ and $\sigma_{\ln K}^2 = 2.0$	36
2.16	Normalized mass flux breakthrough curve, average velocity, and longitudinal macrodispersivity using Model D with $\sigma_{\ln K}^2 = 3.0$ and $\sigma_{\ln K}^2 = 4.0$	37
2.17	Breakthrough curves for an observation well in Model B with $\sigma_{\ln K}^2 = 3.0$ and in Model D with $\sigma_{\ln K}^2 = 3.0$	38
2.18	Average velocity and longitudinal macrodispersivity using a local-scale dispersion of $\alpha = 0.05m$ with Model B for $\sigma_{\ln K}^2 = 4.0$ and with Model D for $\sigma_{\ln K}^2 = 2.0$ and $\sigma_{\ln K}^2 = 4.0$	39
3.1	Comparison of breakthrough curves obtained with CXTFIT (<i>Toride et al., 1995</i>) and random walk particle tracking.	57
3.2	Comparison of breakthrough curves obtained with STAMMT-L (<i>Haggerty and Reeves, 2002</i>) and random walk particle tracking.	62
3.3	Evaluation of the root mean of squared residual errors in dependency of the time step size for different $Da_{I,1}$ numbers. Solute transport for this case is only subject to advection and first-order mass transfer.	64
3.4	Cumulative breakthrough curves obtained using different time step sizes for a Damköhler number of $Da_{I,1} = 200$	66
3.5	Absolute error tolerance δ versus matrix 1-norm of $\ (\mathbf{A}^{-1}\mathbf{B})t\ $ when using a Taylor Series approximation for the matrix exponential with three terms.	67
3.6	Evaluation of the root mean of squared residual errors in dependency of the number of terms used for the multirate series.	68
3.7	Breakthrough curves obtained using the example outlined in Section 3.4.	72
3.8	Relative total mass fraction remaining in the aquifer not having passed the control plane located at $x = 78$ using the example outlined in Section 3.4.	72
4.1	Model domain used for the simulations. Circles denote flowmeter well locations. Triangles denote the five solute injection wells.	87
4.2	Frequency distribution and univariate statistics of the 2495 flowmeter measurements.	88
4.3	Omnidirectional horizontal and vertical isotropic variograms and fitted spherical model for the $\ln K$ flowmeter data.	89

LIST OF FIGURES

xiii

4.4	Directional horizontal and vertical variograms and fitted model with hole effect for the $\ln K$ flowmeter data. The rotation angle of the directional variograms is measured in degrees clockwise from the positive y -axis	91
4.5	Standardized indicator variograms for the following directions and deciles: a) Directional horizontal indicator variogram and fitted model for 0.1 decile b) Directional horizontal indicator variogram and fitted model for 0.4 decile c) vertical indicator variogram and fitted model for 0.4 decile d) Directional horizontal indicator variogram and fitted model for 0.9 decile. The rotation angle of the directional variograms is measured in degrees clockwise from the positive y -axis.	93
4.6	Longitudinal mass distribution profiles of the tritium plume and predictions using ordinary and indicator kriging to generate a hydraulic conductivity field. The ordinary kriged fields are generated using Eq. (4.2) and (4.4), respectively, as random function model with the parameters given in Table 4.2. The indicator kriged field was obtained using Eq. (4.7) with the parameters of Table 4.2.	96
4.7	Longitudinal mass distribution profiles of the tritium plume and predictions using sequential Gaussian simulation using Eq. (4.2) as random function model with the parameters given in Table 4.2.	98
4.8	Longitudinal mass distribution profiles of the tritium plume and predictions using sequential Gaussian simulation using Eq. (4.4) as random function model with the parameters given in Table 4.2.	99
4.9	Longitudinal mass distribution profiles of the tritium plume and predictions of six realizations of the sequential Gaussian simulation exhibiting a strong tailing (using Eq. (4.4) as random function model).	99
4.10	Horizontal slice of the hydraulic conductivity field #80 for $z = 8.1$ m.	101
4.11	(a) Depth integrated normalized concentration distribution after 328 days for realization #80 (b) Laterally integrated normalized concentration distribution after 328 days for realization #80.	102
4.12	Longitudinal mass distribution profiles of the tritium plume and predictions using sequential Indicator simulation.	103
A.1	Flowchart of the RW3D program structure. Part A.	120
A.2	Flowchart of the RW3D program structure. Part B.	121

List of Tables

2.1	Velocity Interpolation Schemes (see Figure 2.1)	16
2.2	Parameters for the random function models C and D (where z_k corresponds to the 9 decile cutoffs of the marginal cumulative distribution function $F(z_k)$)	30
3.1	Input parameters for one-dimensional solute transport in Figures 3.1 and 3.2	58
3.2	Multirate Series for Diffusion (after <i>Haggerty and Reeves, 2002</i>)	59
3.3	Final Terms of Truncated Multirate Series (after <i>Haggerty and Reeves, 2002</i>)	61
3.4	Input parameters for solute transport examples in Figures 3.3, 3.4, and 3.6. Note that α was varied to change the ratio between advection and mass transfer timescale.	68
3.5	Grain sizes and diffusion rate coefficients for a Borden sand sample measured by <i>Ball and Roberts (1991)</i> for PCE desorption	71
4.1	Geostatistical model parameters for Figures 4.3 and 4.4.	90
4.2	Geostatistical model parameters for the indicator variogram model according to Eq.(4.7).	92
4.3	Statistical characteristics for generated hydraulic conductivity fields.	95
A.1	Name file for RW3D	122
A.2	Input parameter file for RW3D	122

1

General Context

1.1 Motivation and Objectives

Solute transport models have become an essential tool for assessing environmental risks to groundwater resources, remediation engineering, or the design of underground repositories of nuclear waste. This development was mainly driven by an increasing interest in groundwater quality and a rapid evolution of computer technology making transport simulations widely available to engineers and consultants. However, although numerical models of solute transport have undergone a significant improvement over the last decades, the claims made from the users have also increased. While users initially intended to simply have a rough idea of, for example, the potential threat of a contaminant source on a drinking water well using homogenous parameters for their solute transport model, the failure of many of these models has led the modeling community to recognize that solute transport models need to be able to account for the complexity of parameters found in field problems.

The complexity of solute transport in subsurface systems is based on a multiplicity of processes: the occurrence of a variety of chemical, physicochemical, and biochemical mechanisms often varying spatially, the temporal variability of the flow field, and the heterogeneity of hydraulic conductivity. Unfortunately, exhaustive knowledge of all these parameters will never be available and hence solute transport models need to be able to quantify the uncertainty associated with the model predictions. One possibility to achieve this is the use of a stochastic approach, where, due to the lack of detailed knowledge

about the aquifer properties, multiple equally plausible representations are generated and analyzed.

A further issue when using solute transport models is the problem of scales. Numerical models are usually discretized into model grid blocks which are almost always much larger than the scale of heterogeneity of the corresponding parameter and/or the measurement support scale. Upscaling methods have been developed to overcome this problem, although principally focussing on flow. Less research has been done on the upscaling of solute transport. The problem of scales for solute transport was first recognized by the apparent scale dependance of dispersivity raising the question whether the classical advection-dispersion equation is capable of correctly simulating solute transport for strongly heterogeneous aquifers using coarse model grid blocks in comparison to the small-scale variability of aquifer properties. In fact, more recent research on solute transport upscaling has demonstrated that, when moving from a highly discretized model to a coarsely discretized one, we need to account additionally for mass transfer between model grid blocks and hence either a mass transfer process has to be added to the advection-dispersion equation or even a different solute transport equation, e.g., continuous time random walk, fractional advection-dispersion equation, etc., has to be used.

Thus, the exigency of analyzing solute transport for hundreds or even thousands of different aquifer realizations to quantify uncertainty and/or reduce uncertainty by inverse modeling techniques and the ongoing research of solute transport upscaling require a numerical approach which is highly computational efficient even for models with millions of grid cells and is virtually free of numerical dispersion. For these cases the random walk particle tracking method represents a valuable alternative and the objectives of this thesis are to review the basic concepts of the random walk approach, to present its limitations and advantages, to extend its capacities to include mass transfer processes, possibly significant when upscaling solute transport, and to demonstrate its applicability for field problems.

1.2 Thesis Organization

The first chapter of this dissertation provides an introduction. It is intended to present the issues motivating this research and it briefly discusses the importance of solute transport modeling tools, capable of dealing with complex aquifer heterogeneity at a small-scale and at the same time being computationally efficient and avoiding numerical errors. Each of the following three chapters is comprised of a separate, self-contained paper which is published or is currently being revised for publication in international journals.

Chapter 2 provides an extensive review of the random walk particle tracking method, discusses its advantages and limitations, and evaluates different numerical approaches to overcome the problem of local solute mass conservation of the random walk methodology.

In Chapter 3 the random walk particle tracking method is extended to be capable of modeling a variety of mass transfer processes, ranging from simple first-order mass transfer, to diffusion into different geometries or any combination of these mass transfer processes. The new approach is compared with analytical and semi-analytical solutions and a three-dimensional synthetic example is presented to demonstrate its applicability.

Finally, Chapter 4 provides a field case application of the random walk method demonstrating its advantages especially for solute transport in advection-dominated cases with a large number of model grid cells. For this purpose a detailed geostatistical analysis of the flowmeter data at the Macrodispersion Experiment site at the Columbus Air Force Base, Mississippi, USA, is performed and a variety of high-resolution hydraulic conductivity fields are generated using kriging and Monte Carlo simulations. Solute transport is analyzed in these fields and the effects of the model support scale in comparison with the scale of heterogeneity, as well as the existence and effects of preferential flow pathways caused by a possible connectivity of high conductivity values are discussed.

Chapter 5 summarizes the principal conclusions of this thesis and identifies the new possibilities opened up for future research as well as questions raised during this work that need further investigation.

Appendix A briefly presents the numerical code of the random walk particle tracking method used throughout this dissertation and describes the programming structure of the model as well as the necessary input files.

2

A review and numerical assessment of the random walk particle tracking method

Journal of Contaminant Hydrology, in press:
doi:10.1016/j.jconhyd.2006.05.005

Abstract

We review the basic mathematical concepts of random walk particle tracking (RWPT) and its advantages and limitations. Three different numerical approaches to overcome the local mass conservation problem of the random walk methodology are examined: (i) the interpolation method, (ii) the reflection principle, and (iii) the generalized stochastic differential equations (GSDE). Analytical solutions of the spatial moments for a two-layer system are compared to model predictions using the different techniques and results demonstrate that the interpolation method reproduces correctly average velocity, but fails to reproduce macrodispersion at higher hydraulic conductivity contrasts between the two layers. On the contrary, the reflection principle and the GSDE approach underestimate average velocity, but reproduce macrodispersion better for high contrasts. The different behavior is based on an artificial shift of mass for increasing heterogeneities for the GSDE approach and the reflection principle, whereas the interpolation method suffers from the smoothing of the dispersion tensor. The behavior of these approaches was furthermore analyzed in two-dimensional heterogeneous hydraulic conductivity fields, which are characterized by different random function models. Solute transport

was simulated correctly by all three approaches for the reference fields having Gaussian structures or non-Gaussian structures with an isotropic spatial correlation, even for a variance of the natural log of hydraulic conductivity of $\sigma_{\ln K}^2 = 4$. However, for the non-Gaussian model with a strong anisotropic spatial correlation and a variance of $\sigma_{\ln K}^2 = 2$ and higher, the interpolation method was the only technique modelling solute transport correctly. Furthermore, we discuss the general applicability of random walk particle tracking in comparison to the standard transport models and conclude that in advection-dominated problems using a high spatial discretization or requiring the performance of many model runs, RWPT represents a good alternative for modelling contaminant transport.

2.1 Introduction

Eulerian transport models are often plagued by numerical dispersion or artificial oscillations, especially for advection-dominated problems. To overcome these problems a higher grid resolution and smaller time steps have to be applied, resulting in long execution times even with the CPUs available nowadays (e.g. Liu et al., 2004).

Furthermore, many aquifers present small-scale geological features that strongly affect solute transport (e.g. high hydraulic conductivity channels, low permeability inclusions, abrupt facies transitions). These systems often require a very fine spatial resolution in the numerical model. One of the most prominent examples is the aquifer at the Columbus Air Force Base, Mississippi (commonly referred to as the Macrodispersion Experiment, or MADE site). Although considerable effort was invested in characterizing the heterogeneity of the aquifer and conservative tracer transport was simulated using up to approximately 200.000 nodes, a correct model, based on the classical advection-dispersion equation, representing the main features of transport at this site has still not been achieved (Feehley et al., 2000). Many authors concluded that for a proper representation of tracer transport in these types of aquifers an even higher resolution of the spatial scale is required or a mass transfer component has to be added to the advection-dispersion model to compensate the loss of spatial resolution (e.g. Feehley et al., 2000; Zinn and Harvey, 2003; Liu et al., 2004).

An alternative to solve transport in heterogeneous porous media is the Lagrangian approach. In particular, the random walk particle tracking (RWPT) method treats the transport of a solute mass via a large number of particles. It moves each particle through the porous medium using the velocity field obtained from the solution of the flow equation to simulate advection and adds a random displacement to simulate dispersion. This approach avoids solving the

transport equation directly and therefore is virtually free of numerical dispersion and artificial oscillations. Furthermore, computational times for models with a very large amount of cells and being characterized by strong heterogeneities are significantly smaller than using the traditional Eulerian, mixed Eulerian-Lagrangian, or total variation diminishing (TVD) schemes. Hence, computational efficiency and the absence of numerical dispersion have turned the Lagrangian transport method into a valuable option for modelling complex, high-resolution transport problems, inverse modelling, and uncertainty assessment of contaminant transport (e.g. Tompson and Gelhar, 1990; Quinodoz and Valocchi, 1993; Tompson et al., 1998; Abulaban and Nieber, 2000; Kunstmann and Kinzelbach, 2000; LaBolle and Fogg, 2001; Fernández-García et al., 2005b).

We emphasize, that random walk particle tracking should not be confused with the so called continuous time random walk concept introduced by Berkowitz et al. (2000). Although continuous time random walk also uses a probabilistic approach to simulate contaminant transport in heterogeneous porous media, it is fundamentally different to RWPT as it combines advective, dispersive, and diffusive transport mechanisms inextricably using a generalized master equation.

RWPT is a method from statistical physics which has been used in the analysis of dispersion and diffusion processes in porous media for a long time (Scheidegger, 1954; De Josselin de Jong, 1958). In the late seventies, the first numerical codes were developed to simulate solute transport in aquifers using the random walk theory (Ahlstrom et al., 1977; Prickett et al., 1981) and since then gained popularity. Nevertheless, it was observed in these early studies that particles accumulate in low permeability zones, resulting in unrealistic concentrations. This subject was first pointed out by Kinzelbach (1987), who noted that a slight dissimilarity between the random walk equation, better known as the Fokker-Planck equation, and the advection-dispersion equation exists. In mildly heterogeneous systems, where groundwater flow velocity changes only slightly, this difference is negligible. However, in aquifers with a high variability in groundwater flow velocity, i.e. very heterogeneous hydraulic conductivity fields or areas with strong sink/source conditions, this difference gains importance, and a correction term to retrieve the advection-dispersion equation has to be included.

The problem of local solute mass conservation has been widely discussed and various approaches have been suggested to overcome this problem. LaBolle et al. (1996) compares various interpolation methods and the reflection principle (Uffink, 1985) for a one-dimensional system with no advection and for solute transport in a stratified system, concluding that both methods work well for these cases, but that the reflection method is difficult to implement for heterogeneous multidimensional systems. In a later review of different reflection

methods LaBolle et al. (1998) conclude that only the reflection techniques presented by Uffink (1985) and Semra et al. (1993) are successful in maintaining a uniform particle number density in a closed system with a discontinuous diffusion coefficient, whereas the approaches of Ackerer (1987) and Cordes and Rouvé (1991) fail to reproduce a correct behavior. In a comment on this article Ackerer and Mosé (2000) disagree with these conclusions and state that the method of Uffink (1985) does not preserve mass balance over a discontinuous interface. More recently, LaBolle et al. (2000) present a technique using generalized stochastic differential equations and demonstrate that, for a closed one-dimensional system with no advection and for a two-dimensional system with advective-dispersive transport in composite media, this approach fulfills local solute mass conservation. Finally, Hoteit et al. (2002) compare again the different reflection methods and the interpolation method for a two-layer stratified aquifer and conclude that only the approach of Semra et al. (1993) preserves a uniform particle number density in both layers.

In this article we first present an overview of the mathematical equations of the random walk methodology, its advantages and limitations, and we briefly discuss the general applicability of the random walk methodology in comparison with the standard transport models. Then, the different numerical approaches to conserve local solute mass balance using the random walk methodology are reviewed and evaluated numerically. For this purpose, a two-layer stratified aquifer system will be used in order to observe the effect of the different approaches on particle transport in a simple scenario. The numerical results of the first- and second-order moments are compared with analytical solutions. In a second step, four two-dimensional heterogeneous hydraulic conductivity fields are generated using stochastic simulation techniques. These fields are characterized by having multi-Gaussian or non-multi-Gaussian random distributions as well as by a different spatial correlation structure. Increasing the variance of these fields (i.e., degree of heterogeneity), the importance of the correction term increases and the effects of the different numerical approaches can be demonstrated. The output is compared with simulations using a highly discretized TVD scheme. Finally, the main results from this paper are summarized.

2.2 Basic Concepts of Random Walk Particle Tracking

2.2.1 Mathematical Formulation

The well known transport equation of a conservative solute in an aquifer is given at the representative elemental volume scale by the following equation

$$\frac{\partial c}{\partial t} + \nabla \cdot (\mathbf{u}c) = \nabla \cdot (\mathbf{D}\nabla c) \quad (2.1)$$

where \mathbf{D} is the dispersion coefficient tensor, usually defined as

$$\mathbf{D} = (\alpha_T|\mathbf{u}| + D_m)\mathbf{I} + (\alpha_L - \alpha_T)\frac{\mathbf{u}\mathbf{u}^t}{|\mathbf{u}|} \quad (2.2)$$

c is the dissolved concentration, t is the time, α_L and α_T is the longitudinal and transverse dispersivity, respectively, D_m is the molecular diffusion coefficient, \mathbf{u} is the velocity vector obtained from the solution of the steady-state flow equation, and $|\mathbf{u}|$ is the magnitude of the velocity vector. Here, porosity is assumed constant and velocity fluctuations are mainly attributed to a spatially varying hydraulic conductivity. This represents a second-order partial differential equation, which can be solved using an Eulerian approach by standard finite-difference or finite-element methods. In order to overcome the problem of artificial oscillation and numerical dispersion, the Peclet and Courant number have to be sufficiently small as shown, for example, by Huyakorn and Pinder (1983). This limitation results, especially for advection-dominated problems, in a required grid resolution that often strongly increases computational times.

RWPT simulates solute transport by partitioning the solute mass into a large number of representative particles. The evolution in time of a particle is driven by a drift term that relates to the advective movement and a superposed Brownian motion responsible for dispersion. The displacement of a particle is written in its traditional form given by the Itô-Taylor integration scheme (Gardiner, 1990)

$$\mathbf{X}_p(t + \Delta t) = \mathbf{X}_p(t) + \mathbf{A}(\mathbf{X}_p, t)\Delta t + \mathbf{B}(\mathbf{X}_p, t) \cdot \boldsymbol{\xi}(t)\sqrt{\Delta t} \quad (2.3)$$

where Δt is the time step, $\mathbf{X}_p(t)$ is the position of a particle at time t , \mathbf{A} is a “drift” vector, \mathbf{B} , the displacement matrix, is a tensor defining the strength of dispersion, and $\boldsymbol{\xi}(t)$ is a vector of independent, normally distributed random variables with zero mean and unit variance.

Itô (1951) demonstrated that the particle density distribution $f(\mathbf{X}_p, t)$, defined as the probability of finding a particle within a given interval $[\mathbf{X}_p, \mathbf{X}_p + d\mathbf{X}_p]$ at a given time t , obtained from Eq. (2.3) fulfills, in the limit of large particle numbers and an infinitesimally small step size, the Fokker-Planck equation. This equation describes the motion of the particle density distribution f and is given by

$$\frac{\partial f}{\partial t} + \nabla \cdot (\mathbf{u}f) = \nabla \nabla : (\mathbf{D}f) \quad (2.4)$$

where the colon refers to the outer product for multiplying two tensors and thus

$$\nabla\nabla : (\mathbf{D}f) \equiv \sum_{i=1}^n \sum_{j=1}^n \frac{\partial^2 D_{ij}}{\partial x_i \partial x_j} f \quad (2.5)$$

where n denotes the number of dimensions.

Both of the equations, the advection-dispersion and the Fokker-Planck equation, are similar to each other as both of them are composed of an advection/drift term and a dispersion/diffusion term. However, in order to establish an analogy between them, Eq. (2.1) has to be modified as follows (Kinzelbach, 1987)

$$\frac{\partial c}{\partial t} + \nabla \cdot (\mathbf{u}c) + \nabla \cdot (c\nabla \cdot \mathbf{D}) = \nabla\nabla : (\mathbf{D}c) \quad (2.6)$$

Using a modified velocity

$$\mathbf{u}^* = \mathbf{u} + \nabla \cdot \mathbf{D} \quad (2.7)$$

it can be demonstrated that the solute transport equation for heterogeneous porous media can be transformed into an equivalent of the Fokker-Planck equation:

$$\frac{\partial c}{\partial t} + \nabla \cdot (\mathbf{u}^*c) = \nabla\nabla : (\mathbf{D}c) \quad (2.8)$$

Substituting now the drift vector \mathbf{A} in Eq. (2.3) with the modified velocity vector of Eq. (2.7), the RWPT scheme is obtained:

$$\mathbf{X}_p(t + \Delta t) = \mathbf{X}_p(t) + (\mathbf{u}(\mathbf{X}_p, t) + \nabla \cdot \mathbf{D}(\mathbf{X}_p, t))\Delta t + \mathbf{B}(\mathbf{X}_p, t) \cdot \boldsymbol{\xi}(t)\sqrt{\Delta t} \quad (2.9)$$

where the displacement matrix \mathbf{B} is related to the dispersion tensor according to the following relationship

$$2\mathbf{D} = \mathbf{B} \cdot \mathbf{B}^T$$

Note that \mathbf{D} is defined in terms of \mathbf{u} and not of \mathbf{u}^* . For isotropic porous media the three-dimensional form of the displacement matrix \mathbf{B} can be expressed as:

$$\mathbf{B} = \begin{pmatrix} \frac{u_x}{|u|} \sqrt{2(\alpha_L|u| + D_m)} & -\frac{u_x u_z}{|u| \sqrt{u_x^2 + u_y^2}} \sqrt{2(\alpha_T|u| + D_m)} & -\frac{u_y}{\sqrt{u_x^2 + u_y^2}} \sqrt{2(\alpha_T|u| + D_m)} \\ \frac{u_y}{|u|} \sqrt{2(\alpha_L|u| + D_m)} & -\frac{u_y u_z}{|u| \sqrt{u_x^2 + u_y^2}} \sqrt{2(\alpha_T|u| + D_m)} & \frac{u_x}{\sqrt{u_x^2 + u_y^2}} \sqrt{2(\alpha_T|u| + D_m)} \\ \frac{u_z}{|u|} \sqrt{2(\alpha_L|u| + D_m)} & \frac{\sqrt{u_x^2 + u_y^2}}{|u|} \sqrt{2(\alpha_T|u| + D_m)} & 0 \end{pmatrix} \quad (2.10)$$

Other forms of the dispersion tensors and displacement matrices for non-isotropic media can be found in Burnett and Frind (1987) and Lichtner et al. (2002). As we will use only two-dimensional examples in the following sections, the displacement matrix \mathbf{B} reduces to

$$\mathbf{B} = \begin{pmatrix} \frac{u_x}{|u|} \sqrt{2(\alpha_L|u| + D_m)} & -\frac{u_y}{|u|} \sqrt{2(\alpha_T|u| + D_m)} \\ \frac{u_y}{|u|} \sqrt{2(\alpha_L|u| + D_m)} & \frac{u_x}{|u|} \sqrt{2(\alpha_T|u| + D_m)} \end{pmatrix} \quad (2.11)$$

However, in stochastic theory two different interpretations exist to demonstrate that the particle density distribution converges to a solution of the Fokker-Planck equation. Using Itô’s interpretation of a stochastic integral, the modified velocity \mathbf{u}^* and the matrix \mathbf{B} are evaluated prior to the particle displacement (see Eq.(2.9)). Stratonovich (1966) showed that using the following particle motion scheme leads also to the Fokker-Planck equation (2.4):

$$\mathbf{X}_p(t + \Delta t) = \mathbf{X}_p(t) + \mathbf{u}^*(\mathbf{X}_p, t + \frac{\Delta t}{2})\Delta t + \mathbf{B}(\mathbf{X}_p, t + \frac{\Delta t}{2}) \cdot \boldsymbol{\xi}(t)\sqrt{\Delta t} \quad (2.12)$$

with

$$\mathbf{u}^* = \mathbf{u} + \frac{1}{2}\mathbf{B} \cdot \nabla \cdot (\mathbf{B}^T) \quad (2.13)$$

and the dispersion tensor \mathbf{D} defined as above.

Here, the drift vector and the dispersion tensor are evaluated at a moment halfway along the time step to the next particle position. The modified velocity still contains a derivative term, however, reduced by a factor of 1/2. From a computational point of view, Itô’s procedure is more attractive as Eq. (2.12) is implicit and therefore requires an iterative procedure for each time step.

Numerical implementation of the random walk equations is relatively simple with one exception. When solving the flow equation using numerical methods, the resulting hydraulic heads and the associated velocity field are usually given as a discrete point information. Yet simulation of solute transport by the random walk methodology requires “continuous” information of the velocity field. Therefore, a map of velocities from this discrete information has to be generated. This velocity map should fulfil the local fluid mass balance at any location and the local solute mass conservation at any grid-cell interface. In general, there is not a simple solution to this problem, but several approaches have been proposed in the literature, which will be presented in Section 2.3.

2.2.2 Advantages

Besides the above-mentioned computational efficiency and the absence of numerical dispersion, random walk particle transport offers some further advantages. Based on the simplicity of the explicit equations it can be easily

implanted over any type of flow model and due to the use of particles as discrete mass parcels, global mass conservation is automatically satisfied. Furthermore, using a constant-displacement scheme (Wen and Gómez-Hernández, 1996), which adjusts automatically the time step for each particle according to the local velocity, computational time is decreased significantly, especially for highly heterogeneous aquifers.

Equilibrium sorption using a linear isotherm can be incorporated by replacing the velocity \mathbf{u}^* with a retarded velocity \mathbf{u}^*/R and \mathbf{D} with \mathbf{D}/R in Eq. (2.9). In this case, it must be remembered that, when calculating the total aqueous or sorbed solute mass, each particle with a total mass of m_p moving at the modified retarded velocity \mathbf{u}^*/R has to be divided into an aqueous phase mass and a sorbed phase mass. A detailed analysis of the implementation of equilibrium sorption into random walk particle tracking has been presented by Tompson (1993). Various authors have also introduced algorithms, which permit the simulation of kinetic sorption (Kinzelbach, 1987; Andričević and Foufoula-Georgiu, 1991; Quinodoz and Valocchi, 1993; Michalak and Kitaniidis, 2000) or first-order mass transfer (Huang et al., 2003) within the random walk particle tracking method. Furthermore, first-order degradation reactions can be included into the model by assigning to every particle a variable pollutant mass, which develops in time according to first-order kinetics (Kinzelbach, 1987).

Random walk theory can also be used for the calculation of the so-called backward probability density, where the positive velocities are exchanged with negative velocities and vice versa, so that particles are tracked backward. This allows, for example, to determine capture zones around groundwater wells taking into account dispersion (Uffink, 1989; Frind et al., 2002).

2.2.3 Limitations

One of the problems of the random walk method are the random fluctuations of computed concentrations. Although these can be diminished by increasing the number of particles, the statistical fluctuation is inversely proportional to the square root of the number of particles in a cell (Kinzelbach, 1987). Hassan and Mohamed (2003) demonstrated that in a homogeneous, two-dimensional aquifer with 20000 cells approximately 2.5 million particles were needed to achieve the same smoothness for the concentration contours as that achieved by the TVD method. A different method to solve this problem, instead of increasing the number of particles, is the use of projection functions, which “smooth” the random fluctuations of the computed concentrations (Bagtzoglou et al., 1992).

A desirable property of the random walk method is that during particle tracking computation of solute concentration may not be necessary, which

implies that statistical errors associated to the calculation of concentrations do not propagate to the next time step. Unfortunately, this also means that concentration-dependent chemical processes, like non-linear equilibrium sorption, reactions between different chemical species, or sequential decay reactions are not easily incorporated or have to be implemented with a significant trade-off with respect to computational efficiency (see Abulaban et al., 1998; Tompson et al., 1996). Similar problems are to be expected for the application of RWPT to heat or density-dependent transport. However, currently no literature exists addressing these issues.

Further problems can be observed in the simulation of particle capture by pumping wells (e.g. Zheng, 1994). Wells are usually incorporated by defining a circle around the well center such that when a particle enters the circle it is removed from the aquifer. The choice of the radius and an incorrect representation of the radial velocity field in the proximity of the well, due to a coarse discretization, may therefore influence the breakthrough curve at the well. This problem can be resolved by using a higher discretization for the flow field, so that the velocity vectors in all cells adjacent to the well point towards the well (Kinzelbach, 1987) or by using an analytical solution of the velocity field for the cell in which the well is located (Zheng, 1994).

Finally, as random walk is based on moving particles it is susceptible to numerical difficulties in the presence of highly distorted grids, e.g. when using a vertically deformed grid associated with a varying layer thickness. This problem is known from the classical particle tracking approach and correction procedures have been presented by Zheng (1994) and Pollock (1988).

2.2.4 Comparison with Other Approaches

Most numerical methods used nowadays for solving solute transport can be grouped into four classes: Eulerian, Lagrangian, mixed Eulerian-Lagrangian, and TVD methods. Unfortunately, no single numerical technique has been effective for all transport conditions as each of those has its own strengths and limitations. Hence, the choice of the proper approach for solving a specific transport problem with efficiency and accuracy is important.

For the case of RWPT the limitations concerning the simulation of non-equilibrium processes and multispecies kinetic reactions as mentioned above are undoubtedly one of the greatest disadvantages in comparison to the other numerical methods. Accounting for these processes is essential in many problems and the Eulerian, mixed Eulerian-Lagrangian, and TVD methods offer a greater flexibility and efficiency in treating such problems. Furthermore, due to the difficulties concerning discontinuous properties and in the presence of a highly distorted grid, RWPT is not an optimal approach when using a zoned hydraulic conductivity distribution. In addition, the advantage concerning

computational efficiency gets less important as computational hardware gets more and more powerful.

However, for advection-dominated problems that are present in many field situations, RWPT offers a good alternative to the other existing methods. Eulerian methods are typically susceptible to excessive numerical dispersion and artificial oscillation for advection-dominated problems. Although numerical dispersion or artificial oscillations can be limited by using a sufficiently fine spatial grid, the computational effort required for a field-scale problem may become prohibitive. The mixed Eulerian-Lagrangian method combines the advantages of Eulerian and Lagrangian methods, in treating the advection term with a Lagrangian approach and the dispersion and other terms with an Eulerian approach. However, most Eulerian-Lagrangian schemes do not guarantee mass conservation and they are computationally not as efficient as RWPT. The TVD methods are higher-order finite-difference methods, which essentially belong to the Eulerian family of solution techniques (Zheng and Wang, 1999). These methods are mass conservative and reduce numerical dispersion and artificial oscillations, but unfortunately are much more computationally demanding than the Lagrangian methods.

Generally speaking, for dispersion-dominated cases, or aquifers with a reasonable number of grid cells and/or complex chemical processes, the standard transport models are a more appropriate choice for simulating contaminant transport, whereas advection-dominated problems, using a high spatial discretization or requiring the performance of many model runs, e.g. Monte-Carlo simulations, are more efficiently solved using RWPT.

2.3 Implementation Methods for the Local Solute Mass Conservation

As was mentioned above, the RWPT method requires a velocity field that conserves the local fluid mass balance for each grid-cell and the local solute mass balance at any interface. In aquifers with homogeneous properties both conditions are met, but for heterogeneous aquifers, where discontinuities in effective subsurface transport properties occur, it is especially difficult to fulfill the local solute mass balance. In practice, this means that we need a divergence-free velocity interpolation scheme and a continuous dispersion tensor in space.

2.3.1 The Interpolation Method

The interpolation method is certainly the most often used approach to address the problem of discontinuities in the dispersion tensor. This technique smoothes the dispersion tensor in the vicinity of the interfaces in order to

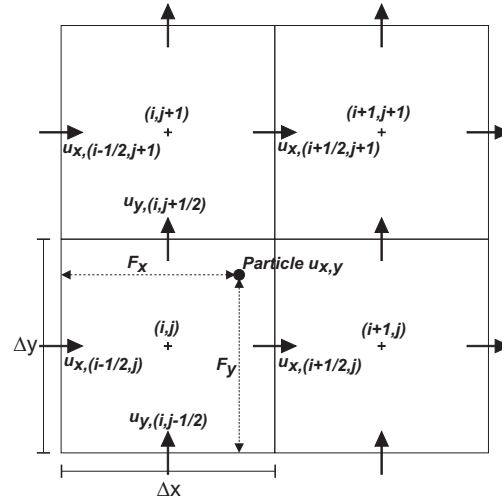


Figure 2.1. Velocity interpolation for a finite-difference flow scheme (LaBolle et al., 1996). Velocities at the particle position can be calculated according to Table 2.1.

produce a continuous gradient term in the drift vector at the interface. It requires not only that the time steps are sufficiently small, but also that the aquifer is sufficiently discretized, in order to minimize errors introduced by the smoothing of the dispersion tensor. LaBolle et al. (1996) presented a detailed analysis of this method.

When the flow equation is solved using a block-centered finite-difference scheme, the usual way to estimate velocity components is to use Darcy’s law to obtain velocities for the cell interfaces from hydraulic heads given at the center of each cell. The interface velocities can then be used to calculate the velocity components at any location within the cell by linear interpolation, as shown in Fig. 2.1 and Table 2.1. Using this method the local fluid mass balance $\nabla \cdot \mathbf{u} = 0$ is fulfilled.

Local mass conservation at the cell interfaces is given as follows (Gardiner, 1990)

$$\mathbf{n} \cdot \mathbf{J}|_{s_+} = \mathbf{n} \cdot \mathbf{J}|_{s_-} \quad (2.14)$$

where $s_{+/-}$ indicate the limits of the quantities from the left and the right hand sides of the interface between two neighboring cells, \mathbf{n} is the outward normal to the interface s , and \mathbf{J} is the solute mass flux, which is given as

$$\mathbf{J} = \mathbf{u}^*c - \mathbf{D} \cdot \nabla c \quad (2.15)$$

Interpolation Scheme
<p>Linear</p> $u_x = (\Delta x - F_x)u_{x,(i-1/2,j)} + F_x u_{x,(i+1/2,j)}$ $u_y = (\Delta y - F_y)u_{y,(i,j-1/2)} + F_y u_{y,(i,j+1/2)}$
<p>Bilinear</p> $u_x = (\Delta x - F_x)(\Delta y - F_y)u_{x,(i-1/2,j-1/2)} + F_x(\Delta y - F_y)u_{x,(i+1/2,j-1/2)} +$ $+(\Delta x - F_x)F_y u_{x,(i+1/2,j-1/2)} + F_x F_y u_{x,(i+1/2,j+1/2)}$ $u_y = (\Delta x - F_x)(\Delta y - F_y)u_{y,(i-1/2,j-1/2)} + F_x(\Delta y - F_y)u_{y,(i+1/2,j-1/2)} +$ $+(\Delta x - F_x)F_y u_{y,(i+1/2,j-1/2)} + F_x F_y u_{y,(i+1/2,j+1/2)}$

Table 2.1. Velocity Interpolation Schemes (see Figure 2.1)

where the first term on the right-hand side represents the advective mass flux and the second term the dispersive mass flux.

In order to fulfill Eq. (2.14) a continuous velocity field is required. When using linear interpolation, velocities are calculated considering only one direction (see Table 2.1) and consequently do not change regarding the orthogonal direction within one cell (Pollock, 1988). Hence, approaching the cell interface between two neighboring cells, e.g. (i,j) and $(i,j+1)$, as shown in Fig. 2.1, when assuming that we have different horizontal velocities u_x in each cell, results in different dispersive solute mass fluxes across the boundary. Neglecting this effect results in an artificial accumulation of particles in low conductivity zones, as was pointed out by Kinzelbach (1987).

In the bilinear approach the velocities are first linearly interpolated in one direction and then in the orthogonal direction using its neighboring grid-cells, so that velocities are obtained for each corner of the cell. The velocity at any point can then be calculated as a weighted average of these four velocities as is shown in Table 2.1. Approaching now the cell interface of cells (i,j) and $(i,j+1)$ from either side, results in a smooth transition of the velocity u_x and thus in an equal dispersive solute mass flux from either side. Nevertheless, bilinear interpolation has two disadvantages: firstly, the interpolated velocity field does not satisfy local fluid mass balance and secondly, bilinear interpolation introduces greater smoothing than linear interpolation. The effect of the second disadvantage can be significant especially in highly heterogeneous aquifers, as will be shown in the following sections.

Considering the condition given in Eq. (2.14), it is sufficient to use bilinear interpolation for the term $\nabla \cdot \mathbf{D}$ and the matrix \mathbf{B} in the particle displacement scheme (Eq.(2.9)), whereas the actual velocity vector \mathbf{u} can be calculated using linearly interpolated velocity components. This raises the possibility of a so called "hybrid" scheme where bilinear interpolation is used only for the

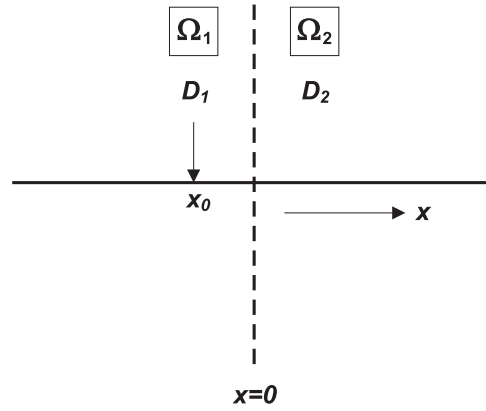


Figure 2.2. A two-layer system with a discontinuous diffusion coefficient across the interface (Uffink, 1990)

dispersion terms and the advective term is obtained applying linear interpolation. LaBolle et al. (1996) demonstrated that this scheme is able to solve solute transport in a heterogeneous aquifer quite accurately.

A hybrid scheme can also be applied to the RWPT method when the Stratonovich interpretation of a stochastic integral is used. Thus, in Eqs. (2.12) and (2.13) the term $\frac{1}{2}\mathbf{B} \cdot \nabla \cdot (\mathbf{B}^T)$ and the matrix \mathbf{B} are calculated using bilinear interpolation, whereas the remaining term is obtained using linear interpolation. In the following sections, where the different numerical approaches will be evaluated, the hybrid scheme is always used with the interpolation method.

2.3.2 The Reflection Method

The reflection method was first presented by Uffink (1985) and is based on the idea of diffusion across a boundary with different diffusion coefficients. If a system of infinite spatial extent as shown in Fig. 2.2 is considered, where Ω_1 and Ω_2 are the two subdomains, D_1 and D_2 are the diffusion coefficients, and c_1 and c_2 are the concentrations on either side of the boundary, the following equations have to be fulfilled

$$\frac{\partial c_1}{\partial t} = D_1 \frac{\partial^2 c_1}{\partial x^2} \quad x < 0 \quad (2.16)$$

$$\frac{\partial c_2}{\partial t} = D_2 \frac{\partial^2 c_2}{\partial x^2} \quad x > 0 \quad (2.17)$$

Conservation of mass requires that

$$\lim_{x \rightarrow 0^-} D_1 \frac{\partial c_1}{\partial x} = \lim_{x \rightarrow 0^+} D_2 \frac{\partial c_2}{\partial x} \quad (2.18)$$

$$\lim_{x \rightarrow 0^-} c_1 = \lim_{x \rightarrow 0^+} c_2 \quad (2.19)$$

The concentration distribution functions for each subdomain for an instantaneous point source at x_0 (delta input) can be described using the method of images (Feller, 1957). Carslaw and Jaeger (1959) demonstrate that the concentration distribution functions for subdomain Ω_1 can be calculated as the sum of two functions, where superscripts s and r, respectively, denote the source and reflected components

$$c_1(x, t) = c_1^s(x, t) + c_1^r(x, t) \quad x < 0 \quad (2.20)$$

$$c_1^s(x, t) = \frac{1}{2\sqrt{\pi D_1 t}} \exp \frac{(x - x_0)^2}{4D_1 t} \quad (2.21)$$

$$c_1^r(x, t) = \frac{R_1}{2\sqrt{\pi D_1 t}} \exp \frac{(x + x_0)^2}{4D_1 t} \quad (2.22)$$

Eqs. (2.21) and (2.22) represent the diffusion in a homogeneous, infinite system with D_1 for a source located at x_0 (see Eq. (2.21)) and for a source located at $-x_0$ and being modified by a reflection coefficient R_1 . The concentration distribution function for subdomain Ω_2 is calculated with an adjusted starting point $x_0^* = x_0\sqrt{D_2}/\sqrt{D_1}$ and using $1 - R_1$

$$c_2(x, t) = \frac{1 - R_1}{2\sqrt{\pi D_2 t}} \exp \frac{(x - x_0^*)^2}{4D_2 t} \quad x > 0 \quad (2.23)$$

In order to satisfy (2.18) and (2.19) R_1 has to be chosen as

$$R_1 = \frac{\sqrt{D_1} - \sqrt{D_2}}{\sqrt{D_1} + \sqrt{D_2}} \quad (2.24)$$

For a source located on the other side of the interface, R_1 has to be replaced with $R_2 = -R_1$ and x_0^* with $x_0^* = x_0\sqrt{D_1}/\sqrt{D_2}$. In the RWPT method the dispersive movement is simulated by drawing a random number from a normal distribution $\xi(t)$ and multiplying it with $\mathbf{B}\sqrt{\Delta t}$ (see Eq. (2.3)). Therefore, the probability density distribution for the dispersive particle movement corresponds to a concentration distribution function for a point source diffusion in a homogeneous medium. When using random walk theory to simulate solute transport across a discontinuous interface, Uffink (1985) suggested to substitute the normal distribution $\xi(t)$ with a modified probability distribution for

particles crossing the interface according to Eqs. (2.20) - (2.24) and thereby to account for the local mass balance at the interface.

Ackerer (1987) suggested a similar, yet slightly different method. It consists in splitting up the time step of a random walk particle into two smaller steps for all the particles that would cross an interface over a time span Δt . The first step Δt_1 moves the particle to the interface. The second step $\Delta t_2 = \Delta t - \Delta t_1$ is performed such that there is a 50% probability for the particle to enter either Ω_1 or Ω_2 . If it enters Ω_2 it will move using the dispersion in Ω_2 . Otherwise, the particle is reflected and it continues its trajectory in Ω_1 .

Cordes and Rouvé (1991) stated that both of the above-mentioned reflection methods fail, based on the fact that the particle density in the vicinity of the interface is not balanced. Therefore, they proposed that for each particle crossing from a cell with high dispersion to a cell with low dispersion, for example, a random number from a uniform distribution over the interval from 0 to 1 should be drawn. If this number is less than $(\sqrt{D_1} - \sqrt{D_2})/\sqrt{D_1}$, the particle is reflected at the interface with no loss of momentum. For the other case the particle continues its trajectory into the other domain.

The most recent variation of the reflection method was presented by Semra et al. (1993) and Hoteit et al. (2002). They use the same time step splitting procedure as presented by Ackerer (1987) in combination with a fully reflecting interface as introduced by Cordes and Rouvé (1991). Nevertheless, the probability that a particle goes into Ω_1 (respectively Ω_2) is calculated slightly different and corresponds to $P_1 = (\sqrt{D_1})/(\sqrt{D_1} + \sqrt{D_2})$ (respectively $P_2 = 1 - P_1 = (\sqrt{D_2})/(\sqrt{D_1} + \sqrt{D_2})$). In the following sections which evaluate the different techniques for a random walk simulation in heterogeneous media the method presented by Semra et al. (1993) and Hoteit et al. (2002) was chosen from the reflection approaches described here.

2.3.3 Generalized Stochastic Differential Equations

The most commonly used stochastic differential equation (SDE) to simulate random walk transport in aquifers is the one presented by Itô (1951). Numerical integration of this SDE leads to Eq. (2.9), which requires the gradient of the dispersion tensor and therefore requires a numerical approach to fulfil local fluid and solute mass conservation. LaBolle et al. (2000) used a Taylor series expansion in order to derive an alternative Itô-SDE for composite porous media and obtained, for the case of constant porosity and isotropic pore-scale dispersion, the following equation

$$\mathbf{X}_p(t + \Delta t) = \mathbf{X}_p(t) + \mathbf{u}(\mathbf{X}_p, t)\Delta t + \mathbf{B}(\mathbf{X}_p + \Delta \mathbf{Y}, t) \cdot \boldsymbol{\xi}(t)\sqrt{\Delta t} \quad (2.25)$$

$$\Delta \mathbf{Y} = \mathbf{B}(\mathbf{X}_p, t) \cdot \boldsymbol{\xi}(t)\sqrt{\Delta t} \quad (2.26)$$

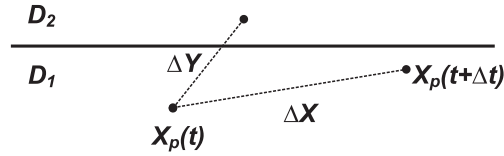


Figure 2.3. Schematic illustration of the two-step process of a random walk simulation in a composite porous media (LaBolle et al., 2000)

It can be observed that the advective step consists only of the actual velocity and therefore linear interpolation can be used to determine the velocity field. Local solute mass balance is included by a two-step procedure: First, the displacement considering only diffusion, denoted as $\Delta \mathbf{Y}$ in Eq. (2.26), is calculated. The velocity at this location is evaluated and used in the $\mathbf{B}(\mathbf{X}_p + \Delta \mathbf{Y}, t)$ term in Eq. (2.25). Then, the actual particle movement is calculated, starting from the particle’s original position $\mathbf{X}_p(t)$ according to Eq. (2.25). The simulation method is graphically illustrated in Fig. 2.3.

This approach can also be extended to the case of a heterogeneous porosity field and anisotropic pore-scale dispersion. However, due to the complexity of the equations for these cases, implementation into a numerical code is not simple. A detailed derivation of the generalized stochastic differential equations can be found in the work presented by LaBolle et al. (2000).

2.4 Method of Moments

In order to evaluate the following numerical simulations, the method of moments approach developed by Aris (1956) is applied. The spatial moments serve as a simple, physically meaningful description of overall plume behavior (e.g. Freyberg, 1986; Garabedian et al., 1991). Usually only the first three moments are considered: the zeroth moment represents the total solute mass contained in the plume, the first moment measures the location of the center of mass of the plume and the second moment corresponds to the spreading of the plume around the center of mass. The general formula to calculate the spatial moments of a plume is given as

$$M_p(t) = \int \int \int_{-\infty}^{\infty} \Theta x^p c(x, y, z, t) dx dy dz \quad (2.27)$$

where M_p is the moment of p th order, Θ is the porosity, and c is the concentration at location x, y, z at time t . In the subsequent cases we will consider only the moments in x -direction, hence mixed moments are not shown.

The center of mass as a function of time can be calculated as

$$X_G(t) = \frac{M_1}{M_0} \quad (2.28)$$

In addition, the second spatial moment in x -direction is defined as

$$S_{xx}(t) = \frac{M_2}{M_0} - \left(\frac{M_1}{M_0} \right)^2 \quad (2.29)$$

Using these moments the apparent average velocity $U(t)$ of the plume center of mass, the apparent longitudinal macrodispersion $D_L(t)$, and the apparent longitudinal macrodispersivity $A_L(t)$ can be calculated with the following formulas

$$U(t) = \frac{\Delta X_G}{\Delta t} = \frac{X_G(t) - X_G(0)}{t} \quad (2.30)$$

$$D_L(t) = \frac{1}{2} \frac{\Delta S_{xx}}{\Delta t} = \frac{1}{2} \frac{S_{xx}(t) - S_{xx}(0)}{t} \quad (2.31)$$

$$A_L(t) = \frac{D_L(t)}{U(t)} = \frac{1}{2} \frac{\Delta S_{xx}}{\Delta X_G} = \frac{1}{2} \frac{S_{xx}(t) - S_{xx}(0)}{X_G(t) - X_G(0)} \quad (2.32)$$

Apparent parameters as calculated in Eqs. (2.30) - (2.32) are viewed as equivalent values in homogeneous porous media that, when used with the classic advection-dispersion equation, lead to the same spatial moments of the plume as observed in the simulations for heterogeneous porous media.

2.5 Numerical Evaluation

All three approaches presented in Section 2.3 were numerically implemented into the random walk transport model RW3D (Fernández-García et al., 2005a). Solute transport in the following synthetic cases is conservative and two-dimensional, and pore-scale dispersion is assumed to be isotropic. Molecular diffusion is neglected in all of the subsequent cases. A constant-displacement scheme is used as it is computationally more efficient than the constant time step scheme. MODFLOW (McDonald and Harbaugh, 1988) was used to solve the flow equation and to compute the cell-interface velocities.

Two problems are considered: (1) transport in a two-layer stratified aquifer and (2) transport in a two-dimensional heterogeneous aquifer with different conceptual random field models. The first problem was chosen to compare the development of first- and second-order moments with analytical solutions and serves as a simple scenario to illustrate the effect of a discontinuous dispersion tensor on particle transport for each of the different numerical approaches. The second problem simulates heterogeneous conditions by creating synthetic,

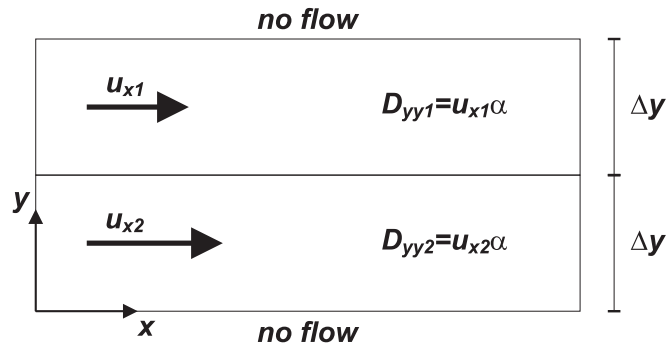


Figure 2.4. Schematic representation of the two-layer aquifer system

two-dimensional aquifers using stochastic simulation. It demonstrates the effects of the different approaches especially with regard to highly heterogeneous aquifers.

2.5.1 Solute Transport in a Two-Layer Stratified Aquifer

Problem Description

The stratified system shown in Fig. 2.4 contains two equally thick horizontal layers with different hydraulic conductivities, a homogeneous porosity of $\Theta = 0.2$, and an isotropic and homogeneous pore-scale dispersivity of $\alpha = 0.01$ m. The system represents a confined aquifer with no flow boundaries at the top and the bottom sides and constant-head boundaries at the left and right-hand sides. Particles were distributed uniformly on a line transverse to the flow direction. The particle source is located on the left-hand side of the aquifer and spans the whole width of the aquifer. A total number of 2000 particles were used in the simulations. The aquifer was chosen to be 0.3 m wide and 1000 m long in order to be able to obtain constant values for the growth of the first- and second-order moments before the particles exit the domain. The system has a hydraulic gradient of 0.01. The natural log of hydraulic conductivity of layer 2 is $\ln K = -4.605$ (where K is in m/s), whereas several alternatives for $\ln K$ in layer 1 were considered between $\ln K = -4.605$ and $\ln K = -11.513$ in order to increase the contrast between the two layers. For the system shown in Fig. 2.4, the explicit Itô-random walk equations reduce to the following simple set of equations

$$x_p(t + \Delta t) = x_p(t) + u_x(t)\Delta t + \xi_x \sqrt{2\alpha \cdot u_x(t)\Delta t} \quad (2.33)$$

$$y_p(t + \Delta t) = y_p(t) + \frac{\partial D_{yy}(t)}{\partial y} \Delta t + \xi_y \sqrt{2\alpha \cdot u_x(t)\Delta t} \quad (2.34)$$

where $u_x(t)$ denotes the velocity and $D_{yy}(t)$ the component of the dispersion tensor in y -direction at the actual position of the particle $x_p(t)$, $y_p(t)$. Using Stratonovich’s interpretation of a stochastic integral, the equations for the two-layer system can be written as

$$x_p(t + \Delta t) = x_p(t) + u_x(t^*)\Delta t + \xi_x \sqrt{2\alpha \cdot u_x(t^*)\Delta t} \quad (2.35)$$

$$y_p(t + \Delta t) = y_p(t) + \frac{1}{2} B_{yy}(t^*) \frac{\partial B_{yy}(t^*)}{\partial y} \Delta t + \xi_y \sqrt{2\alpha \cdot u_x(t^*)\Delta t} \quad (2.36)$$

where $u_x(t^*)$ and $B_{yy}(t^*)$ denote the velocity and the component of the displacement matrix in y -direction at the position $x_p(t + \Delta t/2)$, $y_p(t + \Delta t/2)$ of the particle. The partial derivatives in Eqs. (2.34) and (2.36) represent the gradient of \mathbf{D} and \mathbf{B} with respect to the y -direction resulting from the bilinear interpolation as outlined in Section 2.3.1. Given the two-layer case presented here, the gradient of the dispersion tensor and the displacement matrix, respectively, in x -direction are zero and hence these terms are not included.

When applying the reflection method, the expression for the random walk particle transport is given as

$$x_p(t + \Delta t) = x_p(t) + u_x(t)\Delta t + \xi_x \sqrt{2\alpha \cdot u_x(t)\Delta t} \quad (2.37)$$

$$y_p(t + \Delta t) = y_p(t) + \xi_y \sqrt{2\alpha \cdot u_x(t)\Delta t} \quad (2.38)$$

In Eqs. (2.37) and (2.38) the velocity of a particle is not corrected to preserve local solute mass conservation at interfaces with discontinuous dispersive coefficients as in Eqs. (2.33) to (2.36). Instead, a reflection probability for a particle, which wants to move from layer 1 to layer 2 and vice versa, will be calculated using

$$P_{12} = (\sqrt{D_{yy1}})/(\sqrt{D_{yy1}} + \sqrt{D_{yy2}}) \quad (2.39)$$

$$P_{21} = (\sqrt{D_{yy2}})/(\sqrt{D_{yy1}} + \sqrt{D_{yy2}}) \quad (2.40)$$

in order to account for the local solute mass conservation at the interface. Therefore, every time a particle crosses an interface with discontinuous dispersive coefficients during Δt a Bernoulli trial on the appropriate reflection probability is performed, deciding whether a particle is reflected or not.

Finally, using the generalized stochastic differential equations method, first the particle is moved only using dispersion according to

$$Y_x(t) = x_p(t) + \xi_x \sqrt{2\alpha \cdot u_x(t) \Delta t} \quad (2.41)$$

$$Y_y(t) = y_p(t) + \xi_y \sqrt{2\alpha \cdot u_x(t) \Delta t} \quad (2.42)$$

Then, to calculate the final particle movement, the velocities at $x_p(Y_x, Y_y; t)$, $y_p(Y_x, Y_y; t)$ are used to determine the dispersive step as shown in the following equations

$$x_p(t + \Delta t) = x_p(t) + u_x(t) \Delta t + \xi_x \sqrt{2\alpha \cdot u_x(Y_x, Y_y; t) \Delta t} \quad (2.43)$$

$$y_p(t + \Delta t) = y_p(t) + \xi_y \sqrt{2\alpha \cdot u_x(Y_x, Y_y; t) \Delta t} \quad (2.44)$$

Comparison with Analytical Results

In the following simulations several scenarios were analyzed, in which the hydraulic conductivity contrast between the two layers was increased. The effect of this increasing heterogeneity was assessed using long-time first- and second-order spatial moments. The analytical solution for the apparent average velocity can be written as the arithmetic mean of the two-layer velocities (Marle et al., 1967)

$$U(t \rightarrow \infty) = \frac{u_{x1} + u_{x2}}{2} \quad (2.45)$$

The analytical solution for the macrodispersion is somewhat more complicated. Marle et al. (1967) presented a general solution for a stratified aquifer at large travel times, which can be rewritten for the case presented above as

$$D_L(t \rightarrow \infty) = \frac{D_{xx1} + D_{xx2}}{2} + \frac{\Delta y^2}{24} \left(\frac{1}{D_{yy1}} + \frac{1}{D_{yy2}} \right) (u_{x1} - u_{x2})^2 \quad (2.46)$$

where $D_{xx1} = \alpha u_{x1}$, $D_{xx2} = \alpha u_{x2}$, $D_{yy1} = \alpha u_{x1}$, and $D_{yy2} = \alpha u_{x2}$.

In the following section results are additionally compared with the standard MT3DMS model (Zheng and Wang, 1999) using the TVD scheme.

Results

Fig. 2.5 shows the analytical values calculated using Eq. (2.45) and the apparent average velocity obtained from the different random walk approaches and the TVD scheme with increasing hydraulic conductivity contrast between

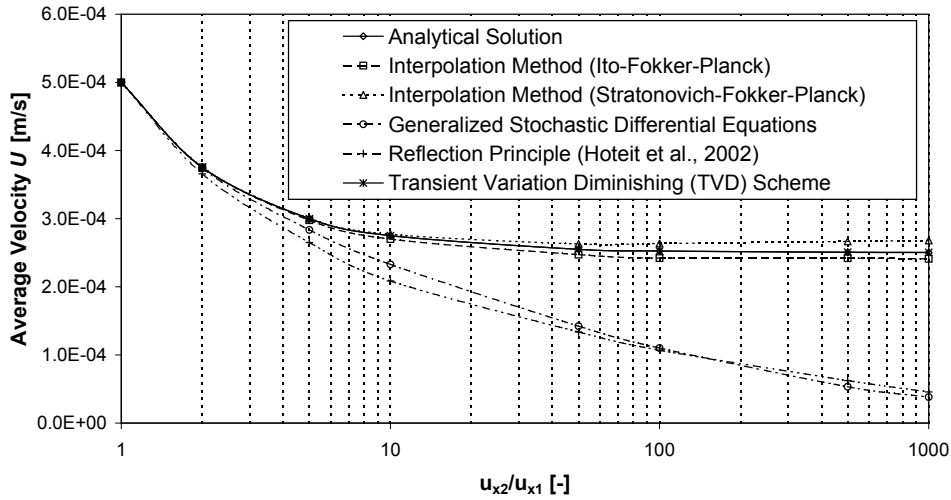


Figure 2.5. Behavior of the average velocity with increasing heterogeneity. (u_{x2} is kept constant and u_{x1} is decreased)

the two layers. As can be observed, the interpolation method for both, the Itô and the Stratonovich interpretation of a stochastic integral, and the TVD scheme are able to reproduce the correct apparent average velocity, even for high hydraulic conductivity contrasts between the two layers. The Generalized Stochastic Differential Equations (GSDE) approach shows an increasingly lower apparent average velocity for contrasts higher than five, whereas the reflection method reproduces an even lower apparent average velocity starting from a hydraulic conductivity contrast of two.

Fig. 2.6 represents the evolution of the late-time longitudinal macrodispersion with increasing velocity differences between the two layers. The TVD scheme and both interpolation methods demonstrate similar behavior, failing to reproduce the analytical macrodispersion for velocity contrasts larger than five between the two layers. On the contrary, the reflection method and the GSDE method represent the macrodispersion fairly good even at high velocity differences up to a contrast of approximately 50. One should note that we have chosen for the two-layer case a vertical discretization that coincides with the width of the layers, for the purpose of a simple example on the effects of a discontinuous dispersion coefficient using the different numerical random walk approaches. Thus, when using a higher vertical discretization, the TVD scheme would correctly approximate the analytical solution.

In order to understand the behavior shown in Figs. 2.5 and 2.6 of the different methods better, we will look at the movement of the centre of mass in the y -direction with respect to time. Gueven et al. (1984) proved that in a

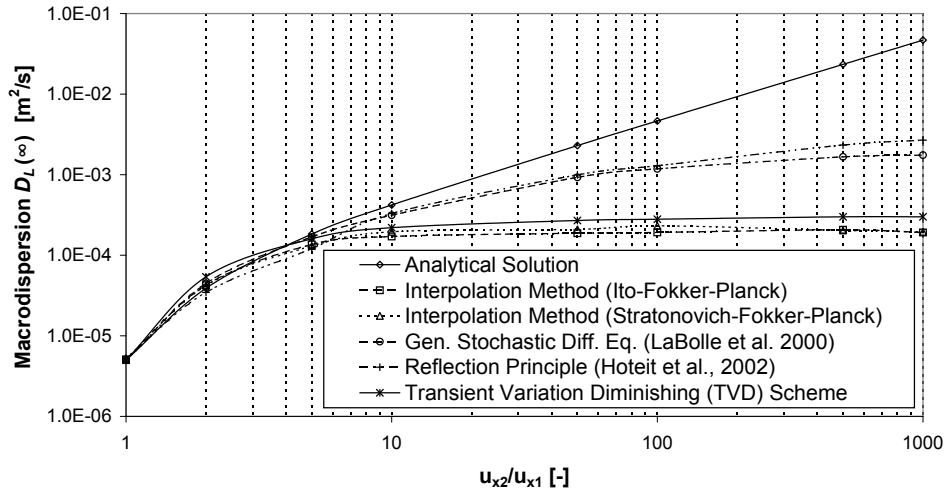


Figure 2.6. Behavior of the longitudinal macrodispersion with increasing heterogeneity. (u_{x2} is kept constant and u_{x1} is decreased)

layered aquifer system with conditions given as described above the mass in a layer is constant with respect to time. Hence, the centre of mass with respect to the y -direction $Y_G(t)$ should always be located at the interface of the two equally thick layers in our system.

The behavior of the centre of mass with respect to the y -axis for the different methods is presented in Figs. 2.7, 2.8, 2.9, and 2.10. The interpolation method for both, the Itô and the Stratonovich interpretation, shows an excellent behavior with respect to conserving the centre of mass at the interface even for strong velocity contrasts. Further, the average velocity of the particle cloud agrees well with the analytical solution, corroborating that particle transfer between layers is accurately captured. Yet due to the increased smoothing of the dispersion tensor introduced by the bilinear interpolation, macrodispersive behavior is not simulated correctly for strong velocity contrasts.

The other two methods display an increasing shift of the centre of mass into the low velocity layer with increasing velocity differences, as they are missing the gradient term forcing the particles into the high velocity layer and it seems that neither the reflection of particles nor the evaluation of the particle’s velocity shifted by a dispersive step, as used in the GSDE method, are able to compensate for the missing drift term. Furthermore, both of these methods result in an average velocity much lower than in the interpolation method, but a better representation of the macrodispersion. This behavior is generated by the artificial transfer of particles into the low conductivity

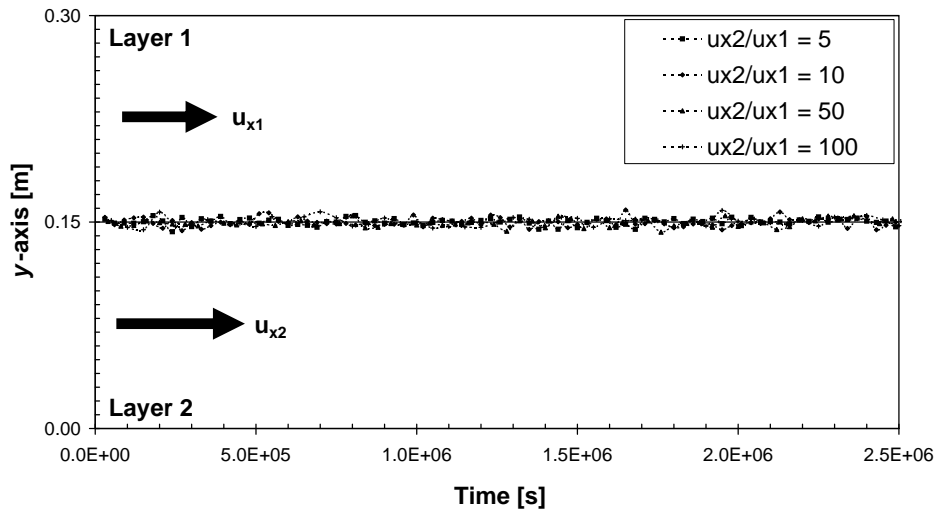


Figure 2.7. Location of the centre of mass with respect to the y -axis using the interpolation method in combination with Itô’s interpretation of a stochastic integral. ($u_{x2} > u_{x1}$)

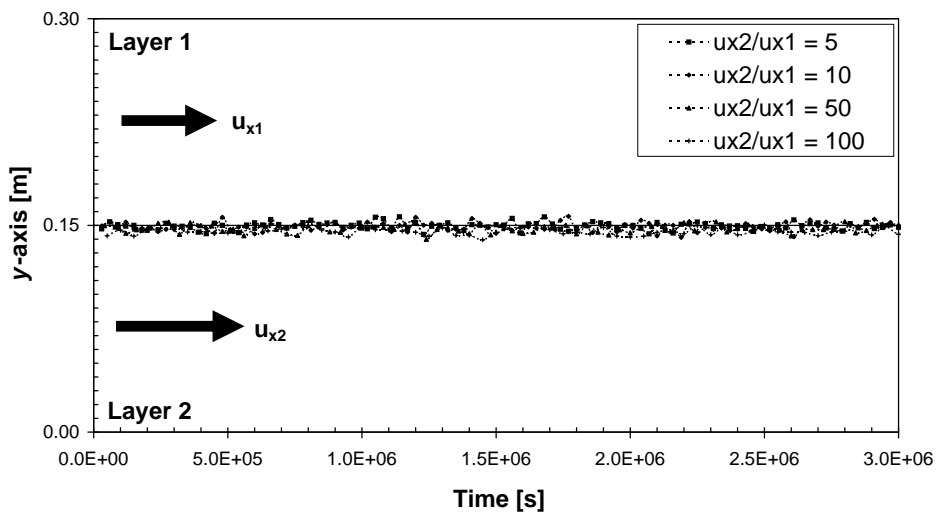


Figure 2.8. Location of the centre of mass with respect to the y -axis using the interpolation method in combination with Stratonovich’s interpretation of a stochastic integral. ($u_{x2} > u_{x1}$)

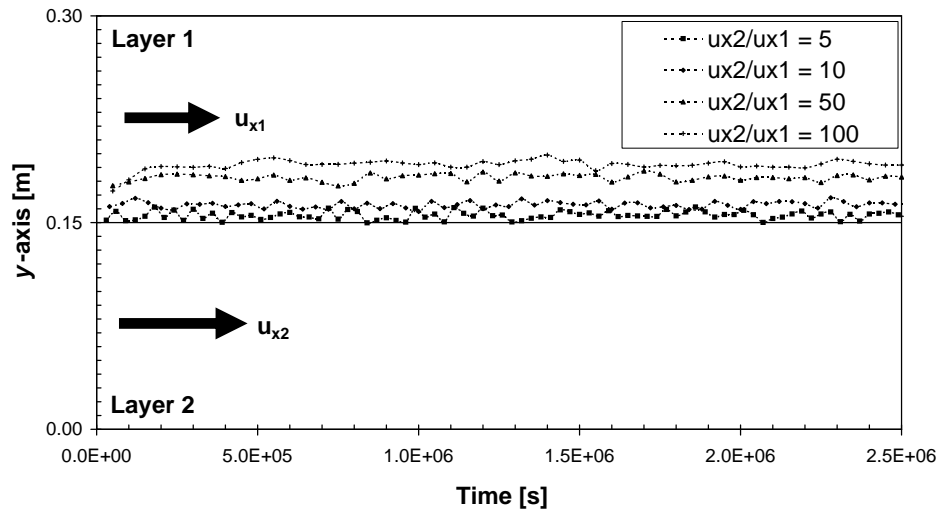


Figure 2.9. Location of the centre of mass with respect to the y -axis using the generalized stochastic differential equations approach. ($u_{x2} > u_{x1}$)

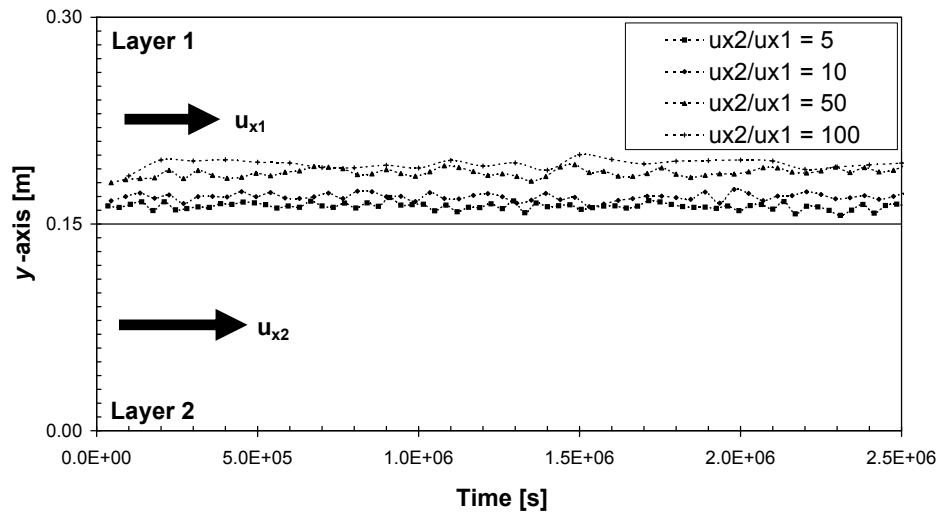


Figure 2.10. Location of the centre of mass with respect to the y -axis using the reflection method. ($u_{x2} > u_{x1}$)

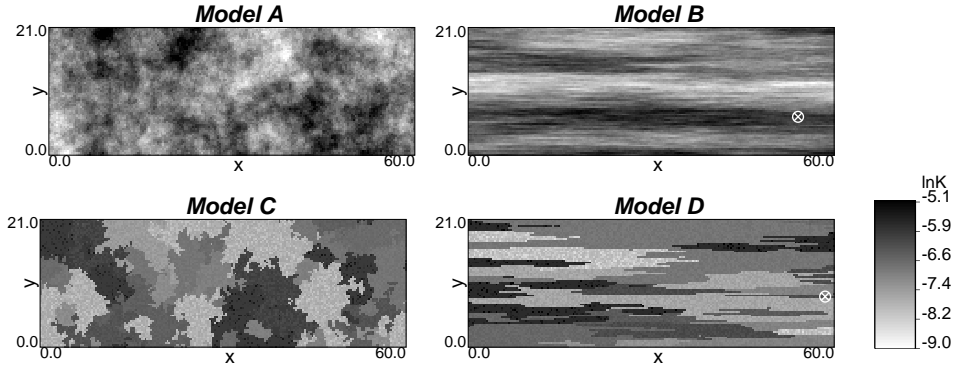


Figure 2.11. The four models generated using Sequential Gaussian and Indicator Simulation with different spatial correlation. Circles in Models B and D denote observation well locations.

layer, and thus, the underlying physical processes are not well reproduced and ultimately will lead to an erroneous mass distribution.

2.5.2 Solute Transport in a Heterogeneous Aquifer

Problem Description

Four reference hydraulic conductivity fields were stochastically generated using different random function models, denoted as A, B, C, and D (Fig. 2.11). All of the reference fields have the same mean $\ln K$ value of -6.908 and variance $\sigma_{\ln K}^2 = 0.5$. In order to simulate increasing heterogeneity the $\ln K$ variance of these fields was increased to values of 2, 3, and 4 by scaling the reference realization. All the reference fields have a spatial discretization of $\Delta x = \Delta y = 0.3$ m and a total length and width of 60 m and 21 m respectively. Reference $\ln K$ fields associated with models A and B were simulated by choosing a realization from a Sequential Gaussian Simulation (GCOSIM3D; Gómez-Hernández and Journel, 1993). Model A is characterized by an isotropic spatial correlation with a correlation length of $\lambda_x = \lambda_y = 1.2$ m and can be described by the following standardized exponential semivariogram

$$\frac{\gamma(h)}{\sigma_{\ln K}^2} = 1 - \exp\left(\frac{-h}{1.2}\right) \quad (2.47)$$

Model B shows a strong anisotropic spatial correlation parallel to the x -axis and was simulated using the following standardized semivariogram, where the anisotropy axes are aligned with the principal coordinate axes and the correlation length in x is $\lambda_x = 20.0$ m and in y is $\lambda_y = 1.2$ m.

Threshold z_k	$F(z_k)$	$F(z_k)[1 - F(z_k)]$	λ_x		λ_y	
			Model C	Model D	Model C	Model D
-8.195	0.1	0.09	1.2	1.2	1.2	60.0
-7.758	0.2	0.16	1.2	1.2	1.2	60.0
-7.44	0.3	0.21	1.2	1.2	1.2	60.0
-7.165	0.4	0.24	1.2	1.2	1.2	60.0
-6.9137	0.5	0.25	1.2	1.2	1.2	60.0
-6.66	0.6	0.24	1.2	1.2	1.2	60.0
-6.386	0.7	0.21	1.2	1.2	1.2	60.0
-6.07	0.8	0.16	1.2	1.2	1.2	60.0
-5.633	0.9	0.09	1.2	1.2	1.2	60.0

Table 2.2. Parameters for the random function models C and D (where z_k corresponds to the 9 decile cutoffs of the marginal cumulative distribution function $F(z_k)$)

$$\frac{\gamma(h_x, h_y)}{\sigma_{\ln K}^2} = 1 - \exp \left(-\sqrt{\left(\frac{h_x}{20.0}\right)^2 + \left(\frac{h_y}{1.2}\right)^2} \right) \quad (2.48)$$

The reference hydraulic conductivity fields associated with models C and D were generated by choosing a realization from a Sequential Indicator Simulation (ISIM3D; Gómez-Hernández and Srivastava, 1990). A mosaic model was used for the corresponding random function as the nine thresholds have all the same standardized exponential semivariogram (Eq.(2.48)). Both of the models have, as with models A and B, a different spatial correlation. The parameters for the indicator variograms used in model C and D are summarized in Table 2.2.

There are two main reasons for choosing these four reference fields. Firstly, the strong anisotropic spatial correlation was chosen in order to study the effects of artificial mass shift into low conductivity zones caused by an incorrect numerical approximation of discontinuous dispersion coefficients as shown in Section 2.5.1. It is expected, especially for the reference fields with a strong variance, that the GSDE approach shows a lower average velocity but a better macrodispersion than the interpolation technique. Secondly, heterogeneous hydraulic conductivity fields generated by Gaussian simulation techniques usually show a smooth transition from high conductivity values to low conductivity values, and vice versa, based on the characteristics of the Gaussian random function (Gómez-Hernández and Wen, 1998). This spatial smoothing will diminish the significance of a correct implementation of the local solute mass balance condition. However, in aquifers formed by alluvial deposits for

example, abrupt changes between different facies with a strong hydraulic conductivity contrast can occur (Heinz et al., 2003). Contrasts between high and low conductivity values in these fields are generally stronger and it is expected that differences in solute transport behavior for the different RWPT approaches will become even more apparent, as a correct implementation of the conservation of the local solute mass balance is more important in these systems. It should be noted that in the following study the reflection principle was not included, as the approach demonstrated a similar behavior as the GSDE approach for the two-layer case and because the correct implementation into a three-dimensional transport model is rather complex as particles can be reflected from different cell interfaces during one time step.

The TVD scheme was, again, used for comparison with the RWPT method. To prevent numerical dispersion and artificial oscillations, the hydraulic conductivity fields were refined to a cell size of $\Delta x = \Delta y = 0.1$ m. Flow and transport was then solved for both, the TVD scheme and the RWPT method, on the refined grid. Although the TVD scheme has proven to be essentially oscillation-free and without excessive numerical dispersion, the reference field for model D (for $\sigma_{lnK}^2 = 2$) was further refined to decrease the Peclet number from 10 to a value of 7.5. The results were compared with the coarser discretized model and neither artificial oscillations nor numerical dispersion were observed for this case.

The aquifer was assumed to be confined and with constant-head boundaries at $x = 0$ m and $x = 60$ m, a head gradient of 0.0833, and with no-flow boundaries at $y = 0$ m and $y = 21$ m. Particles were distributed uniformly on a line transverse to the main flow direction. The source is located 0.45 m away from the constant-head boundary on the left-hand side and 2.25 m from either side of the no-flow boundaries which leaves a total width of the source of 16.5 m. A total number of 2000 particles, a homogeneous porosity of $\Theta = 0.2$, and an isotropic pore-scale dispersion of $\alpha = 0.01$ m was used in all simulations.

Results

In the following figures mass flux breakthrough curves, apparent average velocities, and apparent longitudinal macrodispersivities are used to compare the different numerical approaches to overcome the problem of discontinuous material properties in the RWPT method. Figs. 2.12 and 2.13 present the results for models A and B generated using Sequential Gaussian Simulation, where λ corresponds to $\lambda = 1.2$ m for models A and C and $\lambda = 20$ m for models B and D, respectively. It can be observed that, even for extreme heterogeneities ($\sigma_{lnK}^2 = 4$) and anisotropic spatial correlation, all the approaches produce a similar plume behavior, indicating that all the different numerical implementation methods perform well in aquifers, where a gradual transition

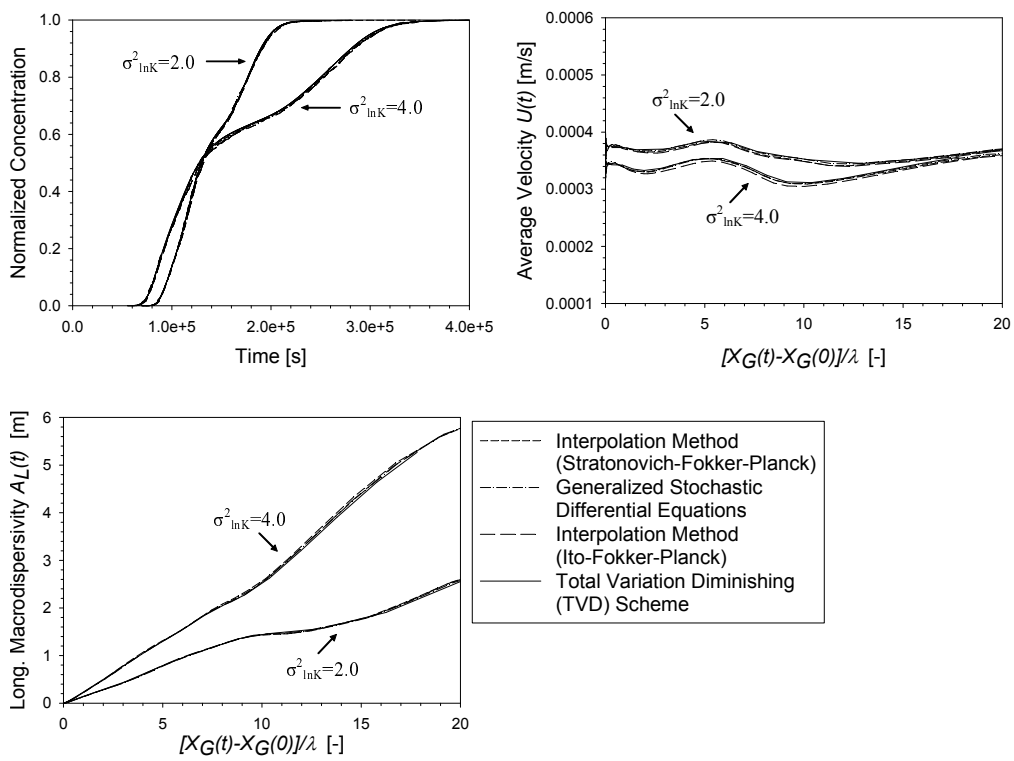


Figure 2.12. Normalized mass flux breakthrough curve, average velocity, and longitudinal macrodispersivity using Model A with $\sigma^2_{inK} = 2.0$ and $\sigma^2_{inK} = 4.0$

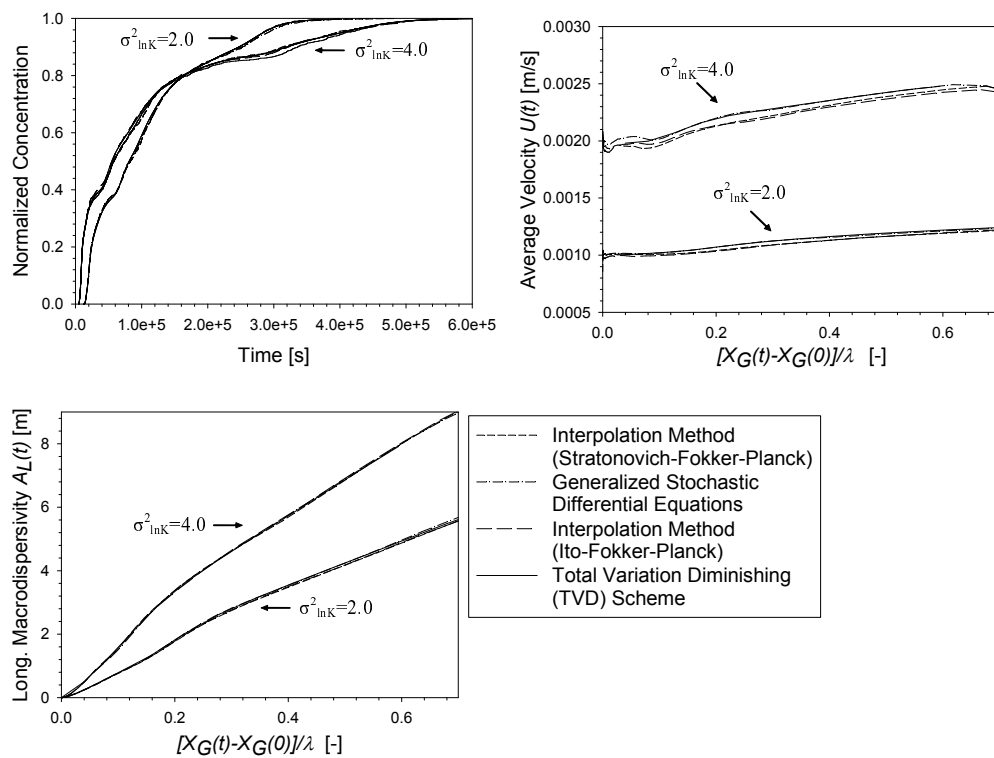


Figure 2.13. Normalized mass flux breakthrough curve, average velocity, and longitudinal macrodispersivity using Model B with $\sigma_{inK}^2 = 2.0$ and $\sigma_{inK}^2 = 4.0$

between high and low conductivity zones exist, despite the strong anisotropic geometry of the aquifer. Similar observations are made for model C generated using Sequential Indicator Simulation (Fig. 2.14). Although contrasts between the different conductivity zones are more abrupt, all of the methods were able to reproduce the correct plume behavior. Only for model D, with a variance of $\sigma_{\ln K}^2 = 2.0$ or higher, a difference in the average velocity between the various approaches is noticeable (Figs. 2.15 and 2.16). For this case only the interpolation method using Itô's or Stratonovich's interpretation of a stochastic integral is able to reproduce the correct apparent average velocity, whereas the GSDE method tends to underestimate the velocity. This observation coincides with the results achieved in the two-layer stratified case. Furthermore, macrodispersivity in Model D, with a variance of $\sigma_{\ln K}^2 = 2.0$ or higher, is overestimated by the GSDE approach. This is caused by an artificial transfer of particles into lower hydraulic conductivity regions already observable in the two-layer scenario. Hence, this artificial mass shift occurring at strong $\ln K$ variances for the GSDE method results in an overall plume retardation, lower peak concentrations, and an increased tailing of the contaminant breakthrough curves.

Fig. 2.17 presents the breakthrough curves obtained in two observation wells located in high-conductivity channels in model B and model D as depicted in Fig. 2.11. The models are characterized by a natural log hydraulic conductivity variance of $\sigma_{\ln K}^2 = 3.0$ and the observation wells have a diameter of 0.4 m. In order to recover a representative number of particles in a well and to obtain smoother breakthrough curves, particle numbers for these simulations have been increased to 50000. Fig. 2.17 illustrates that all approaches produce similar outputs for the Gaussian random function, as expected. When looking at the breakthrough curves in model D it can be observed that, although early particle arrival times agree for all three approaches, the total number of particles arriving at the well is significantly lower when using the GSDE method, since particles are artificially moved to lower $\ln K$ regions. As in real world situations solute mass arrival is measured usually in observation wells and is then compared with numerical simulations, employing the GSDE method can result in a possible underestimation of contaminant breakthrough curves.

In order to examine the performance of the RWPT methods for the case where pore-scale dispersion has a stronger impact on solute transport, the pore-scale dispersion was increased to a value of $\alpha = 0.05$ m. Fig. 2.18 depicts the results for these cases. Although the apparent plume average velocity in model B with a variance of $\sigma_{\ln K}^2 = 4.0$ is slightly underestimated for the GSDE approach, the overall plume behavior agrees well with the results obtained using the TVD scheme. However, Model D presents a lower apparent average velocity for a variance higher than $\sigma_{\ln K}^2 = 2.0$ using the GSDE tech-

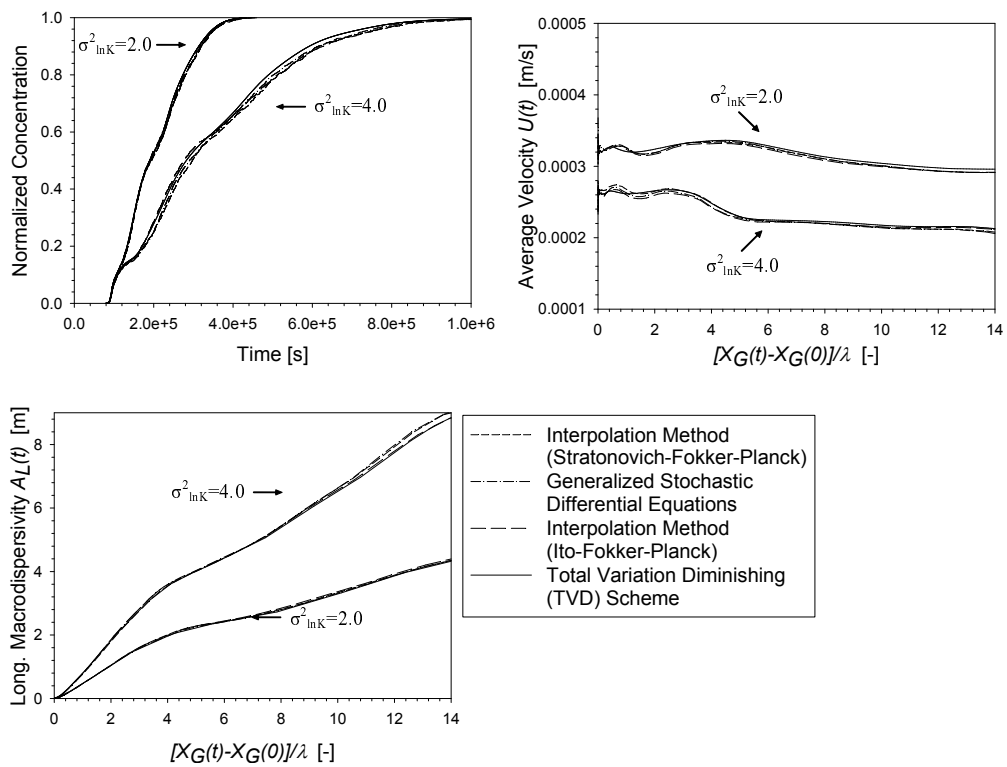


Figure 2.14. Normalized mass flux breakthrough curve, average velocity, and longitudinal macrodispersivity using Model C with $\sigma_{\ln K}^2 = 2.0$ and $\sigma_{\ln K}^2 = 4.0$

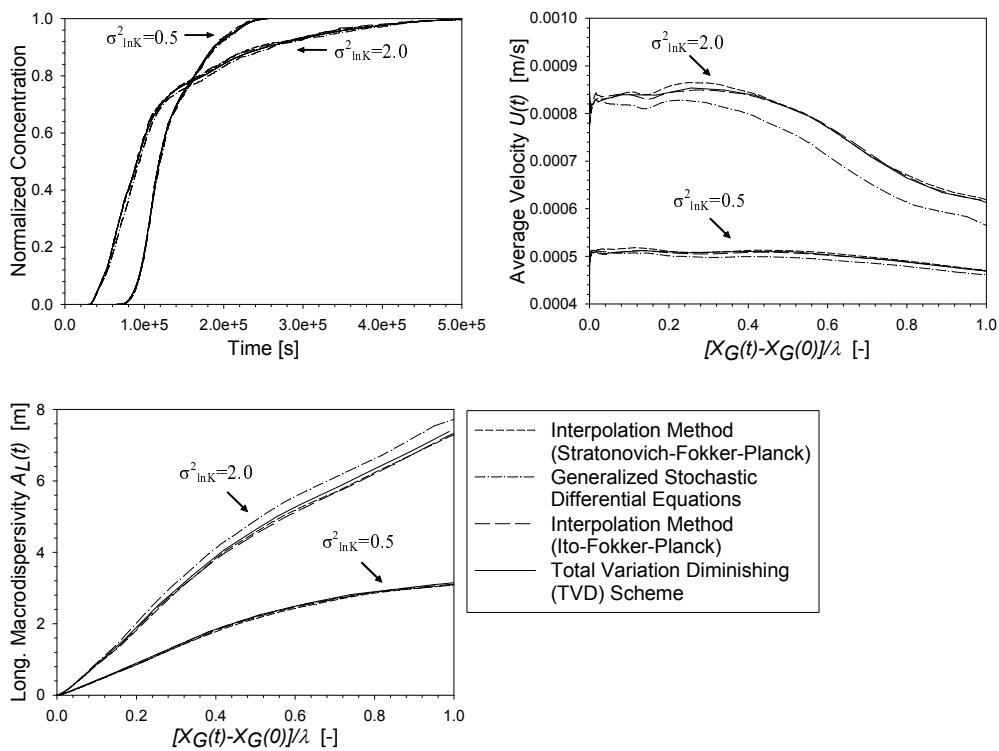


Figure 2.15. Normalized mass flux breakthrough curve, average velocity, and longitudinal macrodispersivity using Model D with $\sigma_{\ln K}^2 = 0.5$ and $\sigma_{\ln K}^2 = 2.0$

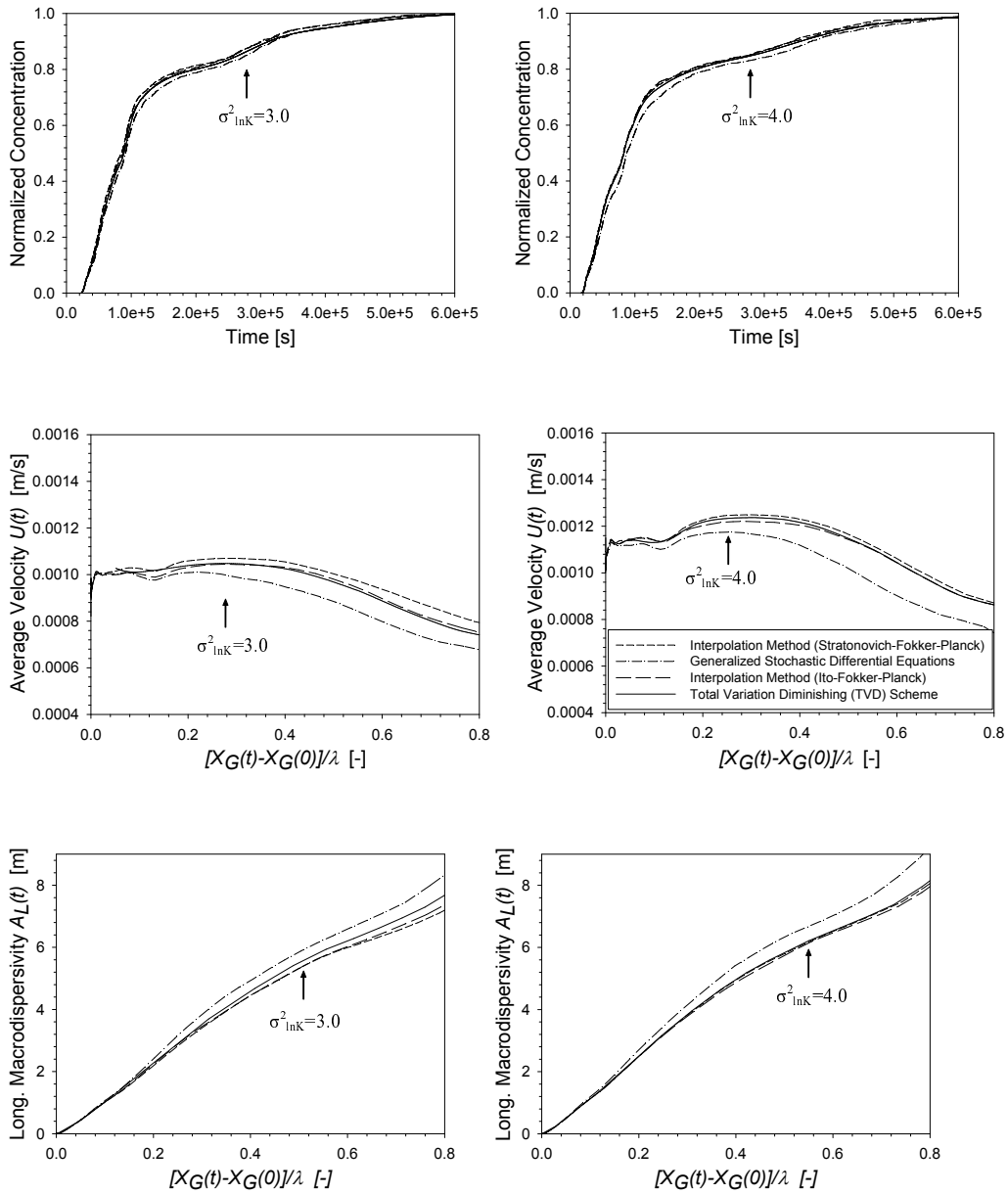


Figure 2.16. Normalized mass flux breakthrough curve, average velocity, and longitudinal macrodispersivity using Model D with $\sigma_{inK}^2 = 3.0$ and $\sigma_{inK}^2 = 4.0$

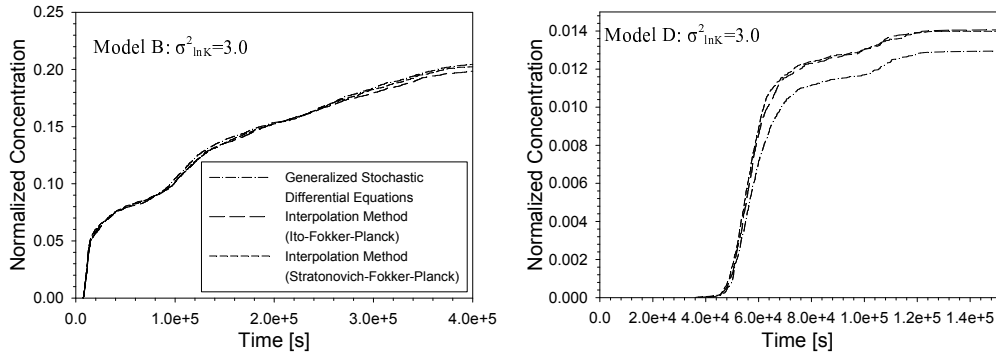


Figure 2.17. Breakthrough curves for an observation well in Model B with $\sigma_{lnK}^2 = 3.0$ and in Model D with $\sigma_{lnK}^2 = 3.0$

nique and the interpolation method in combination with the Itô-Fokker-Planck equation. The interpolation method in combination with the Stratonovich-Fokker-Planck equation seems to represent the best approach for the average velocity for the case of a variance $\sigma_{lnK}^2 = 2.0$ and higher. Macrodispersivity is represented well by the interpolation method, and is overestimated by the GSDE method. Increasing pore-scale dispersion results in a stronger artificial mass shift for the GSDE method and therefore overestimation of macrodispersivity and underestimation of the apparent average velocity of the plume is emphasized.

2.6 Conclusions

We have presented the fundamental concepts of the RWPT method and its advantages and limitations. The different numerical approaches for the random walk methodology to conserve local solute mass balance at interfaces with discontinuous properties were reviewed and evaluated numerically using synthetic test cases. Solute transport in a two-layer stratified aquifer demonstrated that both of the interpolation methods, using Itô’s or Stratonovich’s interpretation of a stochastic integral, are able to reproduce the apparent average velocity even for high hydraulic conductivity contrasts. The reflection principle and the GSDE method underestimate the apparent average velocity at conductivity contrasts between the two layers of higher than five and two, respectively. Macrodispersion is represented insufficiently by both of the interpolation methods at contrasts higher than five between the two layers, whereas the GSDE and the reflection method reproduce macrodispersion fairly well up to velocity contrasts of 50. The different behavior of the RWPT approaches is based on an artificial shift of mass for increasing heterogeneities for the GSDE

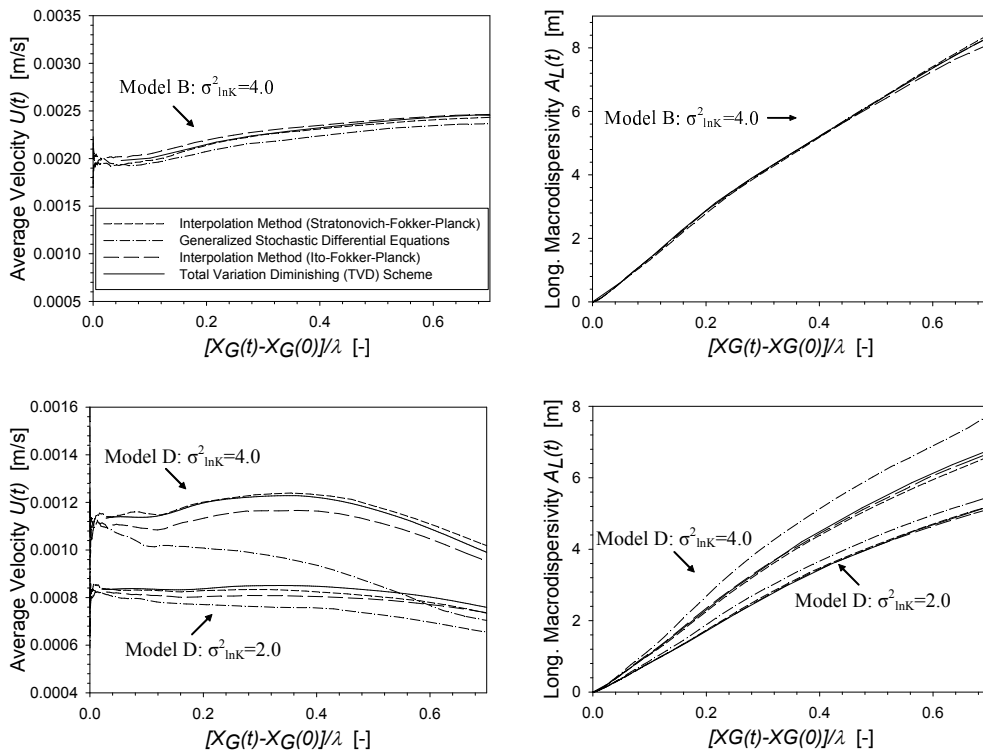


Figure 2.18. Average velocity and longitudinal macrodispersivity using a local-scale dispersion of $\alpha = 0.05m$ with Model B for $\sigma_{lnK}^2 = 4.0$ and with Model D for $\sigma_{lnK}^2 = 2.0$ and $\sigma_{lnK}^2 = 4.0$

and the reflection approach, whereas the interpolation method suffers from the smoothing of the dispersion tensor introduced by bilinear interpolation.

However, the experiments with heterogeneous hydraulic conductivity fields created by sequential Gaussian simulation did not demonstrate any differences for the various approaches, even for highly heterogeneous aquifers with a strong anisotropic spatial correlation and a large pore-scale dispersivity value. This indicates that, when the transition between zones with high and low hydraulic conductivities is relatively gradual, as occurs in Gaussian random function models, differences in the implementation approaches for the conservation of local solute mass balance are not significant.

In fields generated by sequential indicator simulation, only for the case of a strong anisotropic spatial geometry of the aquifer and variances of $\sigma_{lnK}^2 = 2.0$ or higher, a discrepancy in the first-order moment was observed for the different approaches. For these cases only the interpolation method, using Itô's or Stratonovich's interpretation of a stochastic integral, demonstrated a good representation of the apparent average velocity and macrodispersion of the plume. Apparent average velocity is underestimated and longitudinal macrodispersivity is overestimated by the GSDE approach for these cases. Various authors (LaBolle et al., 1996, 1998; Ackerer and Mosé, 2000; LaBolle et al., 2000) demonstrated that the interpolation technique, the reflection principle, and the GSDE method are all able to simulate correctly diffusive processes in discontinuous media with no advection. Nevertheless, advective and dispersive solute transport for highly heterogeneous cases with abrupt transitions between different hydrogeological units and strong anisotropic spatial correlation seems to be represented better using the interpolation method.

Concerning the numerical implementation, the interpolation method in combination with the Itô-Fokker-Planck equation is the easiest method. While the Stratonovich-Fokker-Planck equation requires the implementation of an iterative procedure, the GSDE method becomes especially complex for the case when pore-scale dispersion is anisotropic and porosity is heterogeneous. The reflection principle turns out to be difficult to implement for general three-dimensional problems, where particles can be reflected by various interfaces within one time step as was already mentioned by LaBolle et al. (1996).

Bibliography

- Abulaban, A., Nieber, J.L., Misra, D., 1998. Modelling plume behaviour for nonlinearly sorbing solutes in saturated homogeneous porous media. *Advances in Water Resources*, 21(6), 487-498.
- Abulaban, A., Nieber, J.L., 2000. Modelling the effects of nonlinear equilibrium sorption on the transport of solute plumes in saturated heterogeneous porous media. *Advances in Water Resources*, 23(8), 893-905.
- Ackerer, Ph., 1987. Random-Walk Method to Simulate Pollutant Transport in Alluvial Aquifers or Fractured Rocks. *Advances in Analytical and Numerical Groundwater Flow and Quality Modelling*, Editor: E. Custodio et al., NATO ASI Series C Vol. 224, 475-486.
- Ackerer, P., Mosé, R., 2000. Comment on “Diffusion theory for transport in porous media: Transition-probability densities of diffusion processes corresponding to advection-dispersion equations” by Eric M. LaBolle et al. *Water Resources Research*, 36(3), 819-821.
- Ahlstrom, S.W., Foote, H.P., Arnett, R.C., Cole, C.R., Serne, R.J., 1977. Multi-component mass transport model: theory and numerical implementation (discrete parcel random walk version). Rep. BNWL-2127, Battelle Pacific Northwest Lab., Richland, Washington.
- Andričević, R., Foufoula-Georgiu, E., 1991. Modelling kinetic non-equilibrium using the first two moments of residence time distribution. *Stochastic Hydrol. Hydraul.*, 5, 155-171.
- Aris, R., 1956. On the dispersion of a solute in a fluid flowing through a tube. *Proc. R. Soc. London, Ser. A*, 235, 67-78.
- Bagtzoglou, A., Tompson, A.F.B., Dougherty, D.E., 1992. Projection functions for particle grid methods. *Numer. Methods Partial Differential Equations*, 8, 325-340.
- Berkowitz, B., Scher, H., Silliman, S.E., 2000. Anomalous transport in laboratory-scale, heterogeneous porous media. *Water Resources Research*, 36(1), 149-158.

- Burnett, R.D., Frind, E.O., 1987. Simulation of contaminant transport in three dimensions: 2. Dimensionality effects. *Water Resources Research*, 23(4), 695-705.
- Carslaw, H.S., Jaeger, J.C., 1959. *Conduction of Heat in Solids*. Clarendon, Oxford, 363-365.
- Cordes, C.H.D., Rouvé, G., 1991. A new very efficient algorithm for particle tracking in layered aquifers. *Computer Methods in Water Resources II*, Vol. 1, Groundwater Modelling and Pressure Flow, Editor: D.B. Sari et al., Springer Verlag, New York, 41-55.
- De Josselin de Jong, G., 1958. Longitudinal and transverse diffusion in granular deposits. *Trans. Am. Geophys. Union* 39, 67-74.
- Feehley, C.E., Zheng, C., Molz, F.J., 2000. A dual-domain mass transfer approach for modelling solute transport in heterogeneous aquifers: Application to the Macrodispersion Experiment (MADE) site. *Water Resources Research*, 36(9), 2501-2515.
- Feller, W., 1957. *An introduction to probability theory and its applications*. JohnWiley, New York.
- Fernández-García, D., Illangasekare, T.H., Rajaram, H., 2005a. Differences in the scale dependence of dispersivity and retardation factors estimated from forced-gradient and uniform flow tracer tests in three-dimensional physically and chemically heterogeneous porous media. *Water Resources Research*, 41(3), doi: 10.1029/2004WR003523.
- Fernández-García, D., Illangasekare, T.H., Rajaram, H., 2005b. Differences in the scale dependence of dispersivity estimated from temporal and spatial moments in chemically and physically heterogeneous porous media. *Advances in Water Resources*, 28(7), 745-759.
- Freyberg, D.L., 1986. A natural gradient experiment on solute transport in a sand aquifer. 2. Spatial moments and the advection and dispersion of nonreactive tracers. *Water Resources Research*, 22(13), 2031-2046.
- Frind, E.O., Muhammad, D.S., Molson, J.W., 2002. Delineation of three-dimensional well capture zones for complex multi-aquifer systems. *Ground Water*, 40(6), 586-598.
- Garabedian, S.P., LeBlanc, D.R., Gelhar, L.W., Celia, M.A., 1991. Large-scale natural gradient tracer test in sand and gravel, Cape Cod, Massachusetts. 2. Analysis of spatial moments for a nonreactive tracer. *Water Resources Research*, 27(5), 911-924.

- Gardiner, C.W., 1990. Handbook of Stochastic Methods for Physics, Chemistry, and the Natural Sciences. Springer Verlag, New York.
- Gómez-Hernández, J.J., Srivastava, R.M., 1990. ISIM3D: An ANSI-C three dimensional multiple indicator conditional simulation program. *Computer and Geosciences*, 16(4), 395-440.
- Gómez-Hernández, J.J., Journel, A.G., 1993. Joint sequential simulation of multi-Gaussian fields. *Geostatistics Tróia '92*, Editor: A. Soares, Kluwer, Vol. 1, 85-94.
- Gómez-Hernández, J.J., Wen, X.H., 1998. To be or not to be multi-Gaussian? A reflection on stochastic hydrogeology. *Advances in Water Resources*, 21(1), 47-61.
- Gueven, O., Molz, F.J., Melville, J.G., 1984. An analysis of dispersion in a stratified aquifer. *Water Resources Research* 20(10), 1337-1354.
- Hassan, A.E., Mohamed, M.M., 2003. On using particle tracking methods to simulate transport in single-continuum and dual continua porous media. *Journal of Hydrology*, 275(3-4), 242-260.
- Heinz, J., Kleineidam, S., Teutsch, G., Aigner, T., 2003. Heterogeneity patterns of quaternary glaciofluvial gravel bodies (SW-Germany): application to hydrogeology. *Sedimentary Geology*, 158, 1-23.
- Hoteit, H., Mosé, R., Younes, A., Lehmann, F., Ackerer, Ph., 2002. Three-dimensional Modelling of Mass Transfer in Porous Media Using the Mixed Hybrid Finite Elements and the Random Walk Methods. *Mathematical Geology*, 34(4), 435-456.
- Huang, H., Hassan, A.E., Hu, B.X., 2003. Monte Carlo study of conservative transport in heterogeneous dual porosity media. *Journal of Hydrology*, 275, 229-241.
- Huyakorn, P.S., Pinder, G.F., 1983. *Computational Methods in Subsurface Flow*. Academic Press, San Diego, 473 pp.
- Itô, K., 1951. On stochastic differential equations. Vol. 4: Am. Math. Soc., New York, 289-302.
- Kinzelbach, W., 1987. The random walk method in pollutant transport simulation. *Advances in Analytical and Numerical Groundwater Flow and Quality Modelling*, Editor: E. Custodio et al., NATO ASI Series C Vol. 224, 227-246.

- Kunstmann, H., Kinzelbach, W., 2000. Computation of stochastic wellhead protection zones by combining the first-order second moment method and Kolmogorov backward equation analysis. *Journal of Hydrology*, 237(3-4), 127-146.
- LaBolle, E.M., Fogg, G.E., Tompson, A.F.B., 1996. Random-walk simulation of transport in heterogeneous porous media: Local mass-conservation problem and implementation methods. *Water Resources Research*, 32(3), 583-593.
- LaBolle, E.M., Quastel, J., Fogg, G.E., 1998. Diffusion theory for transport in porous media: Transition-probability densities of diffusion processes corresponding to advection-dispersion equations. *Water Resources Research*, 34(7), 1685-1693.
- LaBolle, E.M., Quastel, J., Fogg, G.E., Gravner, J., 2000. Diffusion processes in composite porous media and their numerical integration by random walks: Generalized stochastic differential equations with discontinuous coefficients. *Water Resources Research*, 36(3), 651-662.
- LaBolle, E.M., Fogg, G.E., 2001. Role of molecular diffusion in contaminant migration and recovery in an alluvial aquifer system. *Transport in Porous Media*, 42, 155-179.
- Lichtner, P.C., Kelkar, S., Robinson, B., 2002. New form of dispersion tensor for axisymmetric porous media with implementation in particle tracking. *Water Resources Research*, 38(8), doi:10.1029/2000WR000100.
- Liu, G., Zheng, C., Gorelick, S.M., 2004. Limits of applicability of the advection-dispersion model in aquifers containing connected high-conductivity channels. *Water Resources Research*, 40, W08308, doi:10.1029/2003WR002735.
- Marle, C.P., Simandoux, J.P., Gaulier, C., 1967. Etude du déplacement de fluids miscibles en milieu poreux stratifié. *Rev. Inst. Français Petrol.*, 22(2), 272-294.
- McDonald, M.D., Harbaugh, A.W., 1988. A modular three-dimensional finite-difference flow model. *Techniques of Water Resources Investigations*, U.S. Geological Survey, Book 6.
- Michalak, A.M., Kitanidis, P.K., 2000. Macroscopic behaviour and random-walk particle tracking of kinetically sorbing solutes. *Water Resources Research*, 36(8), 2133-2146.

- Pollock, D.W., 1988. Semianalytical computation of path lines for finite difference models. *Ground Water*, 26(6), 743-750.
- Prickett, Th.A., Naymik, Th.G., Longquist, C.G., 1981. A random walk solute transport model for selected groundwater quality evaluations. *Illinois State Water Survey, Bulletin 65*, 103pp.
- Quinodoz, H.A., Valocchi, A.J., 1993. Stochastic Analysis of the transport of kinetically sorbing solutes in aquifers with randomly heterogeneous hydraulic conductivity. *Water Resources Research*, 29(9), 3227-3240.
- Scheidegger, A.E., 1954. Statistical hydrodynamics in porous media. *J. Geophys. Res.* 66, 3273-3278.
- Semra, K., Ackerer, P., Mosé, R., 1993. Three-dimensional groundwater quality modelling in heterogeneous media. *Water Pollution II: Modelling, Measuring and Prediction, Comput. Mech., Billerica, Massachusetts*, 3-11.
- Stratonovich, R.L., 1966. A new representation for stochastic integrals and equations. *SIAM. J. Control*, (4), 362-371.
- Tompson, A.F.B., Gelhar, L.W., 1990. Numerical simulation of solute transport in three-dimensional, randomly heterogeneous porous media. *Water Resources Research*, 26(10), 2541-2562.
- Tompson, A.F.B., 1993. Numerical Simulation of Chemical Migration in Physically and Chemically Heterogeneous Porous Media. *Water Resources Research*, 29(11), 3709-3726.
- Tompson, A.F.B., Schafer, A.L., Smith, R.W., 1996. Impacts of physical and chemical heterogeneity on cocontaminant transport in a sandy porous medium. *Water Resources Research*, 32(4), 801-818.
- Tompson, A.F.B., Falgout, R.D., Smith, S.G., Bosl, W.J., Ashby, S.F., 1998. Analysis of subsurface contaminant migration and remediation using high performance computing. *Advances in Water Resources*, 22(3), 203-221.
- Uffink, G.J.M., 1985. A random walk method for the simulation of macrodispersion in a stratified aquifer. *Relation of Groundwater Quality and Quantity. IAHS Publ. 146*, 103-114.
- Uffink, G.J.M., 1989. Application of Kolmogorov's backward equation in random walk simulations of groundwater contaminant transport. *Contaminant Transport in Groundwater*, Editors: Kobus, H.E. and Kinzelbach, W. Rotterdam, The Netherlands, A.A. Balkema.

- Uffink, G.J.M., 1990. Analysis of dispersion by the random walk method. Ph.D. thesis, Delft Univ. of Technol., Delft, Netherlands, 143 pp.
- Wen, X.H., Gómez-Hernández, J.J., 1996. The constant-displacement scheme for tracking particles in heterogeneous aquifers. *Ground Water*, 34(1), 135-142.
- Zheng, C., 1994. Analysis of particle tracking errors associated with spatial discretization. *Ground Water*, 32(5), 821-828.
- Zheng, C., Wang, P.P., 1999. MT3DMS, a modular three-dimensional multi-species transport model for simulation of advection, dispersion, and chemical reactions of contaminants in groundwater systems. Report to the US Army Corps of Engineers, Washington, DC.
- Zinn, B., Harvey, C.F., 2003. When good statistical models of aquifer heterogeneity go bad: A comparison of flow, dispersion, and mass transfer in connected and multivariate Gaussian hydraulic conductivity fields. *Water Resources Research*, 39(3), 1051, doi:10.1029/2001WR001146.

3

Modeling Mass Transfer Processes Using Random Walk Particle Tracking

Water Resources Research, in press.

Abstract

The complexity of mass transfer processes often complicate solute transport simulations. We present a new approach for the implementation of the multirate mass transfer model into random walk particle tracking. This novel method allows for a spatially heterogeneous distribution of mass transfer coefficients as well as hydrodynamic parameters in three dimensions, and it is well suited for avoiding numerical dispersion and solving computationally demanding transport simulations. For this purpose the normalized zeroth spatial moments of the multirate transport equations are derived and used as phase transition probabilities. Performing a simple Bernoulli trial on the appropriate phase transition probabilities the particle distribution between the mobile domain and any immobile domain can be determined. The approach is compared satisfactorily to analytical and semi-analytical solutions for one-dimensional, advective-dispersive transport with different types of mass transfer. Aspects of the numerical implementation of this approach are presented and it is demonstrated that two restrictive criteria for the time step size have to be considered. Adjusting time step size for each grid cell based on the cell specific velocity field and mass transfer rate a correct simulation of solute transport is assured,

while at the same time computational efficiency is preserved. Finally, an example is presented evaluating the effect of a heterogeneous intraparticle pore diffusion in a synthetic aquifer. The results demonstrate, that for this specific case the heterogeneous distribution of mass transfer rates has not a significant influence on mean solute transport behavior, but that at low concentration ranges differences between the different mass transfer models become visible.

3.1 Introduction

Mass transfer processes occur in almost all porous media and over various scales ranging from pore diffusion at the grain scale and diffusion into low hydraulic conductivity inclusions at the centimeter to meter scale to matrix diffusion into fractured rocks. The significance and diversity of these processes has been recognized already for a long time (e.g., *van Genuchten and Wierenga*, 1976; *Neretnieks*, 1980) due to its important effect on solute transport observed in laboratory and field studies. More recent experimental findings showed that, for example, the sorption/desorption mechanism is often limited by the diffusive transport within the fluid phase of the intraparticle pores of the sediment grains (e.g., *Ball and Roberts*, 1991; *Pignatello and Xing*, 1996; *Luthy et al.*, 1997; *Rügner et al.*, 1999). Furthermore, various authors (e.g., *Guswa and Freyberg*, 2002; *Zinn and Harvey*, 2003; *Liu et al.*, 2004) have demonstrated, that solute transport through heterogeneous aquifers with connected high-conductivity pathways and/or lenses of low-conductivity material is often better upscaled using an advection-dispersion model including a mass transfer component. This is believed to be the reason, why a successful modeling of the tracer test at the Macrodispersion Experiment (MADE) site using the classical advection-dispersion model and the hydraulic conductivity data obtained in the field has still not been achieved (*Harvey and Gorelick*, 2000; *Feehley et al.*, 2000). In fact, various authors (*Berkowitz and Scher*, 1998; *Schumer et al.*, 2003) demonstrated that a certain form of a multirate mobile/immobile model reproduces the anomalous tracer plume spreading at the MADE site better than a classical single rate mass transfer model. Thus, the proper modeling of these processes for groundwater risk assessment is critical, especially when assessing the persistence of contaminants in aquifers and the long-term performance of remediation technologies.

Unfortunately, mass transfer processes complicate solute transport simulations and therefore many of the studies performed up to now consider only a simple first-order mass transfer model. This is from a mathematical and numerical point of view a very convenient approach. Yet it does not represent correctly the underlying physical process in many cases, which can lead to a misinterpretation of the fitted values (*Young and Ball*, 1995; *Haggerty et al.*,

2004) and therefore lead to noticeable different results when used for prediction. Moreover, mass transfer processes might not be correctly described by using a spatially homogeneous coefficient and only a small number of authors have investigated the effects when mass transfer rates are treated as a spatial random variable (e.g., *Li and Brusseau, 2000; Huang and Hu, 2000; Huang et al., 2003*). Hence, modeling all these different mass transfer processes requires the implementation of a possibly spatially heterogeneous, small-scale physical process into a coarse-scale numerical model without losing computational efficiency, but yet approximating reality which is often being limited by these small-scale diffusion processes.

In order to encompass all these different mass transfer processes within one mathematical model which is still based on the classical advection-dispersion equation, two formulations have been presented in literature. The first approach was introduced by *Carrera et al. (1998)* and consists of using a source-sink term in the advection-dispersion equation to represent the rate of loss or gain of concentration to or from the immobile domain. The source-sink term is expressed as a convolution product of a memory function. Choosing the adequate memory function simple first-order mass transfer, diffusion using a distribution function of mass transfer rates, e.g., gamma or power law distribution, and diffusion into different geometries, e.g., sphere, layer, or cylinder, can be modeled (*Carrera et al., 1998; Haggerty et al., 2000*).

The second approach was presented by *Haggerty and Gorelick (1995)* and is based on the idea of using the conventional first-order mass transfer equation (*Nkedi-Kizza et al., 1984*) but superimposing multiple first-order mass transfer rates to represent various diffusion processes. In fact, by choosing a certain infinite sum of first-order rates the model permits the simulation of diffusion into different geometries. It is interesting to note that the memory function used by *Carrera et al. (1998)*, necessary when using the convolution approach, has also the form of an infinite sum with the same mass transfer rates as required by the multirate approach. The parallelism between these two formulations was already pointed out by *Carrera et al. (1998)*.

Note that similar models trying to capture the anomalous behavior of solute plumes in heterogeneous aquifers caused by mass transfer processes have been developed recently. For example, continuous time random walk models particle transport in a heterogeneous medium as a random walk in space and time (e.g., *Berkowitz and Scher, 1998; Dentz and Berkowitz, 2003; Dentz et al., 2004*) and can be formulated to be generally equivalent to the multirate mass transfer approach of *Haggerty and Gorelick (1995)*. Furthermore, fractal models have also been expanded to include a mobile/immobile domain for the purpose of a better description of anomalous transport (*Schumer et al., 2003*). Although both approaches have proven to be flexible and have been applied successfully to a variety of field studies (e.g., *Berkowitz and Scher, 1998*), we

do not discuss them here in detail as the method presented here is based on the classical advection-dispersion equation as opposed to the continuous time random walk and the fractal models.

Due to the mathematical complexity of the formulations presented by *Haggerty and Gorelick* (1995) and *Carrera et al.* (1998) only a few numerical solutions exist, which do not impose any restrictive assumptions on the spatial variability of advection, dispersion, and mass transfer rates in a three-dimensional numerical model (e.g., *Carrera et al.*, 1998; *Wang et al.*, 2005). In this paper we will present a new numerical method to implement the multirate mass transfer approach into random walk particle tracking. Random walk particle tracking has been used to model solute transport in aquifers for a long time (e.g., *Prickett et al.*, 1981; *Kinzelbach*, 1987). It consists in moving a cloud of particles advectively according to the flow-pathlines and adding a random displacement for each time step to simulate dispersion. Its main advantages, i.e., the non-existence of numerical dispersion, computational efficiency, and local as well as global mass conservation, have turned random walk particle tracking into a valuable tool for inverse modeling, uncertainty assessment, and solute transport in highly discretized, heterogeneous aquifers (e.g., *Tompson*, 1993; *Salamon et al.*, 2006).

Various methods to include simple linear mass transfer into random walk particle tracking have been presented in literature. *Valocchi and Quinodoz* (1989) compared three techniques for modeling kinetic sorption which is mathematically equivalent to first-order mass transfer as pointed out by *Haggerty and Gorelick* (1995): (1) the continuous time step method which simulates the history of phase changes of a particle for each time step; (2) the arbitrary time step method which uses probability density functions to calculate the time spent in the aqueous/sorbed phase of a particle during a time step; (3) the small time step method originally introduced by *Kinzelbach* (1987), which performs a Bernoulli trial using transition probabilities to determine if the particle will be in the aqueous or sorbed phase for the next time step. *Andricevic and Foufoula-Georgiu* (1991) present a method similar to the arbitrary time step method, however using a different approach to calculate the fraction of time a particle spends in a certain phase. *Michalak and Kitanidis* (2000) again review the methods presented by *Valocchi and Quinodoz* (1989) and add the semi-analytical moment method, which performs a Bernoulli trial using phase transition probabilities, obtained by the method of moments to determine the phase of a particle for the next time step. *Huang et al.* (2003) develop a first-order mass transfer model based on the phase transition probabilities of *Valocchi and Quinodoz* (1989). Finally, a method for the diffusion into fractures using particle tracking was presented by *Tsang and Tsang* (2001). They use analytical solutions to calculate the residence time caused by matrix diffusion into homogeneous finite or infinite matrix blocks.

In this work we will present the implementation of the multirate mass transfer approach with the random walk particle tracking method. Section 3.2 first outlines the general mathematical framework for the multirate mass transfer approach and the calculation of the zeroth spatial moment, required to determine the phase transition probabilities. In the following subsections examples for first-order mass transfer, multirate mass transfer, and diffusion into various geometries are given. Section 3.3 outlines some numerical implementation details with respect to the choice of the time step size for particle tracking, the approximation of a matrix exponential using Taylor series, and the truncation of the series for diffusion into different geometries. Section 3.4 illustrates a numerical example for the influence of a heterogeneous distribution of intraparticle pore diffusion on contaminant transport. Finally, Section 3.5 summarizes the main results and conclusions from this paper.

3.2 Mathematical Framework

3.2.1 The Multirate Model

The multirate model describes mass transfer between a mobile domain and any number of immobile domains with varying properties. The advection-dispersion equation for this model can be written as follows (according to *Haggerty and Gorelick, 1995*):

$$\theta_m R_m \frac{\partial c_m}{\partial t} + \sum_{j=1}^N \theta_{im,j} R_{im,j} \frac{\partial c_{im,j}}{\partial t} = \nabla \cdot (\theta_m \mathbf{D} \nabla c_m) - \nabla \cdot (\theta_m \mathbf{v} c_m) \quad (3.1)$$

where $c_m[M/L^3]$ is the aqueous concentration in the mobile domain; $c_{im,j}[M/L^3]$ is the aqueous concentration in the j th immobile domain; $\mathbf{D}[L^2/T]$ is the hydrodynamic dispersion tensor; $\mathbf{v}[L/T]$ is the velocity vector; θ_m and $\theta_{im,j}[-]$ are the porosities of the mobile and the j th immobile domain, respectively; R_m and $R_{im,j}[-]$ are the retardation factors for the mobile and the j th immobile domain, respectively; and $N[-]$ is the number of distinct immobile phases. Here, changes in porosities with time are assumed negligible as typically used in subsurface hydrology. The retardation factors are given as

$$R_m = 1 + \frac{\rho_b K_d f_m}{\theta_m} \quad R_{im,j} = 1 + \frac{\rho_b K_d f_{im,j}}{\theta_{im,j}} \quad (3.2)$$

where $\rho_b[M/L^3]$ is the bulk density of the porous medium; $K_d[L^3/M]$ is the distribution coefficient; and f_m and $f_{im,j}[-]$ are the mass fractions of the sorbed phase in sorption equilibrium with the mobile domain and the j th

immobile domain, respectively. The sum of all f_m and $f_{im,j}$ is 1. The mass transfer equations for the multirate model are given as

$$\frac{\partial c_{im,j}}{\partial t} = \alpha_j(c_m - c_{im,j}) \quad j = 1, 2, \dots, N \quad (3.3)$$

with

$$\alpha_j = \frac{\alpha'_j}{R_{im,j}} \quad (3.4)$$

where $\alpha'_j[T^{-1}]$ is the first-order mass transfer rate associated with the j th immobile zone.

As can be seen from equations (3.1) and (3.3) the model permits not only to use a spatial heterogeneous distribution of mass transfer rates, but also a distribution of various diffusion processes within one grid cell. *Haggerty and Gorelick* (1995) argue that at the grain scale a contaminant may diffuse into stagnant zones of water, intraparticle pores, and larger aggregates of grains and therefore a numerical model should be able to account for these different processes.

3.2.2 Development of Phase Transition Probabilities

The term transition probability has its origin in the context of continuous time Markov chains and denotes the probability that a process presently in state i will be in state j a time t later (e.g., *Ross*, 2003). Using this principle in particle tracking and provided that we know the transition probability function we can determine if a particle is in the mobile phase and thus susceptible to advection and dispersion or in the immobile phase after a time step Δt by simply performing a Bernoulli trial on the appropriate phase transition probability. *Valocchi and Quinodoz* (1989) demonstrated the analogy between the first-order, reversible, linear rate expression for kinetic sorption and a homogeneous, continuous-time, two-state Markov chain and used the corresponding phase transition probability functions to simulate kinetic sorption.

A second idea important for the development of the following method was introduced by *Michalak and Kitanidis* (2000). They state, that when the spatial moments of concentrations are interpreted as those of particles, the normalized zeroth spatial moment, which describes the distribution of mass in the different phases, can be used as a phase transition probability function. Applying this idea, *Michalak and Kitanidis* (2000) obtained the same phase transition probability functions for the kinetic sorption case as *Valocchi and Quinodoz* (1989).

In this section we will outline the derivation of the zeroth spatial moment for the multirate model. The spatial moments are generally calculated in three

dimensions (*Aris*, 1956). For the sake of simplicity we will present them here only in one dimension:

$$\mu_n(t) = \int_{-\infty}^{\infty} x^n \theta_m R_m c_m(x, t) dx \quad (3.5)$$

$$\nu_{n,j}(t) = \int_{-\infty}^{\infty} x^n \theta_{im,j} R_{im,j} c_{im,j}(x, t) dx \quad (3.6)$$

where μ_n and $\nu_{n,j}$ are the n th mobile and immobile phase moments, respectively.

The concentrations for the mobile and immobile phases are now substituted with their Fourier transforms in order to be able to calculate the zeroth moment in the Fourier domain. The following definition of the Fourier transform and its inverse will be used here

$$\tilde{C}(p, t) = \int_{-\infty}^{\infty} c(x, t) e^{-i2\pi p x} dx \quad (3.7)$$

$$c(x, t) = \int_{-\infty}^{\infty} \tilde{C}(p, t) e^{i2\pi p x} dp \quad (3.8)$$

Using equation (3.8) and assuming spatially uniform coefficients within a grid block, equations (3.1) and (3.3) can be rewritten as

$$\theta_m R_m \frac{\partial \tilde{C}_m}{\partial t} + \sum_{j=1}^N \theta_{im,j} R_{im,j} \frac{\partial \tilde{C}_{im,j}}{\partial t} + \theta_m v 2\pi i p \tilde{C}_m + \theta_m D_L 4\pi^2 p^2 \tilde{C}_m = 0 \quad (3.9)$$

$$\frac{\partial \tilde{C}_{im,j}}{\partial t} = \alpha_j (\tilde{C}_m - \tilde{C}_{im,j}) \quad j = 1, 2, \dots, N \quad (3.10)$$

We note that our objective here is to find the mechanism by which the particle is exchanged between the mobile/immobile domain in the random walk method. Thus, according to *Kitanidis* (1994) we view each particle as a very small plume compared to the grid block so that the effects of boundaries are negligible in equation (3.9).

The spatial moments of the concentration in the real domain can be evaluated from the concentration Fourier coefficients (*Goltz and Roberts*, 1987):

$$\mu_n(t) = \frac{\theta_m R_m}{(-2\pi i)^n} \frac{\partial^n \tilde{C}_m}{\partial p^n} \Big|_{p=0} \quad (3.11)$$

$$\nu_{n,j}(t) = \frac{\theta_{im,j} R_{im,j}}{(-2\pi i)^n} \frac{\partial^n \tilde{C}_{im,j}}{\partial p^n} \Big|_{p=0} \quad (3.12)$$

In this work we only require the zeroth moments, hence from equations (3.11) and (3.12) follows

$$\mu_0(t) = \theta_m R_m \tilde{C}_m |_{p=0} \quad (3.13)$$

$$\nu_{0,j}(t) = \theta_{im,j} R_{im,j} \tilde{C}_{im,j} |_{p=0} \quad (3.14)$$

Substituting equations (3.13) and (3.14) into (3.9) and (3.10) and setting $p = 0$ yields

$$\frac{\partial \mu_0}{\partial t} + \sum_{j=1}^N \frac{\partial \nu_{0,j}}{\partial t} = 0 \quad (3.15)$$

$$\frac{\partial \nu_{0,j}}{\partial t} = \alpha_j \beta_j \mu_0 - \alpha_j \nu_{0,j} \quad j = 1, 2, \dots, N \quad (3.16)$$

with

$$\beta_j = \frac{\theta_{im,j} R_{im,j}}{\theta_m R_m} \quad (3.17)$$

where $\beta_j[-]$ is the so called capacity ratio associated with the j th immobile zone. Equations (3.15) and (3.16) represent a system of linear differential equations, which can be written in matrix form as

$$\mathbf{A} \frac{d\mathbf{M}}{dt} = \mathbf{B}\mathbf{M} \quad (3.18)$$

where

$$\mathbf{A} = \begin{pmatrix} 1 & 1 & \dots & 1 \\ 0 & 1 & 0 & 0 \\ \vdots & 0 & \ddots & 0 \\ 0 & \dots & 0 & 1 \end{pmatrix}$$

$$\mathbf{B} = \begin{pmatrix} 0 & 0 & \dots & 0 \\ \alpha_1 \beta_1 & -\alpha_1 & 0 & 0 \\ \vdots & 0 & \ddots & 0 \\ \alpha_N \beta_N & 0 & 0 & -\alpha_N \end{pmatrix}$$

$$\mathbf{M} = \begin{pmatrix} \mu_0 \\ \nu_{0,1} \\ \vdots \\ \nu_{0,N} \end{pmatrix}$$

The general solution to this problem is given by (e.g., *Haggerty and Gorelick, 1995*)

$$\mathbf{M} = \exp[(\mathbf{A}^{-1}\mathbf{B})\Delta t]\mathbf{M}_0 \quad (3.19)$$

where

$$\mathbf{A}^{-1}\mathbf{B} = \begin{pmatrix} -\sum_{j=1}^N \alpha_j \beta_j & \alpha_1 & \cdots & \alpha_N \\ \alpha_1 \beta_1 & -\alpha_1 & 0 & 0 \\ \vdots & 0 & \ddots & 0 \\ \alpha_N \beta_N & 0 & 0 & -\alpha_N \end{pmatrix} \quad (3.20)$$

$\Delta t[T]$ is the time step, and \mathbf{M}_0 is a vector containing the initial distribution of mass in the different phases.

A general solution to the exponential matrix of equation (3.19) and thus to the vector \mathbf{M} containing the zeroth spatial moments for each domain is not easy to find. This is especially the case when a large number of mass transfer rates is modeled and therefore the corresponding matrices are of a high order. The evaluation of the exponential of a matrix has been subject to intensive research over the last decades and in the work by *Moler and van Loan (2003)* a comprehensive overview of the existing approaches is presented. However, computing the whole exponential matrix numerically for every time step and each particle would decrease computational efficiency of the particle tracking significantly. Fortunately, using particle tracking to simulate contaminant transport provides two important advantages: Firstly, we do not always need to compute the entire matrix (i.e., when no phase transition occurs). Secondly, we can use a low order Taylor series to approximate the exponential matrix, as the time steps used in particle tracking are usually small.

The reader should keep in mind that using a polynomial series as shown in the following sections is not the only way to compute the exponential of a matrix. Methods employing the matrix eigenvalues, differential equations, or approximation theory have been proposed in literature. However, in practice computational stability and accuracy indicate that some of the methods are preferable to others but that none are completely satisfactory (*Moler and van Loan, 2003*). We chose the Taylor series method due to the above mentioned advantages and its simplicity regarding the mathematical formulation and the numerical implementation. Other methods might lead to the same results requiring however different stability and accuracy criteria as given in Sections 3.3.2 and 3.3.3.

Simple first-order mass transfer

The simplest case of mass transfer is described by a single first-order rate coefficient. When using the multirate approach this is done by setting $N = 1$. This results in square matrices of second-order in equation (3.18). For this case an analytical solution for the exponential matrix of equation (3.19) can be found

$$\exp[(\mathbf{A}^{-1}\mathbf{B})\Delta t] = \begin{pmatrix} \frac{1+\beta e^{-(1+\beta)\alpha\Delta t}}{1+\beta} & \frac{1-e^{-(1+\beta)\alpha\Delta t}}{1+\beta} \\ \frac{\beta-\beta e^{-(1+\beta)\alpha\Delta t}}{1+\beta} & \frac{\beta+e^{-(1+\beta)\alpha\Delta t}}{1+\beta} \end{pmatrix} \quad (3.21)$$

On the basis of this analytical solution for the zeroth spatial moments the particle phase transition probabilities can be derived easily. Assuming that at the beginning of the time step all the solute mass M is in the mobile domain and setting the solute mass $M = 1$ ($\mu_0(0) = 1$ and $\nu_0(0) = 0$) the phase transition probabilities can be written as

$$P_{m \rightarrow m} = \mu_0^m(\Delta t) = \frac{1 + \beta e^{-(1+\beta)\alpha\Delta t}}{1 + \beta} \quad (3.22)$$

$$P_{m \rightarrow im} = \nu_0^m(\Delta t) = \frac{\beta - \beta e^{-(1+\beta)\alpha\Delta t}}{1 + \beta} \quad (3.23)$$

where the superscripts m represent solute originating in the mobile domain, and $P_{m \rightarrow m}$ and $P_{m \rightarrow im}$ refer to the probability of a particle starting in the mobile phase and ending in the mobile/immobile phase, respectively.

Conversely, assuming that at the beginning of the time step all the solute mass is in the immobile domain ($\mu_0(0) = 0$ and $\nu_0(0) = 1$) the phase transition probabilities are

$$P_{im \rightarrow m} = \mu_0^{im}(\Delta t) = \frac{1 - e^{-(1+\beta)\alpha\Delta t}}{1 + \beta} \quad (3.24)$$

$$P_{im \rightarrow im} = \nu_0^{im}(\Delta t) = \frac{\beta + e^{-(1+\beta)\alpha\Delta t}}{1 + \beta} \quad (3.25)$$

where the superscript im represents solute originating in the immobile domain, and $P_{im \rightarrow m}$ and $P_{im \rightarrow im}$ refer to the probability of a particle starting in the immobile phase and ending in the mobile/immobile phase, respectively. It can be seen from equations (3.22) to (3.25) that $P_{m \rightarrow m} = 1 - P_{m \rightarrow im}$ and $P_{im \rightarrow im} = 1 - P_{im \rightarrow m}$. *Valocchi and Quinodoz* (1989) and *Michalak and Kitanidis* (2000) obtained equivalent expressions for the case of kinetic sorption, as mentioned above.

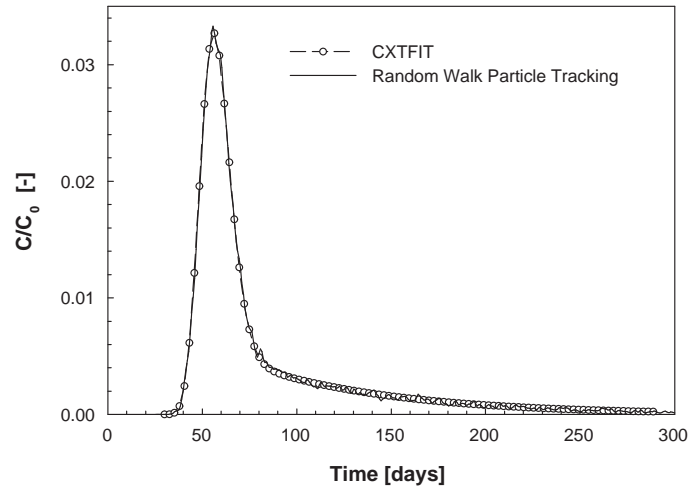


Figure 3.1. Comparison of breakthrough curves obtained with CXTFIT (*Toride et al.*, 1995) and random walk particle tracking.

Having calculated the phase transition probabilities, numerical implementation into particle tracking is done easily. For each time step a uniform $[0, 1]$ random number Y is drawn for each particle and is compared to the corresponding probability. The state of a particle being in the mobile phase is adjusted according to

$$\mathbf{X}_p(t + \Delta t) = \begin{cases} \text{mobile} & \text{if } Y < P_{m \rightarrow m} \\ \text{immobile} & \text{if } Y \geq P_{m \rightarrow m} \end{cases} \quad (3.26)$$

where \mathbf{X}_p is the position of the particle at time $t + \Delta t$. For a particle being in the immobile domain the final state is adjusted according to

$$\mathbf{X}_p(t + \Delta t) = \begin{cases} \text{immobile} & \text{if } Y < P_{im \rightarrow im} \\ \text{mobile} & \text{if } Y \geq P_{im \rightarrow im} \end{cases} \quad (3.27)$$

Having finished the trial a particle is only allowed to move when being in the mobile phase.

Parameter	First-Order Mass Transfer	Spherical Diffusion
Model Length	5.0 m	5.0 m
v_x	0.0864 m/d	0.0864 m/d
α_L	0.05 m	0.05 m
θ_m	0.2	0.2
θ_{im}	0.1	0.1
α	0.01728 1/d	0.00432 1/d ^a
Nr. of Particles ^b	20000	20000
Nr. of Multirate Series	-	8 ^b / 100 ^c
Courant number	0.01	0.01

^a for Spherical Diffusion $\alpha = \frac{D_a}{a^2}$ is the diffusion rate coefficient

^b only Random Walk Particle Tracking

^c STAMMT-L

Table 3.1. Input parameters for one-dimensional solute transport in Figures 3.1 and 3.2

Figure 3.1 and Table 3.1 show the breakthrough curve and input parameters obtained for a one-dimensional system with simple, first-order mass transfer using the random walk model. The curve is compared with the results obtained using the well-known CXTFIT Code (*Toride et al.*, 1995).

Multiple mass transfer and diffusion into various geometries

One of the main advantages of the multirate model is the possibility not only to simulate a certain number of linear mass transfer processes, but to model diffusion into spheres, cylinders, and layers by choosing appropriate values for the first-order rates and capacity coefficients (*Haggerty and Gorelick*, 1995). The series of these coefficients for the different geometries are shown in Tables 3.2 and 3.3. However, modeling these processes usually requires a relatively large number of mass transfer rates resulting into high order matrices in equation (3.18). Analytical solutions, as presented in Section 3.2.2, for equation (3.19) do not exist and thus the exponential matrix has to be calculated using a numerical approach.

In this work we will employ the following Taylor series approximation of exponential matrices

$$\begin{aligned} \exp[(\mathbf{A}^{-1}\mathbf{B})\Delta t] = & \mathbf{I} + (\mathbf{A}^{-1}\mathbf{B})\Delta t + (\mathbf{A}^{-1}\mathbf{B})^2 \frac{\Delta t^2}{2} + \dots \\ & \dots + (\mathbf{A}^{-1}\mathbf{B})^n \frac{\Delta t^n}{n!} + \dots \end{aligned} \quad (3.28)$$

where \mathbf{I} is the identity matrix.

Due to the fact that in random walk particle tracking the time step chosen is normally small, as already mentioned above, we do not require to use a lot of terms in equation (3.28) to approximate the exponential of the matrix $[(\mathbf{A}^{-1}\mathbf{B})\Delta t]$. Instead, using only the terms up to the third-order the zeroth spatial moments for each domain are sufficiently well approximated.

Diffusion Geometry	Multirate Series ^a	
	α_j for $j = 1, \dots, N - 1$	β_j for $j = 1, \dots, N - 1$
Layered Diffusion	$\frac{(2j-1)^2\pi^2}{4}\alpha$	$\frac{8}{(2j-1)^2\pi^2}\beta_{tot}$
Cylindrical Diffusion ^b	$r_{0,j}^2\alpha$	$\frac{4}{r_{0,j}^2}\beta_{tot}$
Spherical Diffusion	$j^2\pi^2\alpha$	$\frac{6}{j^2\pi^2}\beta_{tot}$

^a $\alpha = \frac{D_a}{a^2}$ is the diffusion rate coefficient; $\beta_{tot} = \frac{\theta_{im}R_{im}}{\theta_m R_m}$ is the capacity coefficient.

^b $r_{0,j}$ is the j th root of $J_0(x)$, where J_0 is the zero-order Bessel function of the first kind.

Table 3.2. Multirate Series for Diffusion (after *Haggerty and Reeves, 2002*)

Using these spatial moments the phase transition probabilities for a particle are calculated with a similar procedure as outlined in Section 3.2.2. Assuming that at the beginning of the time step all the solute mass M is in the mobile domain and setting the solute mass $M = 1$ ($\mu_0(0) = 1$ and $\nu_{0,j}(0) = 0$) the probability of a particle originating in the mobile phase and being in the mobile phase $P_{m \rightarrow m}$ at the elapsed time Δt can be approximated as follows

$$\begin{aligned}
 \mu_0(\Delta t)|_m^m \approx & 1 - \left[\sum_{j=1}^N \alpha_j \beta_j \right] \Delta t + \left[\left[\sum_{j=1}^N \alpha_j \beta_j \right]^2 + \sum_{j=1}^N \alpha_j^2 \beta_j \right] \frac{\Delta t^2}{2} \\
 & - \left[\left[\sum_{j=1}^N \alpha_j \beta_j \right]^3 + \sum_{j=1}^N \alpha_j \beta_j \sum_{j=1}^N \alpha_j^2 \beta_j \right. \\
 & \left. + \sum_{j=1}^N \left[\alpha_j^2 \beta_j \left[\sum_{k=1}^N \alpha_k \beta_k \right] + \alpha_j^3 \beta_j \right] \right] \frac{\Delta t^3}{6} \quad (3.29)
 \end{aligned}$$

The probability of a particle originating in the mobile phase and changing into the i th immobile phase $P_{m \rightarrow im,i}$ can be written as

$$\begin{aligned}
 \nu_0(\Delta t)|_{im,i}^m &\approx \alpha_i\beta_i\Delta t - \left[\alpha_i\beta_i \left[\sum_{j=1}^N \alpha_j\beta_j \right] + \alpha_i^2\beta_i \right] \frac{\Delta t^2}{2} \\
 &+ \left[\alpha_i\beta_i \left[\sum_{j=1}^N \alpha_j\beta_j \right]^2 + \alpha_i^2\beta_i \left[\sum_{j=1}^N \alpha_j\beta_j \right] \right. \\
 &\left. + \alpha_i^3\beta_i + \alpha_i\beta_i \sum_{j=1}^N \alpha_j^2\beta_j \right] \frac{\Delta t^3}{6} \tag{3.30}
 \end{aligned}$$

Conversely, assuming that at the beginning of the time step all the solute mass is in the i th immobile domain ($\mu_0(0) = 0$, $\nu_{0,i}(0) = 1$, and $\nu_{0,j}(0) = 0$ for all $j \neq i$) the phase transition probability for a particle to move from the i th immobile domain to the mobile domain $P_{im,i \rightarrow m}$ is

$$\begin{aligned}
 \mu_0(\Delta t)|_m^{im,i} &\approx \alpha_i\Delta t - \left[\alpha_i \left[\sum_{j=1}^N \alpha_j\beta_j \right] + \alpha_i^2 \right] \frac{\Delta t^2}{2} \\
 &+ \left[\alpha_i \left[\left[\sum_{j=1}^N \alpha_j\beta_j \right]^2 + \sum_{j=1}^N \alpha_j^2\beta_j \right] \right. \\
 &\left. + \alpha_i^2 \left[\sum_{j=1}^N \alpha_j\beta_j \right] + \alpha_i^3 \right] \frac{\Delta t^3}{6} \tag{3.31}
 \end{aligned}$$

The probability of a particle to stay in the i th immobile domain $P_{im,i \rightarrow im,i}$ can be approximated as

$$\begin{aligned}
 \nu_0(\Delta t)|_{im,i}^{im,i} &\approx 1 - \alpha_i\Delta t + [\alpha_i^2\beta_i + \alpha_i^2] \frac{\Delta t^2}{2} - \left[\alpha_i^2\beta_i \left[\sum_{j=1}^N \alpha_j\beta_j \right] \right. \\
 &\left. + 2\alpha_i^3\beta_i + \alpha_i^3 \right] \frac{\Delta t^3}{6} \tag{3.32}
 \end{aligned}$$

Although the different immobile domains are not connected with each other there exists still the possibility that a particle moves first from the i th immobile domain to the mobile domain and from there into the k th immobile domain $P_{im,i \rightarrow im,k}$ within one time step, as transition probabilities only describe the initial and the final state during the elapsed time Δt , but do not account for state changes within Δt . The probability for this case can be calculated as

Diffusion Geometry	Final Term in Multirate Series	
	α_N	β_N
Layered Diffusion	$\frac{3\alpha \left[1 - \sum_{j=1}^{N-1} \frac{8}{(2j-1)^2 \pi^2} \right]}{1 - \sum_{j=1}^{N-1} \frac{96}{(2j-1)^4 \pi^4}}$	$\left[1 - \sum_{j=1}^{N-1} \frac{8}{(2j-1)^2 \pi^2} \right] \beta_{tot}$
Cylindrical Diffusion	$\frac{8\alpha \left[1 - \sum_{j=1}^{N-1} \frac{4}{r_{0,j}^2} \right]}{1 - \sum_{j=1}^{N-1} \frac{32}{r_{0,j}^4}}$	$\left[1 - \sum_{j=1}^{N-1} \frac{4}{r_{0,j}^2} \right] \beta_{tot}$
Spherical Diffusion	$\frac{15\alpha \left[1 - \sum_{j=1}^{N-1} \frac{6}{j^2 \pi^2} \right]}{1 - \sum_{j=1}^{N-1} \frac{90}{j^4 \pi^4}}$	$\left[1 - \sum_{j=1}^{N-1} \frac{6}{j^2 \pi^2} \right] \beta_{tot}$

Table 3.3. Final Terms of Truncated Multirate Series (after *Haggerty and Reeves, 2002*)

$$\begin{aligned} \nu_0(\Delta t)|_{im,k}^{im,i} \approx & [\alpha_k \beta_k \alpha_i] \frac{\Delta t^2}{2} - \left[\alpha_k \beta_k \alpha_i \left[\sum_{j=1}^N \alpha_j \beta_j \right] \right. \\ & \left. + \alpha_k^2 \beta_k \alpha_i + \alpha_k \beta_k \alpha_i^2 \right] \frac{\Delta t^3}{6} \quad \text{for } k \neq i \quad (3.33) \end{aligned}$$

It can be observed from equation (3.33) that the probability for this case is very small, as we would expect, because the first-order term is canceled out. Therefore, particles will move from one immobile zone to another only for considerably large time steps.

Numerical implementation is, again, similar to the simple first-order mass transfer case. However, we will now have to keep track of in which immobile domain the particle is currently located. The state of a particle being located in the mobile phase is adjusted according to

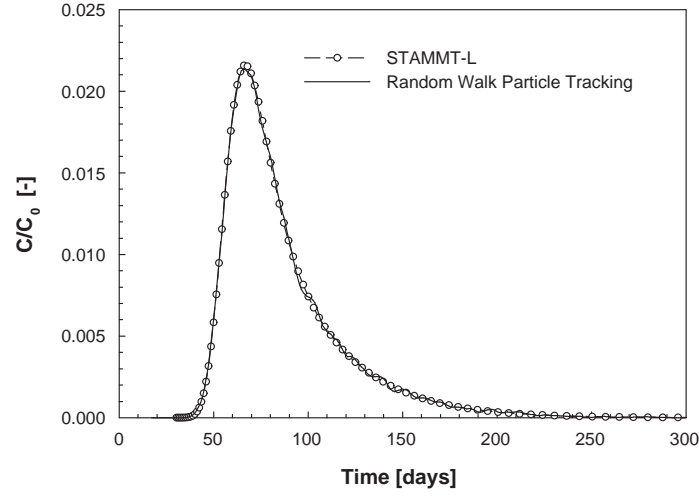


Figure 3.2. Comparison of breakthrough curves obtained with STAMMT-L (*Haggerty and Reeves, 2002*) and random walk particle tracking.

$$\mathbf{X}_p(t + \Delta t) = \begin{cases} \text{mobile} & \text{if } Y < P_{m \rightarrow m} \\ \text{immobile}, 1 & \text{if } P_{m \rightarrow m} \leq Y < P_{m \rightarrow m} + P_{m \rightarrow \text{im}, 1} \\ \dots & \dots \\ \text{immobile}, N & \text{if } Y \geq P_{m \rightarrow m} + \sum_{j=1}^{N-1} P_{m \rightarrow \text{im}, j} \end{cases} \quad (3.34)$$

For a particle being located in the i th immobile phase the final state is being adjusted as follows

$$\mathbf{X}_p(t + \Delta t) = \begin{cases} \text{immobile}, i & \text{if } Y < P_{\text{im}, i \rightarrow \text{im}, i} \\ \text{mobile} & \text{if } P_{\text{im}, i \rightarrow \text{im}, i} \leq Y < \\ & P_{\text{im}, i \rightarrow \text{im}, i} + P_{\text{im}, i \rightarrow m} \\ \text{immobile}, k & \text{if } P_{\text{im}, i \rightarrow \text{im}, i} + P_{\text{im}, i \rightarrow m} \leq Y < \\ & P_{\text{im}, i \rightarrow \text{im}, i} + P_{\text{im}, i \rightarrow m} + P_{\text{im}, i \rightarrow \text{im}, k} \\ \dots & \dots \\ \text{immobile}, N & \text{if } Y \geq P_{\text{im}, i \rightarrow \text{im}, i} + P_{\text{im}, i \rightarrow m} \\ & + \sum_{k=1}^{N-1} P_{\text{im}, i \rightarrow \text{im}, k} \quad \text{for } k \neq i \end{cases} \quad (3.35)$$

A breakthrough curve obtained using random walk and a multirate series for spherical diffusion is presented in Figure 3.2. The input parameters are

shown in Table 3.1. The curve is compared with the results obtained using STAMMT-L (*Haggerty and Reeves, 2002*). STAMMT-L is a code that provides a semi-analytical solution to one-dimensional, dual porosity, advective-dispersive transport, where mass transfer between the mobile and immobile domains is generalized to include multiple immobile domains.

3.3 Numerical Implementation Details

3.3.1 Random Walk Particle Tracking

Random walk particle tracking simulates solute transport by partitioning the solute mass into a large number of representative particles. The evolution in time of a particle is driven by a drift term that relates to the advective movement and a superposed Brownian motion responsible for dispersion. The displacement of a particle is calculated as follows (e.g., *Tompson, 1993*)

$$\mathbf{X}_p(t + \Delta t) = \mathbf{X}_p(t) + \mathbf{B}_1(\mathbf{X}_p, t)\Delta t + \mathbf{B}_2(\mathbf{X}_p, t) \cdot \boldsymbol{\xi}(t)\sqrt{\Delta t} \quad (3.36)$$

where \mathbf{B}_1 is a “drift” vector, \mathbf{B}_2 , the displacement matrix, is a tensor defining the strength of dispersion, and $\boldsymbol{\xi}(t)$ is a vector of independent, normally distributed random variables with zero mean and unit variance. In expression (3.36) \mathbf{B}_1 corresponds to

$$\mathbf{B}_1 = \frac{\mathbf{v} + \nabla \cdot \mathbf{D}}{R_m} \quad (3.37)$$

and the displacement matrix \mathbf{B}_2 is related to the dispersion tensor as

$$\frac{2\mathbf{D}}{R_m} = \mathbf{B}_2 \cdot \mathbf{B}_2^T \quad (3.38)$$

The displacement matrix used here has the form given by *Lichtner et al. (2002)*.

The velocity vector is computed using linear interpolation of interface velocities. The dispersion tensor field is obtained by first extrapolating interface velocities to surrounding nodes. This gives all three components of the vector pore-velocity to each grid node, which is then used to estimate the dispersive component of the random walk using trilinear interpolation. Various authors have demonstrated (*LaBolle et al., 1996; Salamon et al., 2006*), that this hybrid scheme yields local as well as global divergence-free velocity fields within the solution domain and a continuous dispersion tensor field that approximates well mass balance at grid interfaces of adjacent cells with contrasting hydraulic conductivities. Furthermore, a constant-displacement scheme (*Wen*

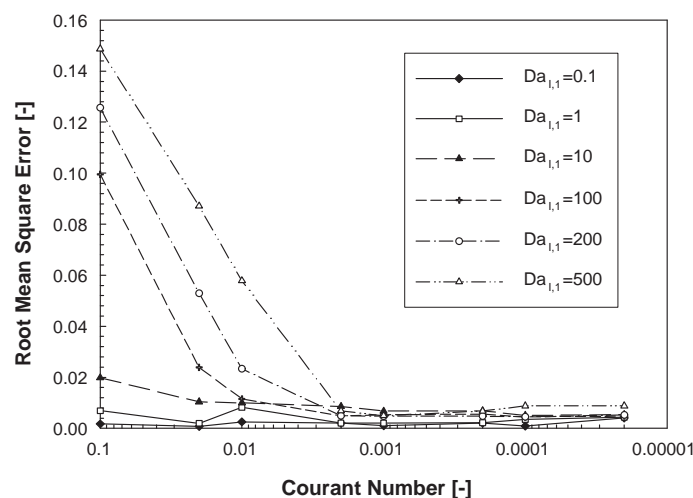


Figure 3.3. Evaluation of the root mean of squared residual errors in dependency of the time step size for different $Da_{I,1}$ numbers. Solute transport for this case is only subject to advection and first-order mass transfer.

and Gómez-Hernández, 1996) which modifies automatically the time step size for each particle according to the local velocity is employed in order to decrease computational effort.

For the examples presented in this article the numerical random walk particle tracking code developed by Fernández-García *et al.* (2005) was extended to simulate mass transfer according to the procedure outlined in Section 3.2.

3.3.2 Choice of Time Step Size

One important problem, when simulating mass transfer processes using particle tracking is, that the phase transition probabilities do not describe the number of phase changes occurring within one time step, but only determine the initial and final state of a particle during the elapsed time Δt (Parzen, 1962). Thus, the time a particle actually spends in the mobile/immobile phase can differ significantly within a time step for the case of high mass transfer rate in relation to the time step size. This problem is complicated further when using a constant displacement scheme which adjusts automatically the time step size according to the particle displacement in the mobile phase. For the case of having various linear mass transfer processes acting at the same time it is therefore possible that a particle moves from the immobile phase i to the mobile phase and from there into the immobile phase k as shown in Section 3.2.2.

One simple way to overcome this problem is to choose a time step size small enough so that the probability of various phase changes within one time step is negligible (Valocchi and Quinodoz, 1989; Kinzelbach, 1987). In order to determine the proper time step size we will look at the case of advective solute transport with first-order mass transfer in a one-dimensional, homogeneous column. Particles will be released at a point on the left border of the column and arrival times will be measured at the right column border. Δt is given here as a function of the Courant number ($Cr = (v\Delta t)/L$, where L is the column length). By varying Cr and comparing the cumulative breakthrough curves with a reference curve obtained using the random walk approach with a very small time step ($Cr = 0.00001$) the root mean of squared residual errors (RMS) is calculated

$$RMS = \left[\frac{1}{N} \sum_{i=1}^N (cal_i - ref_i)^2 \right]^{\frac{1}{2}} \quad (3.39)$$

where N is the total number of observations, cal_i [M/L^3] and ref_i [M/L^3] are the calculated and the reference concentration values of the breakthrough curves at a certain time. An overview of the input parameters for the following examples is given in Table 3.4.

To characterize the ratio of the mass transfer timescale to the advection timescale the Damköhler number is used. In the case of one-dimensional flow and transport and using the multirate model, each mass transfer reaction has a Damköhler number associated, which can be expressed as follows

$$Da_{I,j} = [\alpha_j(\beta_j + 1)R_m L]/v \quad (3.40)$$

where L [L] is the length scale, which for this case corresponds to the column length.

Figure 3.3 shows the RMS for different Damköhler numbers. As expected, increasing the first-order mass transfer rate requires a smaller time step, in order to represent solute transport correctly. Figure 3.4 illustrates the effects of large time steps on the breakthrough curves for the case of a high mass transfer-advection ratio ($Da_{I,1} = 200$). If time step size is not sufficiently small the detention of particles in the immobile compartments is too large and artificial dispersion and an increased tailing in the breakthrough curve is introduced.

However, Bahr and Rubin (1987) stated that for a Damköhler value greater than approximately 100 the mass transfer relationship is effectively at equilibrium and therefore practical problems usually have Damköhler numbers smaller than 100. Thus, for most cases a Cr of 0.01 is sufficient for a correct simulation of mass transfer using random walk.

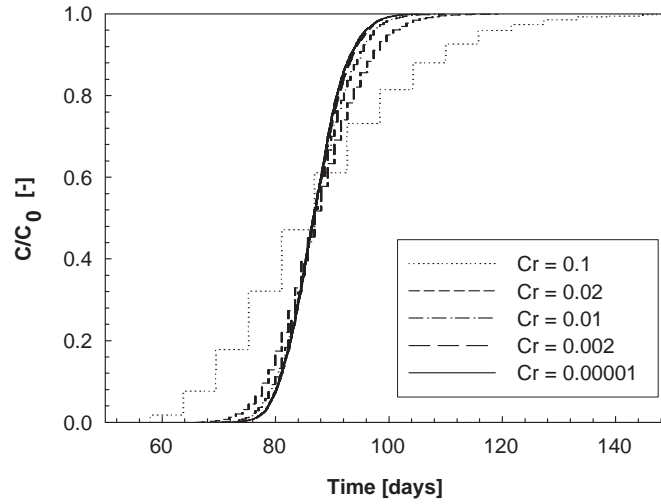


Figure 3.4. Cumulative breakthrough curves obtained using different time step sizes for a Damköhler number of $Da_{I,1} = 200$.

3.3.3 An Approximation Criteria for the Exponential Matrix

A further difficulty concerns the fact that equations (3.29) to (3.33) only represent an approximation to the matrix exponential $\exp[(\mathbf{A}^{-1}\mathbf{B})\Delta t]$. Choosing a very large time step or increasing the number of multirate parameters can result in an erroneous approximation of the phase transition probabilities when only three terms are employed. A variety of restrictive criteria have been suggested in literature concerning the truncation of Taylor series (e.g., *Everling*, 1967; *Bickart*, 1968). Here, the criterion established by *Liou* (1966) will be used

$$\delta \equiv \frac{\|(\mathbf{A}^{-1}\mathbf{B})\Delta t\|^{D+1}}{(D+1)!} \cdot \frac{1}{1 - \|(\mathbf{A}^{-1}\mathbf{B})\Delta t\|/(D+2)} \leq \delta_{max} \quad (3.41)$$

where $D[-]$ is the number of terms used for the approximation, and δ and $\delta_{max}[-]$ are the truncation error bound function and the prescribed absolute error tolerance, respectively. The matrix norm used here is a 1-norm or also called the maximum absolute column sum norm:

$$\|\mathbf{A}\|_1 = \max_j \sum_{i=1}^n |a_{ij}| \quad (3.42)$$

In case of exceeding δ_{max} either the number of multirate parameters or the time steps have to be adjusted. Figure 3.5 shows the relation between the

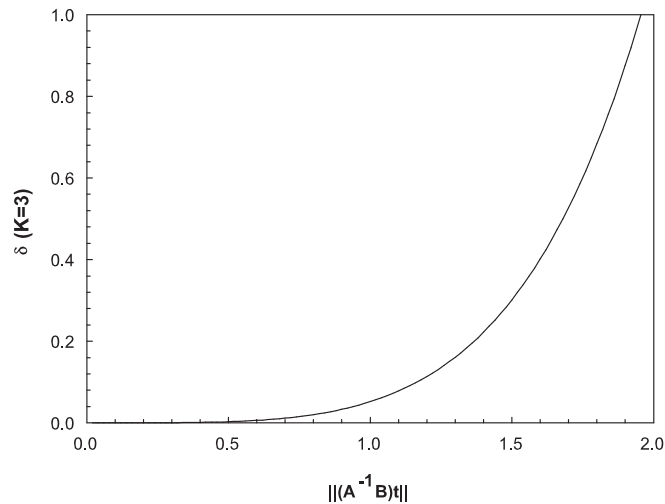


Figure 3.5. Absolute error tolerance δ versus matrix 1-norm of $\|(\mathbf{A}^{-1}\mathbf{B})t\|$ when using a Taylor Series approximation for the matrix exponential with three terms.

matrix norm and the error tolerance for a matrix exponential approximation with terms up to the third order. Experience has shown, that when choosing $\delta_{max} = 0.1$ the matrix exponential is well approximated and for most cases the matrix norm does not exceed the restriction criterion.

3.3.4 Truncation of the Multirate Series

A final issue concerns the truncation of the multirate series when simulating diffusion into different geometries, which was already addressed by *Haggerty and Reeves* (2002). They found that very precise results can be obtained with truncated series as long as appropriate expressions for the final term of the series are used (see Table 3.3). According to *Haggerty and Reeves* (2002) usually less than 30 terms are sufficient for the representation of a diffusion process into a specific geometry.

Unfortunately, when using a multirate series to simulate diffusion, some immobile domain compartments will always have relatively high Damköhler numbers, hence requiring a small Courant number for the random walk simulations. Figure 3.6 shows the root mean square error (see equation (3.39)) for comparing cumulative breakthrough curves obtained using STAMMT-L and the method presented here for one-dimensional, advective-dispersive solute transport with diffusion into spherical grains (input parameters are illustrated in Table 3.4). The curves simulated with STAMMT-L employ 30 terms for the multirate series. It should be noted that the Da_I values presented in Figure

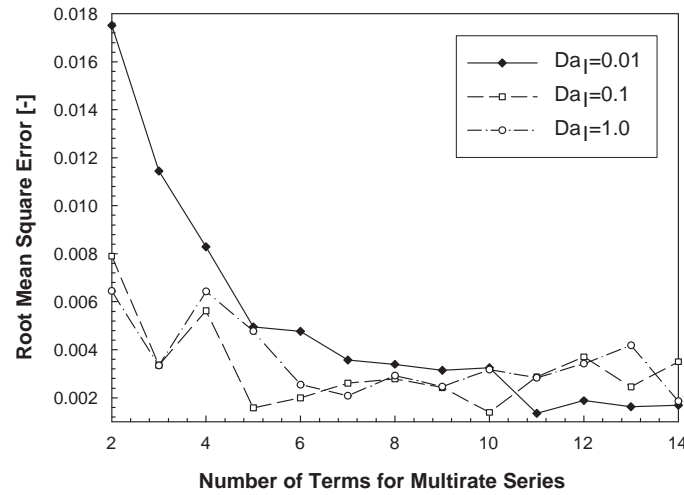


Figure 3.6. Evaluation of the root mean of squared residual errors in dependency of the number of terms used for the multirate series.

3.6 represent the ratio of mass transfer and advective timescale of the spherical diffusion and are calculated using the diffusion rate constant ($\alpha = \frac{D_a}{a^2}$).

Parameter	Figures 3.3 and 3.4	Figure 3.6
Model Length	5.0 m	5.0 m
v_x	0.0864 m/d	0.0864 m/d
α_L	-	0.05 m
θ_m	0.2	0.2
θ_{im}	0.1	0.2
α	0.001152 / 0.01152	8.64×10^{-5}
	0.1152 / 1.152	8.64×10^{-4}
	2.304 / 5.76 1/d	8.64×10^{-3} 1/d ^a
Number of Particles ^b	5000	5000
Number of Multirate Series	-	2 - 14 ^b / 30 ^c
Courant number	- ^d	0.01

^a for Spherical Diffusion $\alpha = \frac{D_a}{a^2}$ is the diffusion rate coefficient

^b only Random Walk Particle Tracking

^c STAMMT-L

^d see Figures 3.3 and 3.4

Table 3.4. Input parameters for solute transport examples in Figures 3.3, 3.4, and 3.6. Note that α was varied to change the ratio between advection and mass transfer timescale.

It can be observed that the error in general is very small and that with significantly less than 30 terms no further improvement is visible. This is not surprising as the capacity ratios of the multirate series approach rapidly very small values whereas the mass transfer rates for the different immobile compartments approximate large $Da_{I,j}$ values. These compartments can therefore be lumped together and modeled with a single equilibrium mass transfer relationship (according to *Haggerty and Gorelick, 1995*). Furthermore, when using particle tracking, an increase in the number of terms used for the multirate series does not necessarily result in a higher precision of the outcome as there are two restrictive constraints to the time step size Δt : the rate of mass transfer and the approximation of the exponential matrix using a third-order Taylor series.

3.4 The Effect of a Heterogeneous Intraparticle Pore Diffusion Distribution - An Example

One of the main advantages of the method presented here is that it does not impose any spatial restrictions on the different types of mass transfer while preserving computational efficiency. To illustrate this a synthetic example of the effect of heterogeneous distribution of intraparticle pore diffusion rates is presented in this section. Some of the parameters of this synthetic example, i.e., spatial correlation, pore-scale dispersivities, mobile/immobile porosities, and diffusion rates, are representative of the Borden aquifer. However, the objective of this example is not to reproduce solute transport at the Borden site, but to illustrate the application of the presented random walk approach in a realistic setting.

For this purpose one realization of a sequential gaussian simulation (*Gómez-Hernández and Journel, 1993*) was chosen. The following standardized exponential semivariogram was applied for the simulation of the hydraulic conductivity field

$$\frac{\gamma(h_{x,y,z})}{\sigma_{\ln K}^2} = 1 - \exp \left[-\sqrt{\left(\frac{h_x}{\lambda_x}\right)^2 + \left(\frac{h_y}{\lambda_y}\right)^2 + \left(\frac{h_z}{\lambda_z}\right)^2} \right] \quad (3.43)$$

where $\lambda_{x,y,z}[L]$ are the directional correlation length scales, $h_{x,y,z}[L]$ are the directional lag spaces, and σ^2 is the variance of the natural logarithm of the hydraulic conductivity $\ln K[L/T]$. According to *Woodbury and Sudicky (1991)* a correlation length of $\lambda_x = \lambda_y = 5.1$ m (horizontal) and $\lambda_z = 0.21$ m (vertical) was selected. It should be noted that the variance of $\ln K$ was increased with respect to the Borden aquifer in this example to a value of $\sigma_{\ln K}^2 = 2.5$ and the average hydraulic gradient to a value of 0.043. The computational domain is

parallelepipedic with dimensions of $x = 80$ m, $y = 15$ m, and $z = 4$ m and a discretization of $\Delta x = \Delta y = 0.5$ m, and $\Delta z = 0.04$ m was chosen, resulting in a total of 480,000 grid cells. The aquifer was assumed to be confined and with constant head boundaries at $x = 0$ m and $x = 80$ m and with no-flow boundaries at the remaining model faces. A total of 20,000 particles randomly distributed in a plane shaped, rectangular area of 10 m width and 3 m height located orthogonal to the principal flow direction at a distance of $x = 5$ m were released at $t = 0$. All particles were initially released in the mobile domain. Mass arrival was measured at a control plane located at $x = 78$ m. Pore-scale longitudinal and transverse dispersivities were assumed to be $\alpha_L = 0.0005$ m and $\alpha_T = 0.00005$ m (*Brusseau and Srivastava, 1997*), and mobile/immobile domain porosities were selected to be $\theta_m = 0.293$ and $\theta_{im} = 0.037$, respectively (*Brusseau and Srivastava, 1997*).

We considered here the following four different models: Solute transport in Model A was purely influenced by advection and dispersion, whereas in models B, C, and D different types of mass transfer were added to the advection-dispersion equation. Model B utilizes a spatially heterogeneous intraparticle pore diffusion. Model C has a uniform coefficient for intraparticle pore diffusion. Finally, model D employs a uniform first-order mass transfer coefficient. Intraparticle diffusion was modeled employing diffusion into a spherical geometry.

In order to obtain the field of intraparticle pore diffusion rates for Model B the Kozeny-Carmen relationship (*Bear, 1972*) was used to calculate a representative grain size diameter for each cell:

$$K = \left(\frac{\rho_w g}{\mu}\right) \frac{\theta^3}{(1 - \theta)^2} \left(\frac{d_{50}^2}{180}\right) \quad (3.44)$$

where $\rho_w [M/L^3]$ is the fluid density, $g [L/T^2]$ is the gravitational constant, $\mu [M/(LT)]$ is the fluid viscosity, $d_{50} [L]$ is the grain size diameter, and θ is the total porosity, which corresponds to the sum of mobile and immobile porosity. The grain sizes were then employed to assign the corresponding diffusion rate coefficients to each grid cell pursuant to *Ball and Roberts (1991)*, which estimated diffusive PCE uptake into different size fractions of a Borden sample (see Table 3.5). The reader should keep in mind that we are not suggesting that d_{50} is necessarily the representative length scale for intraparticle diffusion. In fact, intraparticle diffusion might even be better represented with several grain sizes (e.g., *Haggerty and Gorelick, 1995*). However, in this example we consider the assumptions taken as valid.

The uniform coefficient for Model C was calculated by applying (3.44) to the geometric mean of the conductivity field $K = 6.182$ m/d (*Burr and Sudicky, 1994*) resulting in a grain size diameter of $d_{50} = 0.128$ mm and thus

Size range ($d_{50} = 2a$)	D_a/a^2
0.85 – 1.7 mm	$3.1 \times 10^{-8} s^{-1}$
0.42 – 0.85 mm	$9.2 \times 10^{-8} s^{-1}$
0.25 – 0.42 mm	$2.3 \times 10^{-7} s^{-1}$
0.18 – 0.25 mm	$2.7 \times 10^{-7} s^{-1}$
0.125 – 0.18 mm	$9.4 \times 10^{-7} s^{-1}$
0.075 – 0.125 mm	$1.7 \times 10^{-6} s^{-1}$
< 0.075 mm	$1.4 \times 10^{-6} s^{-1}$

Table 3.5. Grain sizes and diffusion rate coefficients for a Borden sand sample measured by *Ball and Roberts* (1991) for PCE desorption

into a diffusion rate of $D_a/a^2 = 9.4 \times 10^{-7} s^{-1}$ (see Table 3.5). Model D in turn uses the following relationship to calculate the first-order mass transfer rate

$$\alpha = 15D_a/a^2 \tag{3.45}$$

which has shown to be the best effective rate coefficient used in "equivalent" first-order models of mass transfer (e.g., *Young and Ball*, 1995; *Haggerty et al.*, 2000). To calculate α in this example the uniform diffusion rate coefficient of Model C is used resulting in a first-order mass transfer coefficient of $\alpha = 1.41 \times 10^{-5} s^{-1}$.

Concerning the numerical implementation of the presented approach the following issues had to be addressed: (1) the negative correlation between hydraulic conductivity and mass transfer rates in Model B lead to high Damköhler numbers in low velocity zones; (2) due to the constant displacement scheme employed Δt was considerably large in high hydraulic conductivity areas, thus exceeding the criteria for the matrix norm for Models B and C in some grid cells established in Section 3.3.3. Therefore, the Courant number was adapted for each grid cell before starting the solute transport based on the cell specific velocity field and mass transfer rate, in order to avoid defining one maximum time step size for the entire model domain and therewith decreasing computational efficiency.

The breakthrough curves and the relative mass fraction remaining in the aquifer of the four models are presented in Figures 3.7 and 3.8. It can be seen clearly that the diffusion process acts as a retardation factor on solute transport. However, it can also be observed that Models B, C, and D produce similar results for this example, indicating that the heterogeneous rep-

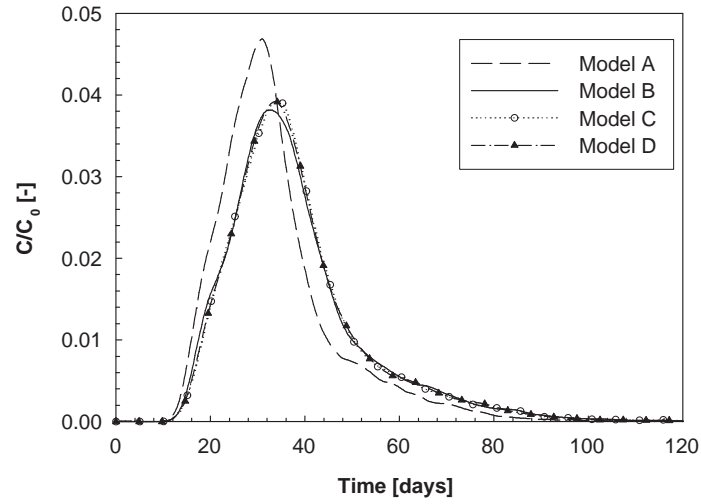


Figure 3.7. Breakthrough curves obtained using the example outlined in Section 3.4.

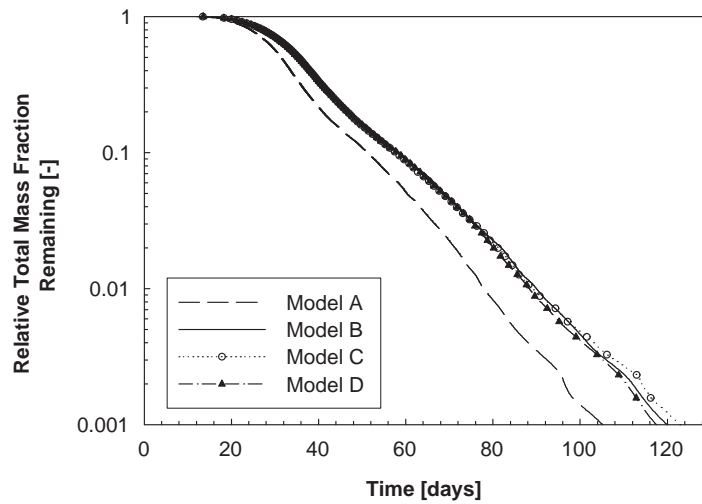


Figure 3.8. Relative total mass fraction remaining in the aquifer not having passed the control plane located at $x = 78$ using the example outlined in Section 3.4.

resentation of mass transfer rates does not influence mean transport behavior significantly for the given input parameters. Instead, it even seems that using an “equivalent” first-order model, is able to reproduce correctly the main features of solute transport. Nevertheless, Model D appears to underestimate the low concentration tailing in comparison to Model B, whereas Model C slightly overestimates the tailing. This indicates that the choice of mass transfer type as well as the spatial distribution of mass transfer rates can potentially have a significant effect on low concentration tailing. Similar observations on the effect of heterogeneous rate-limited mass transfer were also made by *Li and Brusseau* (2000) and *Cunningham and Roberts* (1998).

3.5 Conclusions

We have developed a new numerical method to solve dual-domain multirate mass transfer coupled with advective-dispersive transport using the random walk particle tracking method. Phase transition probabilities which are calculated based on the zeroth spatial moments of the multirate mass transfer equations are used to simulate the particle distribution between the mobile and various immobile domains. The two major advantages of this approach are the flexibility in the sense that it does not impose any restrictive assumptions on the spatial variability of advection, dispersion, and mass transfer and its low computational cost even for highly discretized models having a spatially heterogeneous mass transfer rate. The flexibility of the multirate model to describe a variety of different mass transfer processes is preserved using this approach as well as the advantages of the random walk method: the non-existence of numerical dispersion even for highly advection-dominated solute transport and the local as well as global mass conservation.

However, there are also two disadvantages when using this approach: Firstly, high mass transfer rates require an increasingly smaller time step size. Secondly, using a third-order Taylor series to approximate the matrix exponential can possibly result in an incorrect calculation of the phase transition probabilities when either a large number of immobile domains to simulate diffusion into various geometries is used or the time step is not sufficiently small. Nevertheless, introducing a restrictive criteria for the time step size, which can be adjusted for each grid cell separately instead of defining one maximum time step for the whole model domain, a correct simulation of mass transfer processes can be assured. Hence, the herein presented approach constitutes a valuable tool for the evaluation of the effects of a variety of mass transfer processes on solute transport especially in highly heterogeneous three-dimensional systems.

Bibliography

- Andricevic, R., and E. Foufoula-Georgiu (1991), Modeling kinetic non-equilibrium using the first two moments of residence time distribution, *Stochastic Hydrol. Hydraul.*, 5, 155–171.
- Aris, R. (1956), On the dispersion of a solute in a fluid flowing through a tube, *Proc. R. Soc. London, Ser. A*, 235, 67–77.
- Bahr, J. M., and J. Rubin (1987), Direct comparison of kinetic and local equilibrium formulations for solute transport affected by surface reactions, *Water Resources Research*, 23(3), 438–452.
- Ball, W. P., and P. V. Roberts (1991), Long-term sorption of halogenated organic chemicals by aquifer material. 2. Intraparticle diffusion, *Environmental Science & Technology*, 25(7), 1237–1249.
- Bear, J. (1972), Dynamics of fluids in porous media, 764 pp., Elsevier, New York.
- Berkowitz, B., and H. Scher (1998), Theory of anomalous chemical transport in random fracture networks, *Physical Review E*, 57(5), 5858–5869.
- Bickart, T. A. (1968), Matrix exponential: Approximation by truncated power series, *Proc. IEEE*, 56, 372–373.
- Brusseau, M. L., and R. Srivastava (1997), Nonideal transport of reactive solutes in heterogeneous porous media 2. Quantitative analysis of the Borden natural-gradient field experiment, *Journal of Contaminant Hydrology*, 28, 115–155.
- Burr, D. T., and E. A. Sudicky (1994), Nonreactive and reactive solute transport in three-dimensional heterogeneous porous media: Mean displacement, plume spreading, and uncertainty, *Water Resources Research*, 30(3), 791–815.
- Carrera, J., X. Sánchez-Vila, I. Benet, A. Medina, G. Galarza, and J. Guimerà (1998), On matrix diffusion: formulations, solution methods and qualitative effects, *Hydrogeology Journal*, 6, 178–190.

- Cunningham, J. A., and P. V. Roberts (1998), Use of temporal moments to investigate the effects of nonuniform grain-size distribution on the transport of sorbing solutes, *Water Resources Research*, *34*(6), 1415–1425.
- Dentz, M., and B. Berkowitz (2003), Transport behavior of a passive solute in continuous time random walks and multirate mass transfer, *Water Resources Research*, *39*(5), 1111, doi:10.1029/2001WR001163.
- Dentz, M., A. Cortis, H. Scher, and B. Berkowitz (2004), Transport behavior of solute transport in heterogeneous media: transition from anomalous to normal transport, *Advances in Water Resources*, *27*, 155–173.
- Everling, W. (1967), On the evaluation of e^{At} by power series, *Proc. IEEE*, *55*, 413.
- Feehley, C. E., C. Zheng, and F. J. Molz (2000), A dual-domain mass transfer approach for modeling solute transport in heterogeneous aquifers: Application to the Macrodispersion Experiment (MADE) site, *Water Resources Research*, *36*(9), 2501–2515.
- Fernàndez-Garcia, D., T.H. Illangasekare, and H. Rajaram (2005), Differences in the scale-dependence of dispersivity estimated from temporal and spatial moments in chemically and physically heterogeneous porous media, *Advances in Water Resources*, *28*(7), 745–759.
- Goltz, M. N., and P. V. Roberts (1987), Using the method of moments to analyze three-dimensional diffusion limited solute transport from temporal and spatial perspectives, *Water Resources Research*, *23*(8), 1575–1585.
- Gómez-Hernández, J. J., and A. G. Journel (1993), Joint sequential simulation of multi-Gaussian fields, in *Geostatistics Troia '92*, edited by A. Soares, Vol. 1, 85–94, Kluwer.
- Guswa, A. J., and D. L. Freyberg (2002), On using the equivalent conductivity to characterize solute spreading in environments with low-permeability lenses, *Water Resources Research*, *38*(8), 1132, doi:10.1029/2001WR000528.
- Haggerty, R., and S. M. Gorelick (1995), Multiple-rate mass transfer for modeling diffusion and surface reactions in media with pore-scale heterogeneity, *Water Resources Research*, *31*(10), 2383–2400.
- Haggerty, R., S.A. McKenna, and L. C. Meigs (2000), On the late-time behaviour of tracer test breakthrough curves, *Water Resources Research*, *36*(12), 3467–3479.

- Haggerty, R., and P. Reeves (2002), STAMMT-L: Solute Transport and Multirate Mass Transfer, Version 1.0, User’s Manual, *ERMS#520308*, Sandia Natl. Lab., Albuquerque, N. M.
- Haggerty, R., C. F. Harvey, C. Freiherr von Schwerin, and L. C. Meigs (2004), What controls the apparent timescale of solute mass transfer in aquifers and soils? A comparison of experimental results, *Water Resources Research*, *40*, W01510, doi:10.1029/2002WR001716.
- Harvey, C., and S. M. Gorelick (2000), Rate-limited mass transfer or macrodispersion: Which dominates plume evolution at the Macrodispersion Experiment (MADE) site?, *Water Resources Research*, *36*(3), 637–650.
- Huang, H., and B. X. Hu (2000), Nonlocal nonreactive transport in heterogeneous porous media with interregional mass diffusion, *Water Resources Research*, *36*(7), 1665–1675.
- Huang, H., A. E. Hassan, and B. X. Hu (2003), Monte Carlo study of conservative transport in heterogeneous dual-porosity media, *Journal of Hydrology*, *275*, 229–241.
- Kinzelbach, W. (1987), The random walk method in pollutant transport simulation, *Groundwater Flow and Quality Modelling*, edited by E. Custodio et al., pp. 227–245, D. Reidel Publishing Company, Dordrecht.
- Kitanidis, P. K. (1994), Particle-tracking equations for the solution of the advection-dispersion equation with variable coefficients, *Water Resources Research*, *30*(11), 3225–3227.
- LaBolle, E. M., G. E. Fogg, and A. F. B. Tompson (1996), Random-walk simulation of transport in heterogeneous porous media: Local mass-conservation problem and implementation methods. *Water Resources Research*, *32*(3), 583–593.
- Lichtner, P. C., S. Kelkar, and B. Robinson (2002), New form of dispersion tensor for axisymmetric porous media with implementation in particle tracking, *Water Resources Research*, *38*, 1146, doi:10.1029/2000WR000100.
- Liou, M. L. (1966), A novel method of evaluating transient response, *Proc. IEEE*, *54*, 20–23.
- Li, Z., and M. L. Brusseau (2000), Nonideal transport of reactive solutes in heterogeneous porous media 6. Microscopic and macroscopic approaches for incorporating heterogeneous rate-limited mass transfer, *Water Resources Research*, *36*(10), 2853–2867.

- Liu, G., C. Zheng, and S. M. Gorelick (2004), Limits of applicability of the advection-dispersion model in aquifers containing connected high-conductivity channels, *Water Resources Research*, *40*, W08308, doi:10.1029/2003WR002735.
- Luthy, R. G., R. A. Aiken, M. L. Brusseau, S. D. Cunningham, P. M. Gschwend, J. J. Pignatello, M. Reinhard, S. j. Traina, W. J. Weber Jr., and J. C. Westall (1997), Sequestration of hydrophobic organic contaminants by geosorbents, *Environmental Science & Technology*, *31*(12), 3341–3347.
- Michalak, A. M., and P. K. Kitanidis (2000), Macroscopic behaviour and random-walk particle tracking of kinetically sorbing solutes, *Water Resources Research*, *36*(8), 2133–2146.
- Moler, C., and C. van Loan (2003), Nineteen dubious ways to compute the exponential of a matrix, twenty-five years later, *SIAM Review*, *45*(1), 3–49.
- Neretnieks, I. (1980), Diffusion in rock matrix: an important factor in radionuclide retardation?, *J. Geophys. Res.*, *85*(B8), 4379–4397.
- Nkedi-Kizza, P., J. W. Biggar, H. M. Selim, T. van Genuchten, P. J. Wierenga, J. M. Davidson, and D. R. Nielsen (1984), On the equivalence of two conceptual models for describing ion exchange during transport through aggregated oxisol, *Water Resources Research*, *20*(8), 1123–1130.
- Parzen, E. (1962), *Stochastic Processes*, Holden-Day, San Francisco, CA.
- Pignatello, J. J., and B. Xing (1996), Mechanisms of slow sorption of organic chemicals to natural particles, *Environmental Science & Technology*, *30*(1), 1–11.
- Prickett, Th. A., Th. G. Naymik, and C. G. Longquist (1981), A random walk solute transport model for selected groundwater quality evaluations, *Bulletin 65*, 103pp, Illinois State Water Survey.
- Ross, S. M. (2003), *Introduction to probability models*, 8th ed., 755 pp., Academic Press, Oxford.
- Rügner, H., S. Kleinedamm, and P. Grathwohl (1999), Long term sorption kinetics of phenanthrene in aquifer materials, *Environmental Science & Technology*, *33*(10), 1645–1651.
- Salamon, P., D. Fernández-García, and J. J. Gómez-Hernández (2006), A review and numerical assessment of the random walk particle tracking method, *Journal of Contaminant Hydrology*, doi:10.1016/j.jconhyd.2006.05.005, in press.

- Schumer, R., D. A. Benson, M. M. Meerschaert, and B. Baeumer (2003), Fractal mobile/immobile solute transport, *Water Resources Research*, 39(10), 1–12, doi:10.1029/2003WRR002141.
- Tompson, A. F. B. (1993), Numerical simulation of chemical migration in physically and chemically heterogeneous porous media, *Water Resources Research*, 29(11), 3709–3726.
- Toride, N., F. J. Leij, and M. T. van Genuchten (1995), The CXTFIT code for estimating transport parameters from laboratory or field tracer experiments, version 2.0, U.S. Salinity Lab., U.S. Dep. of Agric., Riverside Calif., 121 pp.
- Tsang, Y. W., and C. F. Tsang (2001), A particle-tracking method for advective transport in fractures with diffusion into finite matrix blocks, *Water Resources Research*, 37(3), 831–835.
- van Genuchten, M. Th., and P. J. Wierenga (1976), Mass transfer studies in sorbing porous media I. Analytical Solutions, *Soil Sci. Soc. Am. J.*, 40(4), 473–480.
- Valocchi, A. J., and H. A. M. Quinodoz (1989), Application of the random walk method to simulate the transport of kinetically adsorbing solutes, paper presented at Groundwater Contamination Symposium of the third IAHS Scientific Assembly, Int. Assoc. of Hydrol. Sci., pp. 35–42, Baltimore, Md.
- Wang, P. P., C. Zheng, and S. M. Gorelick (2005), A general approach to advective-dispersive transport with multirate mass transfer, *Advances in Water Resources*, 28, 33–42.
- Wen, X. H., and J. J. Gómez-Hernández (1996), The constant displacement scheme for tracking particles in heterogeneous aquifers, *Ground Water*, 34(1), 135–142.
- Woodbury, A. D., and E. A. Sudicky (1991), A reexamination of the geo-statistical characteristics of the Borden aquifer, *Water Resources Research*, 27(4), 533–546.
- Young, D. F., and W. P. Ball (1995), Effects of column conditions on the first-order rate modeling of nonequilibrium solute breakthrough, *Water Resources Research*, 31(9), 2181–2192.
- Zinn, B., and C. F. Harvey (2003), When good statistical models of aquifer heterogeneity go bad: A comparison of flow, dispersion, and mass transfer in connected and multivariate Gaussian hydraulic conductivity fields, *Water Resources Research*, 39(3), 1051, doi:10.1029/2001WR001146.

4

Modeling tracer transport at the Macrodispersion Experiment (MADE) site: Only a problem of scales?

submitted to *Water Resources Research*.

Abstract

We present a detailed geostatistical analysis of the flowmeter data at the Macrodispersion Experiment (MADE) site and simulate tracer transport in high-resolution conductivity fields, generated on the basis of this analysis. Evaluating the spatial continuity of the hydraulic conductivity data revealed a hole effect structure indicating an increased occurrence of clustered lenses or facies in the aquifer which appears to improve preferential flow. Furthermore, indicator variography did not show an increased connectivity of high/low hydraulic conductivity values. Tritium transport was modeled in three kriged fields as well as for three sequential simulations all of them using a high grid-resolution with a grid block size similar to the flowmeter measurement support scale to explicitly represent small scale heterogeneity. The kriged fields were not able to simulate anomalous tracer spreading as observed in the field based on an insufficient representation of the variance of $\ln K$. The sequential Gaussian simulations generally demonstrated a better tailing than the sequential Indicator simulation indicating that a multiGaussian distribution of $\ln K$

approximates field conditions better at the Columbus aquifer. Neglecting the hole effect structure for the spatial model of the Gaussian simulations resulted in a reduced tailing of the tracer illustrating the importance of preferential flow on anomalous solute transport. We conclude that, when small-scale variability of hydraulic conductivity is correctly modeled at the flowmeter measurement support scale, the advection-dispersion equation is capable of reproducing the anomalous tracer spreading at the MADE site and that mass transfer effects are principally the results of the use of an inadequate model grid block scale. Furthermore, the model chosen for the spatial correlation of the hydraulic conductivity plays a crucial role in reproducing the anomalous tracer spreading.

4.1 Introduction

Characterizing the spatial variation of hydrogeologic properties in an aquifer and its proper representation in numerical models is a key issue for environmental risk assessment, remediation engineering of contaminated groundwater or the design of underground repositories for radioactive material. Although significant advances were made using stochastic and/or deterministic/analytic approaches in the last decades, heterogeneity of hydrogeologic properties still remains as one of the major areas of concern in hydrogeology (*Carrera, 1993; de Marsily et al., 2005; Gómez-Hernández, 2006*). In order to enhance the understanding of solute transport in geologic formations several natural-gradient tracer tests were performed and detailed data sets were collected. Whereas the majority of the experiments focused on relatively homogeneous aquifers with $\sigma_{\ln K}^2 \approx 0.2$ (e.g. *Mackay et al., 1986; LeBlanc et al., 1991*), hydraulic conductivity measurements at the Columbus Air Force Base in Mississippi, commonly known as the Macrodispersion Experiment (MADE) site, revealed a strongly heterogeneous system with $\sigma_{\ln K}^2 \approx 4.5$ (*Rehfeldt et al., 1992*). Two tracer tests were conducted at this site (*Boggs et al., 1992; Adams and Gelhar, 1992; Boggs et al., 1993*) and both of them resulted in a strong non-Gaussian behavior, i.e., a highly asymmetric spreading of the plume with high concentrations maintained near the source and a far reaching tail with low concentrations.

A variety of modeling studies using many different approaches ranging from the classical advection-dispersion equation (ADE) to continuous time random walk has been performed, resulting in successful/unsuccessful reproduction of the spreading of the tracer plume. All of these studies give a range of arguments and hypotheses on why the tracer movement at the MADE site could or could not be predicted employing a certain model. This paper intends to examine some of the arguments presented and to give some new insights concerning the tracer transport at the MADE site. Therefore, we first briefly

summarize the previous studies performed and the conclusions presented in the following paragraphs.

During the first series of articles describing the MADE tracer test, *Adams and Gelhar* (1992) performed a spatial moment analysis of the concentration measurements. They found that the plume shape is strongly non-Gaussian and that, although the lower order moments could be reproduced reasonably well with two different analytical transport models (advection only from a continuous source in a uniform flow field and advection-dispersion in a converging nonuniform flow field), the rapidly advancing leading tracer plume edge and the decline of solute mass given by the zeroth spatial moment were not captured by the models. Though not referring directly to the strong asymmetry of the plume *Adams and Gelhar* (1992) concluded that the representation of large-scale flow nonuniformity is essential when trying to account for plume spreading and dilution at this site.

Eggleston and Rojstaczer (1998) examined the large-scale spatial trends in hydraulic conductivity and their influence on contaminant transport at the MADE site using flowmeter measurements of hydraulic conductivity and a three-dimensional transport model considering advection only. None of their different hydraulic conductivity fields could recreate the non-Gaussian shape of the tracer plume successfully. *Eggleston and Rojstaczer* (1998) attributed this failure to three possible factors: (1) failure of the trend estimation methods to capture large-scale trends present in the aquifer, (2) use of incorrect model parameters other than hydraulic conductivity, or (3) local-scale hydraulic conductivity variations exerting significant control over tracer movement. Although all three factors possibly contribute to the failure of the model, *Eggleston and Rojstaczer* (1998) conclude that it is the local-scale variability of hydraulic conductivity not being captured by their model, which exerts the most significant control over the observed plume behavior.

Finally, the most recent attempt to model the MADE site tracer plume using the macrodispersion model was presented by *Barlebo et al.* (2004). Using only hydraulic head and concentration measurements for the calibration of an inverse flow and transport model, they reproduced reasonably well the highly irregular plume shape. However, calibrated hydraulic conductivities for their zoned distribution were generally as much as a factor of 5 higher than the measured hydraulic conductivities in the field using a flowmeter. *Barlebo et al.* (2004) conclude therefore that the macrodispersion model is able to reproduce the extensive plume spreading, but that flowmeter measurements of hydraulic conductivity could be biased and that random errors in these measurements obscure abrupt lateral variations of hydraulic conductivity.

Another approach used to explain solute transport at the MADE site is the dual-domain mass transfer model. *Feehley et al.* (2000) compare this model with the ADE using two heterogeneous hydraulic conductivity fields

obtained by ordinary kriging and by choosing one realization of a conditional geostatistical simulation based on fractional Brownian motion. The results demonstrated that tracer spreading using the ADE with a numerical grid scale of $2 \times 2 \times 0.5$ m was not modeled correctly with neither of the two heterogeneous fields. *Feehley et al.* (2000) attribute this to the fact that preferential flow pathways, which strongly influence asymmetric tracer spreading, may exist at a scale smaller than the grid spacing. To overcome this inability they suggest the use of the dual domain approach which, after calibrating the immobile porosity and the mass transfer rate, was able to recreate the non-Gaussian shape of the tracer plume.

A similar study was performed by *Harvey and Gorelick* (2000). They attempt to predict one-dimensional concentration profiles of the MADE experiment using the macrodispersion model and an analytical homogeneous solution of the mass transfer model. Results indicate that the mass transfer model accounts better for the dominant behavior of the system. *Harvey and Gorelick* (2000) argue that this is based on large contrasts in hydraulic conductivity at the centimeter to decimeter scale. They support their argument demonstrating that the conductivity profiles obtained with the permeameter, which has a smaller measurement support scale (7.6 cm) as the flowmeter (15 cm), show a significantly higher variability than the flowmeter measurements. They furthermore argue that physical mass transfer caused by the intragranular pore diffusion and diffusion into dead-end pores might significantly influence the non-Gaussian behavior of the tracer plume.

The MADE site experiment was also analyzed by *Berkowitz and Scher* (1998) using the continuous time random walk formalism. They compare the field experiment with the dominant aspects of anomalous solute transport in fracture networks. Characterizing key features of fracture properties (i.e. segment length and fluid flow) and mapping them on probability distributions, the spatial distribution of the plume concentration as well as breakthrough curves can be calculated analytically using the continuous time random walk approach. Comparing the results of the fracture network to the MADE site *Berkowitz and Scher* (1998) demonstrate that time-dependent anomalous, i.e. non-Gaussian, transport also exists in other geological formations than rock fractures. They conclude that when mapping preferential flow paths and high flow variability of the heterogeneous aquifer at the Columbus Air Force Base to a series of channels or “fractures” tracer transport can be reproduced using the continuous time random walk method.

Finally, fractional derivatives were applied either using a fractional ADE (*Benson et al.*, 2001), a fractal mobile/immobile equation (*Schumer et al.*, 2003), or a subordination model governed by a fractional partial differentiation (*Baeumer et al.*, 2001) to simulate the MADE experiment. These approaches were developed having all the same underlying assumption that the

small-scale variability of the hydraulic conductivity induces the non-Gaussian behavior and anomalous spreading of the plume, and hence using the classical ADE approaches would not lead to a successful reproduction of the tracer experiment. All of these approaches were able to provide a good fit to the observed field data after calibrating the necessary additional parameters.

The reader should note that a few other articles exist dealing with the MADE site (*MacIntyre et al.*, 1993; *Zheng and Jiao*, 1998; *Julian et al.*, 2001; *Brauner and Widdowson*, 2001; *Bowling et al.*, 2005, 2006). However, as some of these studies focus on other aspects of the MADE aquifer or do present similar results as the ones outlined above we do not review them here for the sake of conciseness.

Considering the reviewed articles the principal reason why the macrodispersion model is not successful in reproducing the tracer plume appears to be the inadequate representation of the small scale heterogeneities. Some authors claim that the grid resolution used is not sufficiently small, implying that with an adequately high grid-resolution and the flowmeter measurements solute transport could be reproduced correctly. Others state that the measurement scale for the flowmeter measurements is too large, hence leading to a smaller variance in the hydraulic conductivity data set or even to a measurement bias, which in turn results into an incorrect reproduction of the spatial variability of the conductivity field. In fact, if this would be the case, one would even have to question the usefulness of the flowmeter technique to evaluate local-scale hydraulic conductivity distribution in highly heterogeneous aquifers. Finally, some authors maintain that heterogeneity at the pore-scale has a significant impact via pore-scale mass transfer and therefore even the use of an extremely small grid-scale in combination with the ADE cannot reproduce the non-Gaussian features of the plume and hence one has to employ different types of models, e.g. dual domain, continuous time random walk, or fractional derivatives.

Another often used hypothesis for the failure of the macrodispersion model is the possible existence of connected, small scale high-conductivity channels at the MADE site aquifer. In a variety of synthetic studies (*Wen and Gómez-Hernández*, 1998; *Zheng and Gorelick*, 2003; *Zinn and Harvey*, 2003; *Liu et al.*, 2004) it was demonstrated that these preferential flowpaths can create extensive downstream spreading of low concentrations while maintaining high concentrations near the source. These flowpaths might even exist in aquifers, which have a near-identical lognormal conductivity distribution as is the case for the MADE site. Furthermore, results showed that when describing the upscaled flow and solute transport for these cases, only the mobile-immobile domain mass transfer model was able to model solute transport well. It is interesting to note that all these issues are still the topic of a controversial

discussion amongst hydrogeologists as published in a comment and its corresponding reply by *Molz et al. (2006)* and *Hill et al. (2006)*.

In this study we intend to examine the question whether the flowmeter measurement support scale is small enough to correctly simulate tracer spreading at the MADE site using the ADE or if it is the heterogeneity below this scale dominating tracer spreading. In contrast to other studies we utilize to this end a model grid block scale which has the same size as the flowmeter measurement support scale and hence explicitly includes small-scale variability of hydraulic conductivity. We first perform an extensive univariate and bivariate geostatistical analysis of the flowmeter measurements in order to infer the two-point statistics (i.e., mean, variance, variogram) of the $\ln K$ field and its associated indicator variables for different thresholds. We present several forms of variogram models and analyze the use of indicator variables. Then, the modeling approach is briefly outlined and the simulation results of the hydraulic conductivity fields, using kriging and Monte Carlo simulations are presented. Limitations of the kriging interpolation at the MADE site are shown and the benefits of stochastic simulations at the measurement scale are illustrated. Furthermore, we investigate the possible existence of connected high-conductivity channels and comment on the effects of upscaling of the model grid block scale on the simulated tracer plume. Finally, we discuss the results in the light of the previously mentioned hypotheses and summarize the main results and conclusions of this paper.

4.2 Geostatistical Analysis

This geostatistical analysis is based on 2495 flowmeter measurements of the hydraulic conductivity performed in 62 boreholes (see Figure 4.1). Note that in contrast to the analysis presented by *Rehfeldt et al. (1992)* only measurements located within the model domain plus 11 additional locations for the MADE-2 test are used and hence the mean and the variance differ slightly from the values presented by *Rehfeldt et al. (1992)*. The frequency distribution and the univariate statistics of the data set are illustrated in Figure 4.2.

To determine the spatial continuity for $\ln K$ we employ the commonly used experimental semivariogram (e.g. *Journel and Huijbregts, 1978*)

$$\gamma(\mathbf{h}) = \frac{1}{2N(\mathbf{h})} \sum_{\alpha=1}^{N(\mathbf{h})} [z(\mathbf{u}_{\alpha}) - z(\mathbf{u}_{\alpha} + \mathbf{h})]^2 \quad (4.1)$$

where $N(\mathbf{h})$ is the number of data pairs within the class of distance and direction, \mathbf{h} is the separation vector, and $z(\mathbf{u}_{\alpha})$ denotes a measurement with \mathbf{u}_{α} being the vector of spatial coordinates of the α th individual. In the following study we assume that depositional structures in the aquifer, e.g. clay lenses,

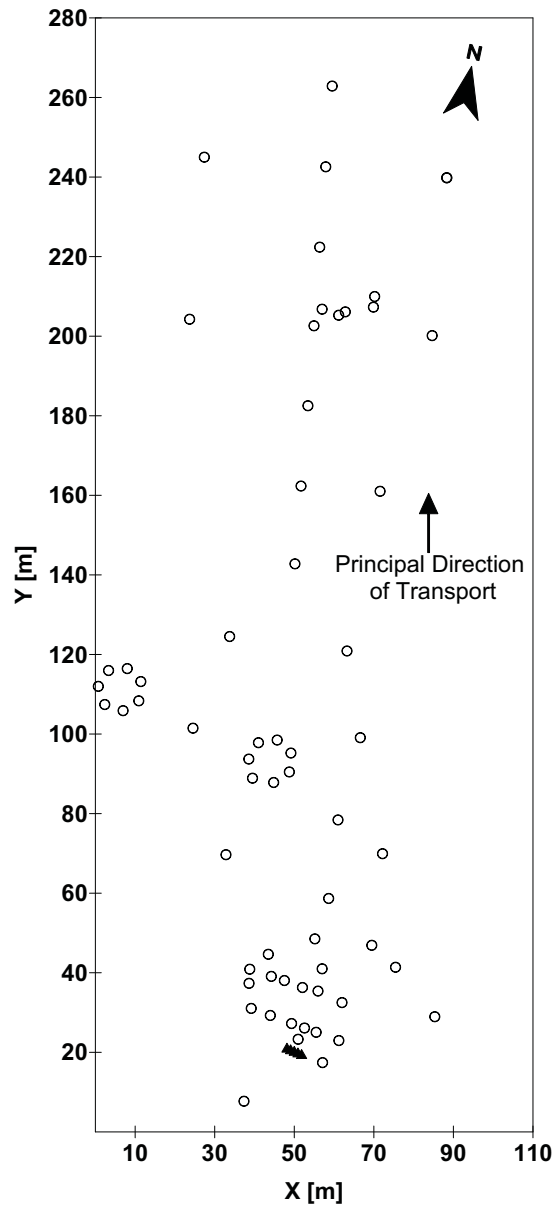


Figure 4.1. Model domain used for the simulations. Circles denote flowmeter well locations. Triangles denote the five solute injection wells.

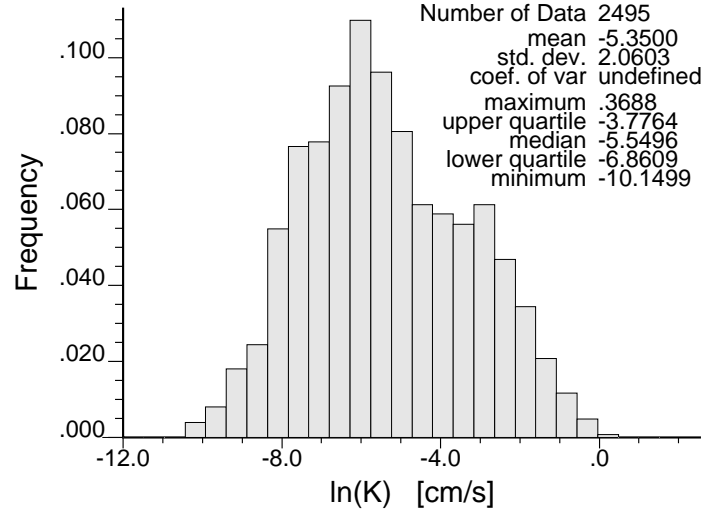


Figure 4.2. Frequency distribution and univariate statistics of the 2495 flowmeter measurements.

high permeability zones, are approximately horizontal, as sustained by various other authors (e.g. *Rehfeldt et al.*, 1992; *Bowling et al.*, 2005). Hence, only horizontal and vertical spatial continuity will be analyzed.

Figure 4.3 shows the omnidirectional horizontal and vertical experimental semivariogram and the corresponding fitted spherical model, which has the following equation

$$\gamma(\mathbf{h}) = c_0 + c_1 \cdot \text{Sph}(\|\mathbf{r}(\mathbf{h})\|) = \begin{cases} c_1 \cdot [1.5\|\mathbf{r}(\mathbf{h})\| - 0.5\|\mathbf{r}(\mathbf{h})\|^3] & \text{if } \|\mathbf{h}\| \leq \|\mathbf{r}(\mathbf{h})\| \\ c_1 & \text{if } \|\mathbf{h}\| \geq \|\mathbf{r}(\mathbf{h})\| \end{cases} \quad (4.2)$$

where c_0 is the nugget, c_1 is the sill, and $\mathbf{r}(\mathbf{h})$ is the corresponding separation vector for an analog variogram model, oriented parallel to the correlation structure and with unitary ranges, that is obtained by rotation and translation of coordinates as

$$\mathbf{r}(\mathbf{h}) = \mathbf{T} \cdot \mathbf{R} \cdot \mathbf{h} \quad (4.3)$$

The translation matrix \mathbf{T} and the rotation matrix \mathbf{R} are given as

$$\mathbf{T} = \begin{pmatrix} \frac{1}{a_1} & 0 & 0 \\ 0 & \frac{1}{a_2} & 0 \\ 0 & 0 & \frac{1}{a_3} \end{pmatrix} \quad \mathbf{R} = \begin{pmatrix} \cos\alpha & \sin\alpha & 0 \\ -\sin\alpha & \cos\alpha & 0 \\ 0 & 0 & 1 \end{pmatrix}$$

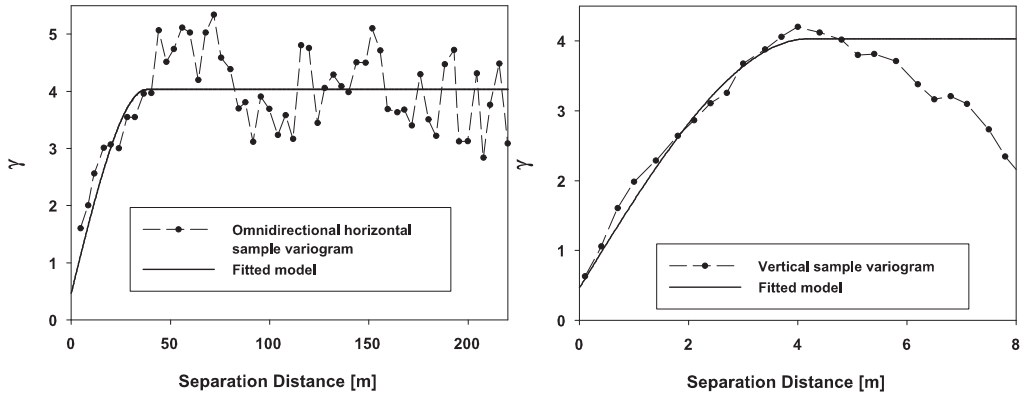


Figure 4.3. Omnidirectional horizontal and vertical isotropic variograms and fitted spherical model for the $\ln K$ flowmeter data.

where $a_{1,2,3}$ are the ranges of the corresponding axes of anisotropy and α is the rotation angle. Note that the rotation matrix only includes one rotation of the y -axis in the horizontal plane, where the rotation angle is measured in degrees clockwise from the positive y -axis, as the presented variogram models in this section solely consider geometric anisotropy in the horizontal plane. Table 4.2 presents the parameters for the model used in Figure 4.3. Similarly to *Rehfeldt et al. (1992)* the directional analysis did not reveal a horizontal anisotropy and the parameters for the isotropic spherical model fit of Figure 4.3 are comparable to the exponential semivariogram model obtained by *Rehfeldt et al. (1992)*.

However, it can be observed that the omnidirectional horizontal experimental semivariogram in Figure 4.3 shows a non-monotonic behavior with a cyclic pattern for separation distances larger than $\sim 40\text{m}$, which is not captured well by the corresponding model. *Rehfeldt et al. (1992)* accounted for this uncertainty defining upper and lower confidence limits for the sill values. Another approach to include this periodic behavior is using a variogram model consisting of a nested structure which contains a spherical and a so called "hole effect" model (see Figure 4.4):

$$\gamma(\mathbf{h}) = c_0 + c_1 \cdot \text{Sph}(\|\mathbf{r}_1(\mathbf{h})\|) + c_2 \cdot [1 - \cos(\|\mathbf{r}_2(\mathbf{h})\|\pi)] \quad (4.4)$$

Hole effect structures most often indicate a form of periodicity, e.g. lenses of high/low conductivity, which is a common spatial characteristic in geology (*Journal and Huijbregts, 1978; Pyrcz and Deutsch, 2003*). It was demonstrated by various authors (e.g. *Ritzi, 2000; Barrash and Clemo, 2002*) that aquifers dominated by distinct hydrofacies, as is also the case for the fluvial aquifer at the MADE site, often exhibit periodic structures in their variograms.

Model	Nugget c_0	Ranges [m]			Structure sill c_i	$\sum_{i=0}^n c_i$	Rotation angle α
		a_1	a_2	a_3			
Spherical (Eq.(4.2))	0.4669	38	38	4.2	3.5657	4.0326	0°
Nested structure (Eq.(4.4))							
Spherical	0.4245	80	32	4.1	3.8204		0°
Hole effect	-	80	-	-	0.8914	5.1363	0°

Table 4.1. Geostatistical model parameters for Figures 4.3 and 4.4.

In order to be positive definite the chosen cosine model may only exist in one direction (*Journal and Huijbregts, 1978*). Directional variogram analysis demonstrated that a good fit is obtained when the y -axis coincides with the principal direction of correlation. Figure 4.4 illustrates the disappearance of the hole effect in the direction orthogonal to the y -axis. Parameters values for the matched model of Eq.(4.4) are presented in Table 4.2.

When evaluating spatial uncertainty the conditional cumulative distribution function (cdf) for each location of the aquifer has to be determined. The most widely used method to infer the parameters of the conditional cdf is to assume a multiGaussian distribution of the $\ln K$ random field. However, this approach has several shortcomings possibly significant to the site characteristics of the MADE aquifer. Firstly, it assumes not only that the one-point cdf of the data is normally distributed, but also that multiple-point distributions of the data exhibit multi-normality. Unfortunately, although the univariate frequency distribution shows a near-identical lognormal behavior (see Figure 4.2 and also *Rehfeldt et al. (1992)*) multiple point experimental cdfs cannot be checked in practice. Secondly, under the multiGaussian approach, extremely large/small values are spatially uncorrelated. However, as already mentioned above, connectivity of high hydraulic conductivity values may play a crucial role for tracer transport at the MADE site. To overcome these shortcomings the indicator approach, which does not assume any particular shape of the conditional distributions, can be applied.

The first step in the indicator approach is the selection of the number of thresholds and their values. In order to provide a reasonable discretization of the local distribution the nine deciles of the sample cumulative distribu-

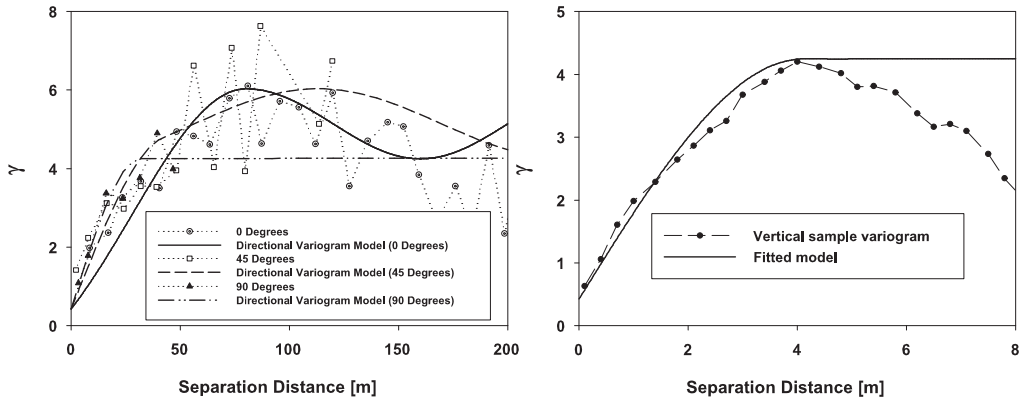


Figure 4.4. Directional horizontal and vertical variograms and fitted model with hole effect for the $\ln K$ flowmeter data. The rotation angle of the directional variograms is measured in degrees clockwise from the positive y -axis

tion were chosen and transformed to the corresponding indicator categories according to

$$i(\mathbf{u}_\alpha; z_k) = \begin{cases} 1 & \text{if } z(\mathbf{u}_\alpha) \leq z_k \\ 0 & \text{otherwise} \end{cases} \quad (4.5)$$

where z_k are the threshold values. Spatial continuity for the different thresholds is then evaluated using the standardized indicator semivariogram (e.g. *Goovaerts, 1997*):

$$\frac{\gamma_I(\mathbf{h}; z_k)}{\sigma_I^2} = \frac{1}{2N(\mathbf{h})} \sum_{\alpha=1}^{N(\mathbf{h})} [i(\mathbf{u}_\alpha; z_k) - i(\mathbf{u}_\alpha + \mathbf{h}; z_k)]^2 \quad (4.6)$$

where σ_I^2 is the indicator variance given as $\sigma_I^2 = F(z_k)[1 - F(z_k)]$. Directional variogram analysis of the indicator categories demonstrated that the best fit was obtained using a nested structure consisting of a spherical and an exponential model according to

$$\frac{\gamma_I(\mathbf{h}; z_k)}{\sigma_I^2} = c_0 + c_1 \cdot \text{Sph}(\|\mathbf{r}_1(\mathbf{h})\|) + c_2 \cdot [1 - \exp(-3\|\mathbf{r}_2(\mathbf{h})\|)] \quad (4.7)$$

Figure 4.5 illustrates the experimental variograms and the corresponding model fit of the 0.1, 0.4, and 0.9 decile cutoffs. The complete set of matched indicator model parameters is presented in Table 4.2. It can be observed that the spatial continuity increases from the 0.1 decile to the 0.7 decile and then

Threshold		Model	Nugget c_0	Ranges [m]			Structure sill c_i	Rotation angle α
z_k	$F(z_k)$			a_1	a_2	a_3		
-7.948	0.1	Spherical	0.2	10	10	1.2	0.26	0°
		Exponential		15	15	4.0	0.57	0°
-7.212	0.2	Spherical	0.2	50	50	4.5	0.37	0°
		Exponential		2.8	2.8	1.8	0.49	0°
-6.556	0.3	Spherical	0.2	65	65	4.7	0.32	0°
		Exponential		8	8	2.5	0.54	0°
-6.066	0.4	Spherical	0.2	90	60	4.6	0.32	150°
		Exponential		20	10	2.7	0.51	150°
-5.550	0.5	Spherical	0.2	100	85	5.4	0.32	150°
		Exponential		30	15	3.5	0.51	150°
-5.011	0.6	Spherical	0.2	130	110	6.0	0.32	150°
		Exponential		40	25	4.0	0.51	150°
-4.227	0.7	Spherical	0.2	150	120	6.4	0.32	150°
		Exponential		40	28	5.6	0.51	150°
-3.339	0.8	Spherical	0.2	90	90	7.6	0.32	0°
		Exponential		20	20	3.3	0.51	0°
-2.454	0.9	Spherical	0.2	65	40	5.8	0.32	0°
		Exponential		13	13	1.4	0.51	0°

Table 4.2. Geostatistical model parameters for the indicator variogram model according to Eq.(4.7).

decreases until the 0.9 decile. No significantly higher spatial continuity in the horizontal direction of the 0.9 decile could be observed. A slight anisotropy in the horizontal plane was detected for the 0.4 to 0.7, and 0.9 deciles, whereas the anisotropy axis was additionally rotated 150° for the deciles 0.4 to 0.7.

Note that some authors have also performed a multifractal analysis of the hydraulic conductivity data at the MADE site suggesting a truncated power law variogram with fractional Brownian motion as a possible model for the spatial variations of K (e.g. *Liu and Molz, 1997; Feehley et al., 2000*). Although this might be a valid approach, we focused here on the more classical geostatistical techniques and do not assess the ability of fractional Brownian motion to characterize subsurface heterogeneity at the MADE site.

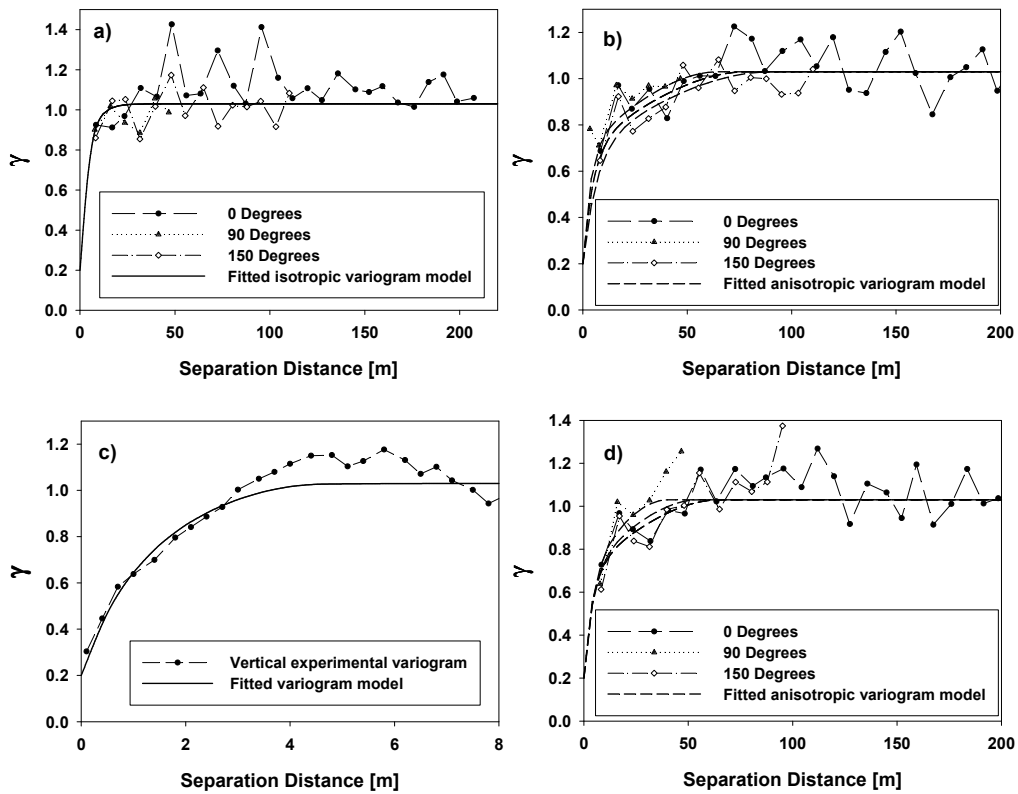


Figure 4.5. Standardized indicator variograms for the following directions and deciles: a) Directional horizontal indicator variogram and fitted model for 0.1 decile b) Directional horizontal indicator variogram and fitted model for 0.4 decile c) vertical indicator variogram and fitted model for 0.4 decile d) Directional horizontal indicator variogram and fitted model for 0.9 decile. The rotation angle of the directional variograms is measured in degrees clockwise from the positive y -axis.

4.3 Modeling Approach

A three-dimensional block centered finite difference grid with a total size of $110 \times 280 \times 10.5$ m was used for modeling the aquifer (see Figure 4.1). The grid spacing was chosen to be of a similar magnitude or smaller than the flowmeter measurement support scale. Hence, grid blocks are 1×1 m in the horizontal direction and 0.15 m in the vertical direction resulting in a total of 2,156,000 nodes. Constant head boundaries at $y = 0$ m and $y = 280$ m as well as no-flow boundaries at $x = 0$ m and $x = 110$ m limit the model domain.

Although being aware of the possible significance of transient flow on tracer transport at the MADE site, we simulated only steady state flow in a confined system using the well-known MODFLOW code (*Harbaugh et al.*, 2000) as we focused during this work on the influence of the heterogeneity of hydraulic conductivity. Flow model calibration was performed similarly to *Feehley et al.* (2000). The hydraulic heads monitored within 1 year of the tracer test were averaged and used as the observed steady state heads. Boundary heads were adjusted manually to a hydraulic conductivity field created using ordinary kriging (see the following section for details) until a satisfactory match between observed and modeled heads was obtained. These boundary heads were then used for the remaining flow simulations.

Tracer transport using the classical, Fickian advection-dispersion transport equation for conservative transport was simulated with the random walk particle tracking code RW3D (*Fernández-García et al.*, 2005; *Salamon et al.*, 2006). We chose the random walk approach because of its computational efficiency and the non-existence of numerical dispersion especially concerning advection-dominated cases with a high spatial discretization as is the case here. The random walk code uses a hybrid scheme for the velocity interpolation which has demonstrated to provide local as well as global divergence-free velocity fields within the solution domain and a continuous dispersion tensor field that approximates well mass balance at grid interfaces of adjacent cells with contrasting hydraulic conductivities (*LaBolle et al.*, 1996; *Salamon et al.*, 2006). Furthermore, a constant-displacement scheme (*Wen and Gómez-Hernández*, 1996) which modifies automatically the time step size for each particle according to the local velocity is employed in order to decrease computational effort. A Courant number of 0.0125 for the constant-displacement was used for all simulations. The local-scale longitudinal dispersivity was fixed at 0.1 m which corresponds approximately to the value calculated by *Harvey and Gorelick* (2000) for a column experiment with a 1 m long soil column from the MADE site aquifer. Transverse horizontal and vertical local-scale dispersivity values were chosen to be one order of magnitude lower than the longitudinal dispersivity resulting in a value of 0.01 m. Apparent diffusion for tritium was selected to be $1.0 \text{ cm}^2/\text{d}$ according to *Gillham et al.* (1984). An

average total porosity of 0.32 as determined from the soil cores by *Boggs et al.* (1992) was assigned to the entire model area.

During the field experiment tritium was injected through five injection wells for a period of 48.5 hours. However, as tracer injection generally is strongly subject to specific local conditions which are difficult to reproduce, e.g. well characteristics, hydraulic head cone during injections, etc., we decided to employ the mass distribution measured for the 27 days snapshot as an initial condition. For this purpose the measured concentrations of the corresponding snapshot were used to achieve a spatial interpolation of the tracer concentration in the aquifer. Then the tracer mass for each cell was calculated and a total of 50,000 particles, where each particle was assigned the same mass, was allocated according to the total amount of mass in each cell.

In the following section longitudinal mass profiles of the tritium plume (MADE-2 tracer experiment, *Boggs et al.*, 1993) and the simulated plumes at 328 days are compared. These profiles were obtained by integrating the mass of 28 equally spaced zones, each of 10 m width, along the general flow direction (the y axis) and normalizing it by the total injected mass.

Model	mean $\ln K$ [cm/s]	variance $\ln K$
<i>Flowmeter Measurements</i>	-5.35	4.245
<i>Ordinary Kriging</i>		
Sph. Model (Eq. (4.2))	-5.218	1.676
Sph. + Hole Effect Model (Eq. (4.4))	-5.3024	2.0433
<i>Indicator Kriging</i>		
Sph. + Exp. Model (Eq. (4.7))	-5.217	2.376
<i>Sequential Gaussian Simulation</i>		
Sph. Model (Eq. (4.2))	$\langle -5.169 \rangle^a$	$\langle -4.652 \rangle^a$
Sph. + Hole Effect Model (Eq. (4.4))	$\langle -5.281 \rangle^a$	$\langle 4.736 \rangle^a$
Realization #7	-5.1589	5.3814
Realization #19	-4.914	4.754
Realization #26	-4.8234	4.6195
Realization #47	-5.229	4.54
Realization #56	-5.343	4.969
Realization #80	-5.2897	5.166
<i>Sequential Indicator Simulation</i>		
Sph. + Exp. Model (Eq. (4.7))	$\langle -5.237 \rangle^a$	$\langle 3.815 \rangle^a$

^aensemble mean

Table 4.3. Statistical characteristics for generated hydraulic conductivity fields.

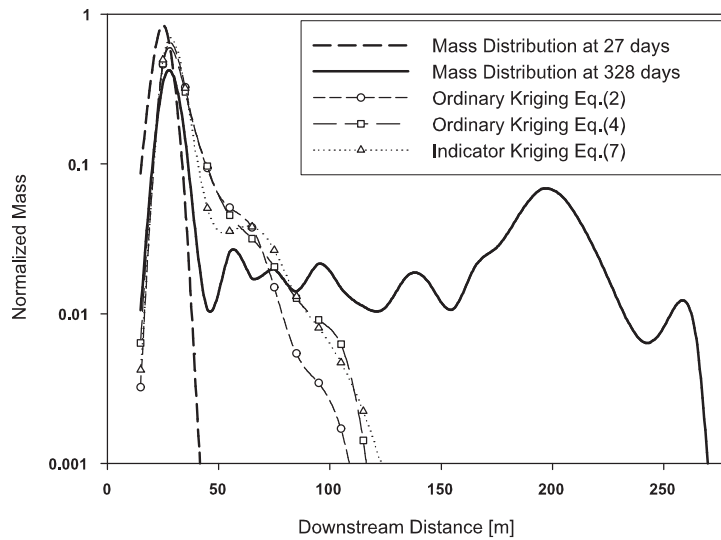


Figure 4.6. Longitudinal mass distribution profiles of the tritium plume and predictions using ordinary and indicator kriging to generate a hydraulic conductivity field. The ordinary kriged fields are generated using Eq. (4.2) and (4.4), respectively, as random function model with the parameters given in Table 4.2. The indicator kriged field was obtained using Eq. (4.7) with the parameters of Table 4.2.

4.4 Simulation Results

4.4.1 Kriging

The most common approach to interpolate sparse hydraulic conductivity data is the kriging algorithm, which was also applied by various authors to the MADE site (e.g. *Eggleston and Rojstaczer, 1998; Fehley et al., 2000*). These methods are basically variations of a least-squares linear regression incorporating the ability to account for different models of spatial continuity. All kriging algorithms have the objective to find an optimal estimate for an unmeasured location and thereby minimizing the estimation variance. In order to evaluate the useability of this geostatistical approach for the herein examined aquifer three conductivity fields generated by ordinary kriging and indicator kriging conditioned to the flowmeter measurements were generated employing the GSLIB code (*Deutsch and Journel, 1998*). Two ordinary kriging fields are obtained using the random function model of Eq. (4.2) and (4.4), respectively, with the parameter values presented in Table 4.2. The indicator kriging field was generated using Eq. (4.7) with the parameters of Table 4.2.

Figure 4.6 illustrates the results for the tritium transport in those fields. Clearly, none of the different kriging methods reproduces the strong non-

Gaussian shape of the tritium plume. This is actually not surprising as it demonstrates one of the shortcomings of this approach, which is especially significant for highly heterogeneous aquifers: interpolation algorithms tend to smooth out local details of the spatial variability of the random variable, i.e. small values are overestimated and large values are underestimated (e.g. *Goovaerts, 1997*). Unfortunately, solute transport is highly sensitive to the extreme values of hydraulic conductivity, particularly for the anomalous tracer spreading at the MADE site. A second disadvantage of the kriging algorithm is that the smoothing is greater at locations being estimated farther away from the data locations whereas smoothing gets smaller closer to the data measurements. That is, in regions with scarce $\ln K$ data kriging interpolation yields values close to the geometric mean whereas in regions with dense data points kriging interpolation more closely follows the "true" variability. These deficiencies become evident when looking at the statistical characteristics of the interpolated fields as shown in Table 4.3. While reproducing well the mean of $\ln K$, all interpolated fields severely underestimate the variance. These negative effects could only be alleviated by using an extremely dense network of measurement points, which is not feasible in practice. Hence, kriging is an inappropriate method for estimating the hydraulic conductivity field at the MADE site and thus reproducing solute transport using the kriged fields in combination with the advection-dispersion concept must fail, independently of an incorrect choice of the model grid scale or the potential incapacity of the ADE to simulate anomalous transport.

4.4.2 Sequential Simulation

Sequential simulation generates multiple, equally probable realizations of the joint distribution of the hydraulic conductivity values in space. In contrast to the kriging algorithm it closely reproduces the statistics considered decisive for the problem in hand, i.e. a better reproduction of the histogram and the variogram model, however with the cost of having to deal with a set of tens or often hundreds alternative representations. In this study a sequential Gaussian simulation, which assumes a multiGaussian random function model for the entire multivariate distribution, was used as well as sequential Indicator simulation, which does not assume any particular shape for the conditional distributions. All simulations are conditioned to the 2495 flowmeter measurements.

Simulations performed are comprised of a total of 40 realizations. Note that when performing Monte Carlo simulations it is desirable to have approximately 100 or more realizations in order to characterize better the uncertainty of solute transport. However, due to the very large amounts of data created with a model of more than 2 million nodes and limitations in computational time, only 40 realizations for each sequential simulation were performed.

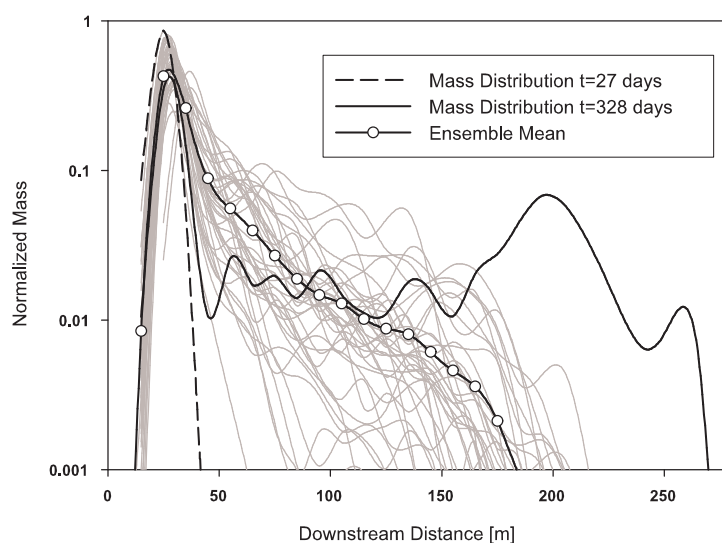


Figure 4.7. Longitudinal mass distribution profiles of the tritium plume and predictions using sequential Gaussian simulation using Eq. (4.2) as random function model with the parameters given in Table 4.2.

Figure 4.7 illustrates the longitudinal mass distribution profiles of the sequential Gaussian simulation generated using the GCOSIM code (*Gómez-Hernández and Journel, 1993*) with the spatial model of Eq. (4.2) and the corresponding parameters of Table 4.2. The ensemble statistics of the 40 realizations are presented in Table 4.3. It can be observed that the solute transport uncertainty in this simulation is considerable and that some realizations exhibit a significantly better tailing in comparison to the kriged fields as a result of the improved representation of the variability of hydraulic conductivity (see Table 4.3) and the variogram model. Nevertheless, none of the realizations is able to reproduce a similarly extensive spreading as observed in the field.

Figure 4.8 presents the results of the sequential Gaussian simulation with the spatial model of Eq. (4.4) and the corresponding parameters of Table 4.2. Note that in this case for a better definition of the solute transport uncertainty the Monte Carlo simulation is comprised of 80 realizations. It can be observed that the uncertainty for the different realizations increases in comparison to Figure 4.7 leading to six realizations which reproduce well the tailing measured in the field (see Figure 4.9). The statistical characteristics of the sequential simulation and the six realizations producing a strong tailing are shown in Table 4.3. A horizontal section of the conditioned hydraulic conductivity field of realization #80 at a relative elevation of $z = 8.1$ m is presented in Figure 4.10 and a horizontal, depth integrated concentration distribution as well as

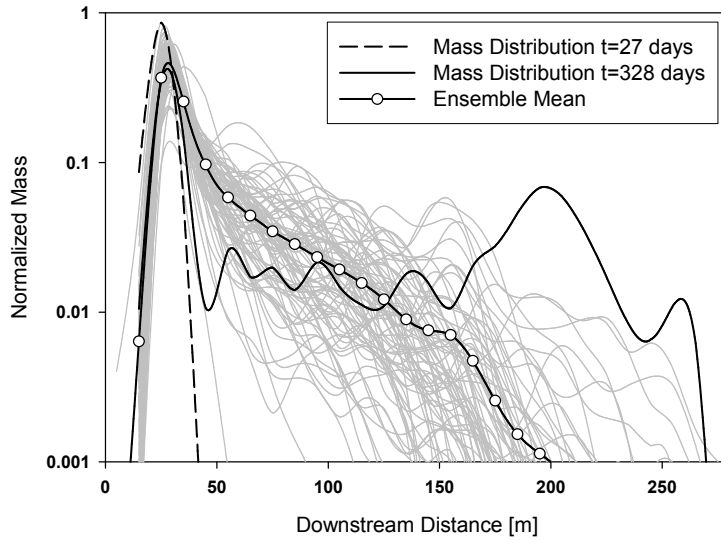


Figure 4.8. Longitudinal mass distribution profiles of the tritium plume and predictions using sequential Gaussian simulation using Eq. (4.4) as random function model with the parameters given in Table 4.2.

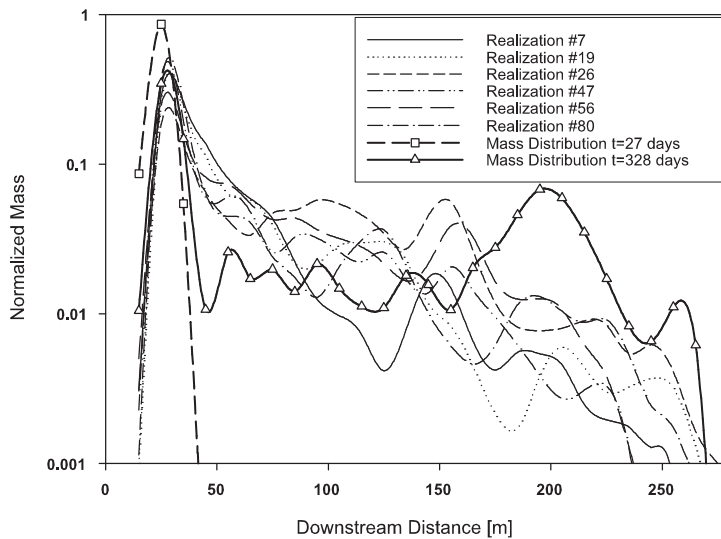


Figure 4.9. Longitudinal mass distribution profiles of the tritium plume and predictions of six realizations of the sequential Gaussian simulation exhibiting a strong tailing (using Eq. (4.4) as random function model).

a vertical, laterally integrated concentration distribution of realization #80 is shown in Figure 4.11. The concentration distribution of Figure 4.11b is in very good agreement with the data observed in the field (see Figure 4-1, *Boggs et al.*, 1993), whereas the tracer plume of Figure 4.11a displays a more narrower appearance than in the field. Evidently this is the effect of approximating a transient flow field, which shows a complex temporal variability of the direction of hydraulic gradient (*Boggs et al.*, 1992), with a steady state model. Furthermore, none of the realizations is able to simulate the increase in tracer mass at a downstream distance between approximately 170 m and 240 m. This is most likely due to an artificial overestimation of the tracer mass in this area caused by the combination of two factors: (1) rapid solute transport in very narrow zones of the aquifer caused by strong preferential flow, and (2) the sampling well network discretization is increased significantly at downstream distances of approximately larger than 160 m. Hence, interpolating the local tracer concentration measurements to the neighboring cells in order to obtain isocontours from which the mass distribution can be calculated leads most likely to an overestimation of mass downstream. Nevertheless and most importantly, it is clear that a similarly anomalous tracer spreading can be obtained with the spatial model of Eq. (4.4) and a model grid scale which corresponds to the flowmeter measurement scale.

Finally, Figure 4.12 illustrates the results of the sequential Indicator simulation generated using the ISIM code (*Gómez-Hernández and Srivastava*, 1990) with the geostatistical model parameters given in Table 4.2. Clearly, the sequential Indicator simulation using the variography obtained from the field data is not able to create the anomalous tracer behavior. This is somewhat surprising as alluvial aquifers, where normally distinct hydrofacies with strongly varying characteristics prevail, are generally modeled better with an indicator approach or other structure-imitating methods (e.g. *Johnson*, 1995; *Koltermann and Gorelick*, 1996; *Zappa et al.*, 2006), which do not assume the multivariate distribution to be Gaussian. However, as the hydraulic conductivity field at the MADE site appears to have a multiGaussian-like behavior expressed by the fact that extreme threshold values of the indicator variables exhibit decreasing integral scales, realizations of a Gaussian simulation constitute a better approximation to the aquifer variability than those provided by sequential Indicator simulation which are instead hindered by the limited number of thresholds.

4.5 Discussion

The herein presented geostatistical analysis and the results of the transport model support or weaken certain arguments used to explain the anomalous

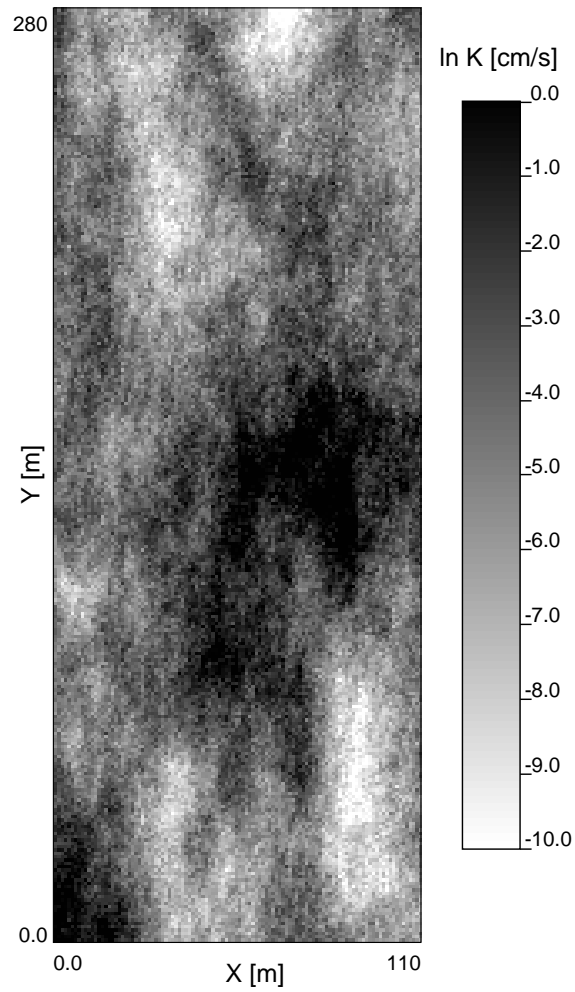


Figure 4.10. Horizontal slice of the hydraulic conductivity field #80 for $z = 8.1$ m.

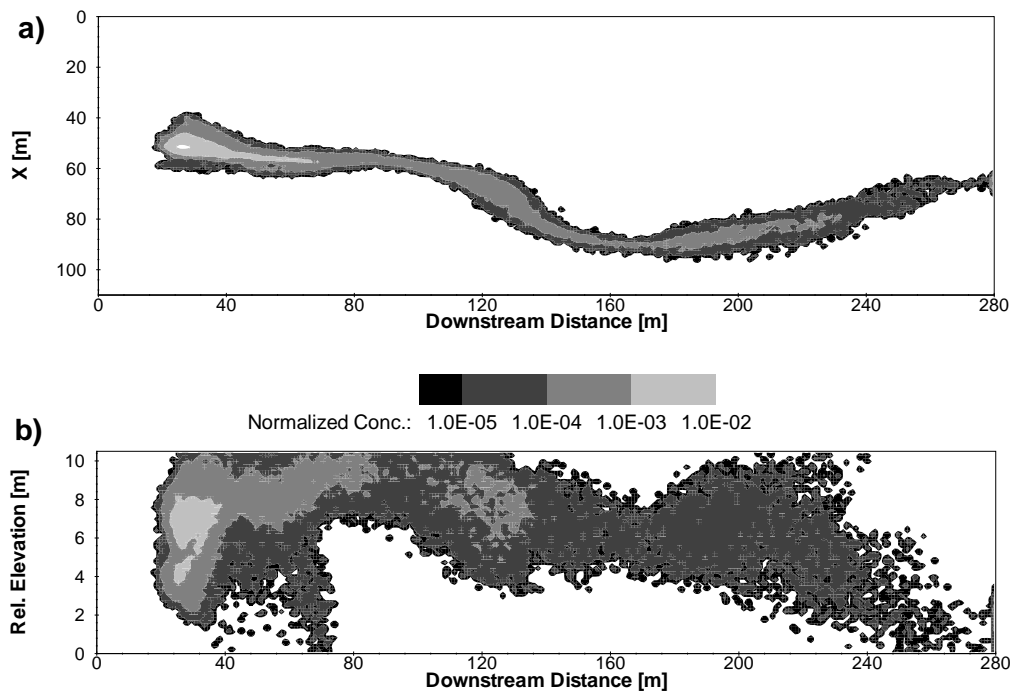


Figure 4.11. (a) Depth integrated normalized concentration distribution after 328 days for realization #80 (b) Laterally integrated normalized concentration distribution after 328 days for realization #80.

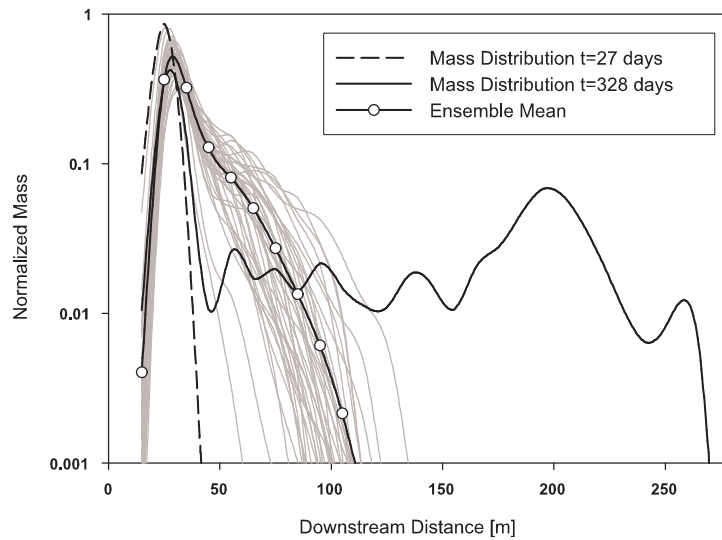


Figure 4.12. Longitudinal mass distribution profiles of the tritium plume and predictions using sequential Indicator simulation.

tracer transport behavior at the MADE site. Our discussion will focus here on the following issues: (1) the scale of aquifer heterogeneity versus the flowmeter sampling scale and the model grid scale, (2) the existence and effects of preferential flow pathways caused by a possible connectivity of high conductivity values.

4.5.1 Support Scale of the Transport Model

Column permeameter studies of vertical core samples at the MADE site (*Boggs et al.*, 1990) indicated a significant variability of hydraulic conductivity at the centimeter to decimeter scale. This strong small-scale variability was analyzed and discussed in detail by *Harvey and Gorelick* (2000) which found a standard deviation of $\ln K$ of as high as 6.0 for one of the column permeameter tests. Furthermore, laboratory studies of tritium transport in soil columns with aquifer material from the Columbus aquifer demonstrated a slight retardation which was attributed to the presence of intragranular porosity and dead-end pores (*Boggs and Adams*, 1992; *Harvey and Gorelick*, 2000). Finally, recovery of tracer from soil cores using physical and chemical extraction also indicated the strong influence of diffusion into small immobile portions of the aquifer material (e.g. *Boggs and Adams*, 1992; *Molz et al.*, 2006). Many authors concluded on the basis of this data that this is a direct evidence for a significant storage/release of tracer from immobile/mobile pore domains at the

Columbus aquifer and hence only a model accounting for these effects (e.g., continuous time random walk, fractional ADE, or dual domain model) is able to reproduce the anomalous tracer spreading. Moreover, specifically the dual-domain approach provides a further advantage: It offers an explanation of the mass overestimation at early times and underestimation at late times as observed in the field (*Harvey and Gorelick, 2000*).

Nevertheless, the simulation illustrated in Figure 4.8 shows that, although heterogeneity exists at a scale smaller than the flowmeter measurement support, it appears to be sufficient to account for the hydraulic conductivity variability which is characterized by the flowmeter data by using a similar grid resolution as the measurement support to reproduce anomalous solute transport at the MADE site. Note that we do not suggest that centimeter to pore-scale heterogeneity plays no role at all. In fact, we do believe that when accounting for these mass transfer processes additionally transport predictions might improve. However, our results suggest that the heterogeneity at the flowmeter measurement scale is the main contributor to the non-Gaussian plume behavior and that mass transfer effects are principally the results of the use of an inadequate model grid block scale.

Upscaling of the model grid blocks and hence not accounting for the heterogeneity at this scale (using a coarser grid-scale can be considered a simple form of upscaling), leads to the inability of the ADE to simulate the increased solute delay and hence additional mechanisms have to be added to the ADE, e.g. mass transfer, or even a different transport equation has to be used, e.g. continuous time random walk or a fractional ADE. In fact, the scalability of the mass transfer rate with the grid block size for the dual domain models applied to the MADE site was already recognized by *Feehley et al. (2000)*. They noted that their estimated factor for mass transfer at the MADE site, when accounting for local scale heterogeneity at a grid scale of $2 \times 2 \times 0.5$ m was about one order of magnitude lower than the one obtained by *Harvey and Gorelick (2000)* who used a homogeneous flow field. More recent synthetic studies have also demonstrated the necessity to include mass transfer mechanisms when upscaling solute transport in strongly heterogeneous fields (*Fernández-García and Gómez-Hernández, 2006*).

Finally, our results also indicate that the mass imbalance observed in the field is mainly caused by a measurement bias as argued by *Molz et al. (2006)* and not by the diffusion of tracer into intragranular porosity or dead-end pores. Water with high concentrations is preferentially sampled from high conductivity zones leading to an overestimation of the plume mass at early times because the same high concentrations were interpolated to the low conductivity regions. At late times mass is underestimated as more mass has spread into the low conductivity zones and is not captured by the sampling.

4.5.2 Connectivity

Connectivity of high-conductivity values has been suggested by various authors to produce the anomalous tracer spreading at the MADE site (e.g. *Zinn and Harvey, 2003; Zheng and Gorelick, 2003; Liu et al., 2004*). One possibility to evaluate patterns of continuity of a particular category, e.g. high or low conductivity values, is the indicator variography. Considering the experimental indicator semivariograms of Section 4.2 it is evident that no significantly larger spatial correlation of neither the 0.9 decile nor the 0.1 decile could be observed (see Table 4.2). Rather, comparing the sequential indicator simulation (Figure 4.12) with the sequential Gaussian simulations (Figures 4.7 and 4.8) it seems that a cdf assuming a multivariate Gaussian model approximates field conditions much better. This is quite surprising as in multiGaussian models extremely large and small values of the modeled variable are generally spatially uncorrelated (e.g. *Gómez-Hernández and Wen, 1998*).

Although the indicator variography does not reveal the existence of connected patches of high-conductivity values the measured tracer spreading still suggests some form of preferential flowpaths. In fact, various authors have demonstrated that indicator statistics is not always a good measure of connectivity (e.g. *Western et al., 2001; Knudby and Carrera, 2005*). Furthermore, the absence of a direct evidence of the connectivity of extreme values from the flowmeter data does not necessarily prove that in the field these connections do not exist. The similarity of the non-Gaussian spreading observed in various studies with synthetic aquifers having a near-identical lognormal conductivity distribution and a connectivity of extreme values (e.g. *Wen and Gómez-Hernández, 1998; Zinn and Harvey, 2003*) is a convincing argument that similar conditions might exist at the MADE site.

Nevertheless, connectivity of extreme values is not the only way to create strong preferential flowpaths resulting in a non-Gaussian plume spreading. Alluvial aquifers are typically made up of lenses or facies of sand and gravel as is also the case for the aquifer at the MADE site (e.g., *Rehfeldt et al., 1992*). The strongly varying hydraulic properties of these geological structures favor preferential flow and solute transport. One potential indication of an increased occurrence of these lenses is the cyclic behavior, or hole effect structure, that can be observed in the experimental semivariogram of Figure 4.4. Hole effect structures are the most prominent signs of the existence of regular/irregular clustered lenses or facies within an aquifer (*Pyrcz and Deutsch, 2003*) and non-monotonic structures of experimental variograms have been observed in practice especially for alluvial aquifers (e.g. *Barrash and Clemo, 2002; Ritzi, 2000*). The presence of these structures increases the probability of having realizations with strong preferential flowpaths as is demonstrated in the solute transport simulations of Figures 4.8 and 4.9 and it hence represents a valuable

alternative able to explain the occurrence of significant preferential flow and transport.

4.6 Conclusions

We have presented a detailed geostatistical analysis of the flowmeter data at the MADE site. Furthermore, we have analyzed tracer transport for different models of spatial correlation in comparison with the tritium tracer experiment (MADE-2). One of the principal conclusions of this research is that, when small-scale variability of hydraulic conductivity is correctly modeled at the flowmeter measurement support scale, the advection-dispersion equation is capable of reproducing the anomalous tracer spreading observed in the field. Furthermore, it was demonstrated that the model chosen for the spatial correlation of hydraulic conductivity plays a crucial role when simulating solute transport at the MADE site. Below, we list the specific conclusions of this work.

1.) The geostatistical analysis of the flowmeter data did not reveal the existence of a significantly larger spatial correlation of the high or low conductivity values. However, a hole effect structure could be observed in the experimental semivariogram, indicating the occurrence of irregularly clustered lenses or facies.

2.) Using kriging for the generation of the hydraulic conductivity field at the MADE site does not lead to a proper reproduction of tracer spreading due to an insufficient representation of the variability of hydraulic conductivity, independently of a potentially insufficient small grid scale, the potential inability of the ADE to simulate anomalous solute transport, or the type of spatial correlation chosen.

3.) Sequential simulations demonstrated that a cdf assuming a multivariate Gaussian distribution approximates field conditions better for the MADE site conditions than the random function model of the indicator approach, which is hampered by the limited number of indicator thresholds.

4.) Neglecting the hole effect structure in the sequential Gaussian simulation leads to a reduced tailing of the tracer. This indicates that, although connectivity of extreme values could not be detected from the field data, preferential flow still plays a significant role and is enhanced by the appearance of clustered lenses and facies.

5.) While direct evidence of the occurrence of diffusion into intragranular porosity and dead-end pores was found in laboratory studies, the solute transport results presented in this work suggest that the heterogeneity at the flowmeter measurement scale is the main contributor to the non-Gaussian

plume behavior and that mass transfer effects are principally the results of the use of an inadequate model grid block scale.

Although we could demonstrate that, when explicitly representing small-scale heterogeneity, anomalous spreading of solute transport for highly heterogeneous aquifers can be simulated using the ADE, in practice these high-resolution models are often not feasible due to the computational effort or the lack of adequate field data. Dual domain models, continuous time random walk or other models, able to account for the strongly delayed solute transport when not explicitly representing small-scale heterogeneity via for example mass transfer processes are therefore good alternatives when trying to predict transport as demonstrated by many authors. However, quantifying the relationship between the occurrence of non-Gaussian solute spreading and the scale of heterogeneity represented in a numerical model remains still a field of ongoing research.

Bibliography

- Adams, E. E., and L. W. Gelhar (1992), Field study of dispersion in a heterogeneous aquifer 2. Spatial moments analysis, *Water Resources Research*, *28*(12), 3293–3307.
- Baeumer, B., D. A. Benson, M. M. Meerschaert, and S. W. Wheatcraft (2001), Subordinated advection-dispersion equation for contaminant transport, *Water Resources Research*, *39*(10), 1296, doi:10.1029/2003WR002141.
- Barlebo, H. C., M. C. Hill, and D. Rosbjerg (2004), Investigating the Macrodispersion Experiment (MADE) site in Columbus, Mississippi, using a three-dimensional inverse flow and transport model, *Water Resources Research*, *40*, W04211, doi:10.1029/2002WR001935.
- Barrash, W., and T. Clemo (2002), Hierarchical geostatistics and multifacies systems: Boise hydrogeophysical research site, Boise, Idaho, *Water Resources Research*, *38*(10), 1196, doi:10.1029/2002WR001436.
- Benson, D. A., R. Schumer, M. M. Meerschaert, and S. W. Wheatcraft (2001), Fractional dispersion, Lévy motion, and the MADE tracer tests, *Transport in Porous Media*, *42*, 211–240.
- Berkowitz, B., and H. Scher (1998), Theory of anomalous chemical transport in random fracture networks, *Physical Review E*, *57*(5), 5858–5869.
- Boggs, J. M., S. C. Young, D. J. Benton, and Y. C. Chung (1990), Hydrogeological characterization of the MADE site, *Top. Rep. EA-6915*, Electr. Power. Res. Inst., Palo Alto, Calif.
- Boggs, J. M., S. C. Young, and L. M. Beard (1992), Field study of dispersion in a heterogeneous aquifer 1. Overview and site description, *Water Resources Research*, *28*(12), 3281–3291.
- Boggs, J. M., and E. E. Adams (1992), Field study of dispersion in a heterogeneous aquifer 4. Investigation of adsorption and sampling bias, *Water Resources Research*, *28*(12), 3325–3336.

- Boggs, J. M., L. M. Beard, and W. R. Waldrop (1993), Transport of tritium and four organic compounds during a natural-gradient experiment (MADE-2), *Tech. Rep. EPRI TR-101998*, Electr. Power. Res. Inst., Palo Alto, Calif.
- Bowling, J. C., A. B. Rodriguez, D. L. Harry, and C. Zheng (2005), Delineating alluvial aquifer heterogeneity using resistivity and GPR data, *Ground Water*, 43(6), 890–903.
- Bowling, J. C., C. Zheng, A. B. Rodriguez, and D. L. Harry (2006), Geophysical constraints on contaminant transport in a heterogeneous fluvial aquifer, *Journal of Contaminant Hydrology*, 85, 72–88.
- Brauner, J. S., and M. A. Widdowson (2001), Numerical simulation of a natural attenuation experiment with a petroleum hydrocarbon NAPL source, *Ground Water*, 39(6), 939–952.
- Carrera, J. (1993), An overview of uncertainties in modeling groundwater solute transport, *Journal of Contaminant Hydrology*, 13, 23–48.
- de Marsily, G., F. Delay, J. Gonçalves, P. Renard, V. Teles, and S. Violette (2005), Dealing with spatial heterogeneity, *Hydrology Journal*, 13, 161–183.
- Deutsch, C. V., and A. G. Journel (1998), *GSLIB, Geostatistical Software Library and User’s Guide*, 2nd ed., 369 pp., Oxford Univ. Press, New York.
- Eggleston, J., and S. Rojstaczer (1998), Identification of large-scale hydraulic conductivity trends and the influence of trends on contaminant transport, *Water Resources Research*, 34(9), 2155–2168.
- Feehley, C. E., C. Zheng, and F. J. Molz (2000), A dual-domain mass transfer approach for modeling solute transport in heterogeneous aquifers: Application to the Macrodispersion Experiment (MADE) site, *Water Resources Research*, 36(9), 2501–2515.
- Fernández-García, D., T. H. Illangasekare, and H. Rajaram (2005), Differences in the scale dependence of dispersivity and retardation factors estimated from forced-gradient and uniform flow tracer tests in three-dimensional physically and chemically heterogeneous porous media, *Water Resources Research*, 41(3), doi:10.1029/2004WR003523.
- Fernández-García, D., and J. J. Gómez-Hernández (2006), Impact of upscaling on solute transport: travel times, scale-dependence of dispersivity and propagation of uncertainty, *Water Resources Research*, accepted for publication.

- Gillham, R. W., M. J. L. Robin, K. J. Dytynshyn, and H. M. Johnston (1984), Diffusion of nonreactive and reactive solutes through fine-grained barrier materials, *Can. Geotech. J.*, *21*, 117–123.
- Gómez-Hernández, J.J., and A. G. Journel (1993), Joint sequential simulation of multi-Gaussian fields, *Geostatistics Tróia '92*, Editor: A. Soares, Kluwer, Vol. 1, 85-94.
- Gómez-Hernández, J.J., and R. M. Srivastava (1990), ISIM3D: An ANSI-C three dimensional multiple indicator conditional simulation program, *Computer and Geosciences*, *16*(4), 395-440.
- Gómez-Hernández, J.J., and X. H. Wen (1998), To be or not to be multi-Gaussian? A reflection on stochastic hydrogeology, *Advances in Water Resources*, *21*(1), 47–61.
- Gómez-Hernández, J. J. (2006), Complexity, *Ground Water*, currently in press.
- Goovaerts, P. (1997), *Geostatistics for Natural Resources Evaluation*, 483 pp., Oxford University Press, NY, NY.
- Harvey, C., and S. M. Gorelick (2000), Rate-limited mass transfer or macrodispersion: Which dominates plume evolution at the Macrodispersion Experiment (MADE) site?, *Water Resources Research*, *36*(3), 637–650.
- Hill, M. C., H. C. Barlebo, and D. Rosbjerg (2006), Reply to comment by F. Molz et al. on “Investigating the Macrodispersion Experiment (MADE) site in Columbus, Mississippi, using a three-dimensional inverse flow and transport model”, *Water Resources Research*, *42*, W06604, doi:10.1029/2005WR004624.
- Johnson, N. M. (1995), Characterization of alluvial hydrostratigraphy with indicator semivariograms. *Water Resources Research*, *31*(12), 3217–3227.
- Journel, A. G., and C. J. Huijbregts (1978), *Mining Geostatistics*, 600 pp., Academic Press, San Diego, Calif.
- Julian, H. E., J. M. Boggs, C. Zheng, and C. E. Feehley (2001), Numerical simulation of a natural gradient tracer experiment for the natural attenuation study: Flow and physical transport, *Ground Water*, *39*(4), 534–545.
- Knudby, C., and J. Carrera (2005), On the relationship between indicators of geostatistical, flow and transport connectivity, *Advances in Water Resources*, *28*, 405–421.

- Koltermann, C. E. (1996), Heterogeneity in sedimentary deposits: A review of structure-imitating, process-imitating and descriptive approaches. *Water Resources Research*, 32(9), 2617–2658.
- LaBolle, E. M., G. E. Fogg, and A. F. B. Tompson (1996), Random-walk simulation of transport in heterogeneous porous media: Local mass-conservation problem and implementation methods. *Water Resources Research*, 32(3), 583–593.
- LeBlanc, D. R., S. P. Garabedian, K. M. Hess, L. W. Gelhar, R. D. Quadri, K. G. Stollenwerk, and W. W. Wood (1986), Large-scale natural gradient tracer test in sand and gravel, Cape Cod, Massachusetts: 1. Experimental design and observed tracer movement, *Water Resources Research*, 27(5), 895–910.
- Liu, G., C. Zheng, and S. M. Gorelick (2004), Limits of applicability of the advection-dispersion model in aquifers containing connected high-conductivity channels, *Water Resources Research*, 40, W08308, doi:10.1029/2003WR002735.
- Liu, H. H., and F. J. Molz (1997), Multifractal analyses of hydraulic conductivity distributions, *Water Resources Research*, 33(11), 2483–2488.
- Mackay, D. M., D. L. Freyberg, P. V. Roberts and J. A. Cherry (1986), A natural gradient experiment on solute transport in a sand aquifer: 1. Approach and overview of plume movement, *Water Resources Research*, 22(13), 2017–2029.
- MacIntyre, W. G., J. M. Boggs, C. P. Antworth, and T. B. Stauffer (1993), Degradation kinetics of aromatic organic solutes introduced into a heterogeneous aquifer, *Water Resources Research*, 29(12), 4045–4051.
- Harbaugh, A. W., E. R. Banta, M. C. Hill, and M. G. McDonald (2000), MODFLOW-2000, the U.S. Geological Survey modular ground-water model - user guide to modularization concepts and the ground-water flow process, *U.S. Geol. Surv., open-file report 00-92*, pp. 121.
- Molz, F. J., C. Zheng, S. M. Gorelick, and C. F. Harvey (2006), Comment on “Investigating the Macrodispersion Experiment (MADE) site in Columbus, Mississippi, using a three-dimensional inverse flow and transport model” by Heidi Christiansen Barlebo, Mary C. Hill, and Dan Rosbjerg, *Water Resources Research*, 42, W06603, doi:10.1029/2005WR004265.
- Pyrzcz, M. J., and C. V. Deutsch (2003), The whole story on the hole effect, Geostatistical Association of Australasia, Editor: S. Searston, Newsletter 18.

- Rehfeldt, K. R., J. M. Boggs, and L. W. Gelhar (1992), Field study of dispersion in a heterogeneous aquifer 3. Geostatistical analysis of hydraulic conductivity, *Water Resources Research*, 28(12), 3309–3324.
- Ritzi, R. W. (2000), Behavior of indicator variograms and transition probabilities in relation to the variance in lengths of hydrofacies, *Water Resources Research*, 36(11), 3375–3381.
- Salamon, P., D. Fernández-García, and J. J. Gómez-Hernández (2005), A review and numerical assessment of the random walk particle tracking method, *Journal of Contaminant Hydrology*, accepted for publication.
- Schumer, R., D. A. Benson, M. M. Meerschaert, and B. Baeumer (2003), Fractal mobile/immobile solute transport, *Water Resources Research*, 39(10), 1296, doi:10.1029/2003WR002141.
- Wen, X. H., and J. J. Gómez-Hernández (1996), The constant displacement scheme for tracking particles in heterogeneous aquifers, *Ground Water*, 34(1), 135–142.
- Wen, X. H., and J. J. Gómez-Hernández (1998), Numerical modeling of macrodispersion in heterogeneous media: a comparison of multi-Gaussian and non-multi-Gaussian models, *Journal of Contaminant Hydrology*, 30, 129–156.
- Western, A. W., G. Blöschl, and R. B. Grayson (2001), Toward capturing significant connectivity in spatial patterns, *Water Resources Research*, 37(1), 83–97.
- Zheng, C., and S. M. Gorelick (2003), Analysis of solute transport in flow fields influenced by preferential flowpaths at the decimeter scale, *Ground Water*, 41(2), 142–155.
- Zheng, C., and J. J. Jiao (1998), Numerical simulation of tracer tests in heterogeneous aquifer, *Journal of Environmental Engineering*, 124(6), 510–516.
- Zinn, B., and C. F. Harvey (2003), When good statistical models of aquifer heterogeneity go bad: A comparison of flow, dispersion, and mass transfer in connected and multivariate Gaussian hydraulic conductivity fields, *Water Resources Research*, 39(3), 1051, doi:10.1029/2001WR001146.
- Zappa, G., Bersezio, R., Felletti, F., and M. Giudici (2006), Modeling heterogeneity of gravel-sand, braided stream, alluvial aquifers at the facies scale, *Journal of Hydrology*, 325, 134–153.

5

General Conclusions

5.1 Summary

The complexity of solute transport in heterogeneous porous media has caused many models, assuming a simple homogeneous parameter distribution, to fail when used for prediction and decision making. The awareness of the necessity to include heterogeneity in flow and transport models has triggered the development of more sophisticated approaches to characterize these processes, e.g. the use of stochastic models to quantify and reduce uncertainty using Monte Carlo simulations and inverse modeling, or the development of methods to upscale parameters which have a small-scale variability in order to be used in coarsely discretized models. However, these more sophisticated approaches often require the analysis of hundreds or even thousands of aquifer realizations or the study of the effects on transport behavior moving from a highly discretized model grid to a coarsely discretized one. One valuable alternative of modeling solute transport for this purpose is the random walk particle tracking method.

In Chapter 2 the basic mathematical concepts of this method have been presented. The principal advantages of the random walk methodology are the high computational efficiency and the absence of numerical dispersion. The limitations in simulating nonequilibrium processes like non-linear sorption or the reactions between different chemical species constitute its main disadvantages. Three different numerical implementation methods to overcome the problem of local solute mass conservation were examined: (1) the interpolation

method, (2) the reflection method, and (3) the generalized stochastic differential equations approach. The different methods were analyzed for solute transport in a simple two-layer case and in various synthetic heterogeneous aquifers. It was demonstrated that the interpolation method using a hybrid scheme, i.e., linear interpolation for velocities and tri/bilinear interpolation for the dispersion tensor field, provides a local as well as global divergence-free velocity field and that it approximates well mass balance at grid interfaces of adjacent cells with contrasting hydraulic conductivities. The generalized stochastic differential equations method and the reflection method suffer both from an artificial shift of mass into zones of low hydraulic conductivity, hence not conserving well local mass balance, which results in an overestimation of the macrodispersion and an underestimation of the average velocity for strongly heterogeneous cases with abrupt transitions between different zones of hydraulic conductivity.

Chapter 3 introduced a new numerical approach to include multirate mass transfer into random walk particle tracking. For this purpose the normalized zeroth spatial moments of the multirate transport equations were derived and used as phase transition probabilities. The particle distribution between the mobile domain and any immobile domain can then be simply determined by performing a Bernoulli trial on the appropriate phase transition probabilities. Examples for the first-order mass transfer and the multirate mass transfer were illustrated and compared satisfactorily with analytical and semi-analytical solutions. Furthermore, the effects of the time step size, the approximation of the matrix exponential with a third order Taylor series, and the truncation of the multirate series were evaluated. It was demonstrated that if a criteria for the matrix exponential approximation and the time step size is introduced mass transfer processes can be efficiently simulated using this new approach. Furthermore, the applicability of this method was illustrated using a synthetic example of the effects of a heterogeneous intraparticle pore diffusion distribution. The major advantages of this newly developed approach are the flexibility in the sense that it does not impose any restrictive assumptions on the spatial variability of advection, dispersion, and mass transfer and its low computational cost even for highly discretized models having a spatially heterogeneous mass transfer rate. It furthermore preserves the principal capacities of the multirate model to describe a variety of different mass transfer processes as well as the advantages of the random walk method.

Finally, Chapter 4 presented the advantages of modeling solute transport using random walk particle tracking for a field application (the tracer test at the Macrodispersion Experiment site) where the strong aquifer heterogeneity requires a highly discretized model grid. For this purpose a detailed geostatistical analysis of the flowmeter data was performed. Evaluating the spatial continuity of the hydraulic conductivity data revealed a hole effect structure

indicating an increased occurrence of clustered lenses or facies in the aquifer apparently improving preferential flow. Indicator variography did not show an increased connectivity of high/low hydraulic conductivity values. Tritium transport was modeled in three kriged fields as well as for three sequential simulations all of them using a high grid-resolution with a grid block size similar to the flowmeter measurement support scale to explicitly represent small-scale heterogeneity. The kriged fields were not able to simulate anomalous tracer spreading as observed in the field based on an insufficient representation of the variance of $\ln K$. The sequential Gaussian simulations generally demonstrated a better tailing than the sequential Indicator simulation indicating that a multiGaussian distribution of $\ln K$ approximates field conditions better at the Columbus aquifer. Using the hole effect structure for the spatial model of the Gaussian simulations resulted in an increased tailing of the tracer and a good reproduction of the non-Gaussian plume shape observed in the field, illustrating the importance of preferential flow on anomalous solute transport. These results furthermore suggest that the heterogeneity at the flowmeter measurement scale is the main contributor to the non-Gaussian plume behavior and that mass transfer effects, claimed to be responsible for the anomalous transport at the MADE site, are principally the consequence of the use of an inadequate model grid block scale. It is concluded that, when small-scale variability of hydraulic conductivity is correctly modeled at the flowmeter measurement support scale, the advection-dispersion equation is capable of reproducing the anomalous tracer spreading. If not representing explicitly this small-scale variability other models, able to account for the strongly delayed solute transport (e.g., dual domain, continuous time random walk, fractional ADE) have to be employed. However, quantifying the relationship between the occurrence of non-Gaussian solute spreading and the scale of heterogeneity represented in a numerical model remains still a field of ongoing research.

5.2 Recommendations for Future Research

This dissertation has demonstrated that the random walk particle tracking method is a valuable alternative to other numerical approaches for modeling solute transport. However, this work has also highlighted some of the numerical disadvantages related to this method, which still require a research effort in order to be overcome. Furthermore, the results of this work have also opened up new possibilities for future lines of investigation. Some of the recommendations for the future research, either employing random walk particle tracking method as a numerical tool, or improving the method itself are listed below:

- *Further development and improvement of the RW3D program code:* Although the RW3D code has been used in a large number of scientific

papers for the numerical solute transport simulations (see Appendix A), its flexibility to model solute transport for a broader range of boundary conditions, e.g. modeling solute transport under transient flow conditions or in unconfined systems, still can be improved. Furthermore increasing the adaptability to MODFLOW2000 output files would increase the user-friendliness and increase its applicability.

- *Including concentration-dependant processes into random walk:* As stated in Chapter 2 one of the disadvantages of the random walk methodology is the difficulty of including concentration-dependant processes, e.g. non-linear sorption or reactions between different chemical species. Although some work has been done on this topic the results all demonstrated a significant decrease in computational efficiency and an increase in numerical errors as concentrations have to be calculated for each time step and each grid cell. However, using a similar probabilistic approach as illustrated in Chapter 3 for the mass transfer might enable a better implementation of these processes into the random walk methodology.
- *Evaluating the effects of heterogeneous mass transfer processes:* The implementation of the multirate mass transfer model as outlined in Chapter 3 provides a powerful tool to assess the influence of a variety of heterogeneous mass transfer processes on solute transport. Although the example for a heterogeneous intraparticle pore diffusion presented in Chapter 3 did not reveal a strong effect on solute transport in comparison to the homogeneous first-order mass transfer model the herein presented approach permits the investigation of the effects of spatially variable, small-scale mass transfer processes (e.g., intraparticle pore diffusion, diffusion into low permeability zones, diffusion into a rock matrix) in models with a high grid-resolution on solute transport.
- *Upscaling of solute transport:* Recent studies have demonstrated that when upscaling solute transport the classical macrodispersion model is not capable of accounting for the mass transfer between model grid blocks. While these results have led some researchers to employ a different transport equation for modeling upscaled solute transport, e.g., fractional advection-dispersion equation or continuous time random walk, others added a simple first-order mass transfer process to the advection-dispersion equation. Random walk particle tracking represents an ideal tool for the numerical studies of solute transport upscaling due to its excellent computational efficiency for highly discretized models and the easiness of implementing first-order mass transfer as illustrated in Chapter 3. Furthermore, the upscaling theories developed can be applied and tested for the field case at the MADE site, presented in Chapter 4.



RW3D - A three-dimensional object-oriented solute transport model based on random walk particle tracking

Throughout this dissertation a numerical code (RW3D), initially developed by Daniel Fernández-García at the Colorado School of Mines, was used and further developed to perform the solute transport simulations. RW3D is written in FORTRAN 95 and has an object-oriented structure in order to facilitate its extension and ongoing improvement. A flowchart diagram outlining the program structure of RW3D is shown in Figures A.1 and A.2.

RW3D uses a hybrid scheme for the velocity interpolation as described in Chapter 1 which has demonstrated to provide local as well as global divergence-free velocity fields within the solution domain and a continuous dispersion tensor field that approximates well mass balance at grid interfaces of adjacent cells with contrasting hydraulic conductivities. For a detailed illustration of the random walk equations see Chapter 1. Furthermore, a constant-displacement scheme which modifies automatically the time step size for each particle according to the local velocity is employed in order to decrease computational effort. RW3D is capable of simulating advection, dispersion/diffusion, retardation via linear sorption, and simple first-order mass transfer as well as mass transfer into a spherical geometry. Currently, RW3D only allows for solute

transport in confined aquifers either with a regular or irregular grid geometry. RW3D can use flow velocities either provided by a file having GSLIB format or can directly use the binary output file of MODFLOW2000. Tables A.1 and A.2 present the necessary input files.

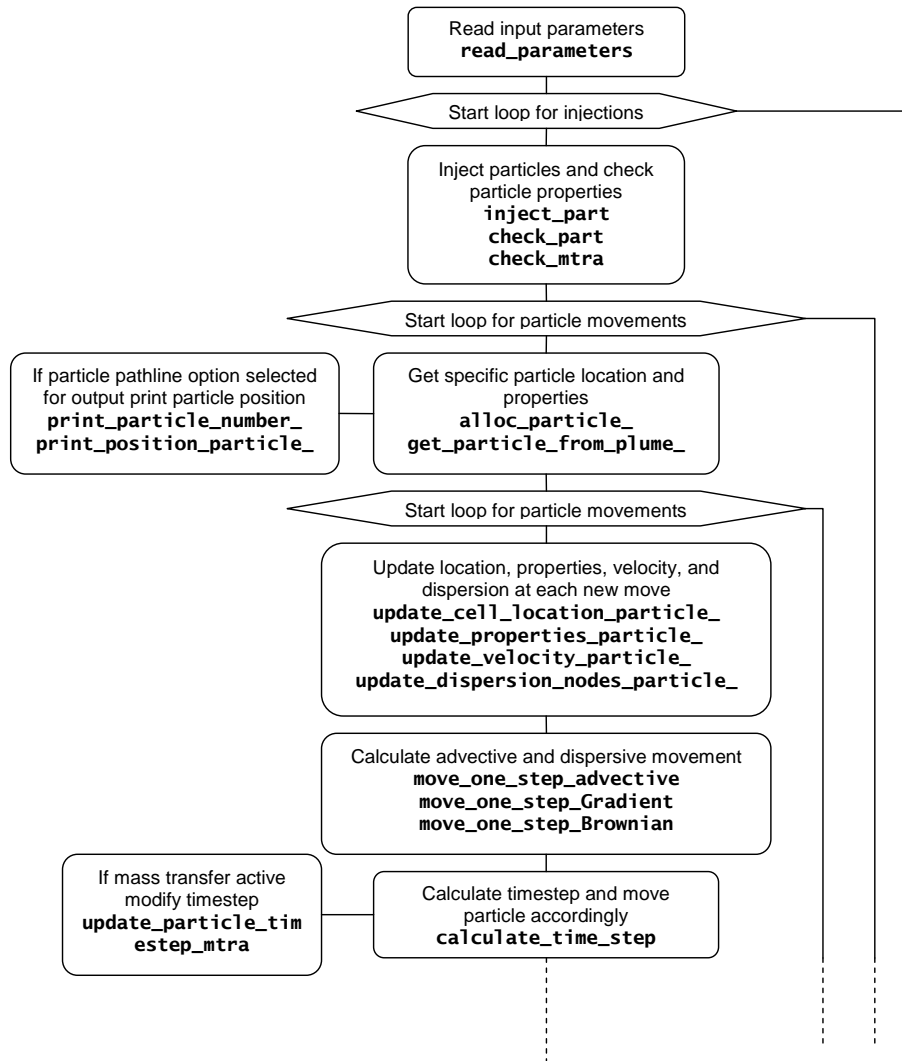


Figure A.1. Flowchart of the RW3D program structure. Part A.

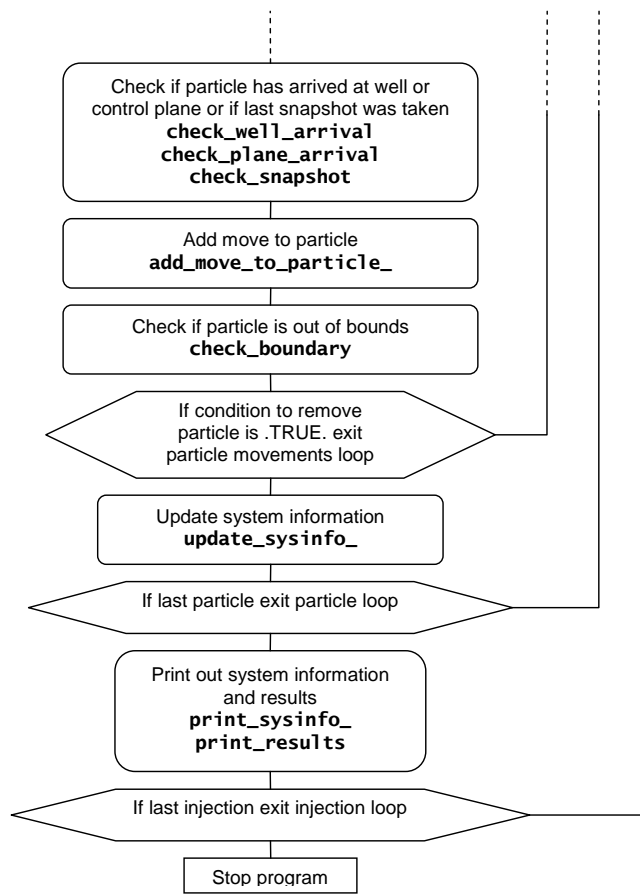


Figure A.2. Flowchart of the RW3D program structure. Part B.

Line	Variable	Description
1	<i>Text</i>	
2	<i>Text</i>	
3	<i>Text</i>	
4	<i>Text</i>	
5	file	Parameter file
6	<i>Text</i>	
7	<i>Text</i>	
8	<i>Text</i>	
9	file	File with histogram (pdf) of particle arrival times (bte)
10	file	File with cumulative pdf particle arrival times (cbtc)
11	file	File with particle snapshots with time
12	file	File with particle paths
13	file	File with cartesian spatial moments
14	file	File with spatial moments of particle position
15	file	File with particle position at control planes
16	file	File with dilution index of Kitanidis
17	file	File with radial spatial moments
18	file	File with temporal moments
19	file	File with dispersivities from control planes
20	file	File with quartiles (5%, 25%, 50%, 75%, 90 %)

Table A.1. Name file for RW3D

Table A.2. Input parameter file for RW3D

Line	Variable	Description
1	<i>Text</i>	
2	<i>Text</i>	
3	nx,ny,nz	number of cells in x,y,z direction
4	file,const,ivar,flag	Size of cells in x-direction: if flag=0 → dx= const , else if → flag=1 use file of for- mat GSLIB where ivar is the column to read and the read values are multiplied with const
5	file,const,ivar,flag	Size of cells in y-direction: if flag=0 → dx= const , else if → flag=1 use file of for- mat GSLIB where ivar is the column to read and the read values are multiplied with const

- continues on the following page -

Line	Variable	Description
6	<code>file, const, ivar, flag</code>	Size of cells in z-direction: if <code>flag=0</code> → <code>dx=const</code> , else if → <code>flag=1</code> use <code>file</code> of format GSLIB where <code>ivar</code> is the column to read and the read values are multiplied with <code>const</code>
7	<code>ibx1, ibx2, iby1, iby2, ibz1, ibz2</code>	Boundary conditions: <code>ib = 0</code> for flux boundary condition, <code>ib = 1</code> for impermeable boundary condition
8	<i>Text</i>	
9	<code>ixmom, irmom, itmom, iwbtc, iwcbrtc, iwshot, idilut, iwpath</code>	Program Options: <code>ixmom</code> = calculate spatial cartesian moments, <code>irmom</code> = calculate spatial radial moments, <code>itmom</code> = calculate temporal moments, <code>iwbtc</code> = write breakthrough curve, <code>iwcbrtc</code> = write cumulative breakthrough curve, <code>iwshot</code> = write snapshots of particles, <code>idilut</code> = calculate kitani-dis dilution index (Not Available), <code>iwpath</code> = write particle paths
10	<code>ixmompl, iwshotpl, ipldisp</code>	Program Options: <code>ixmompl</code> = spatial moments at control planes, <code>iwshotpl</code> = write particle position at planes, <code>ipldisp</code> = write equivalent parameters at planes
11	<i>Text</i>	
12	Logical Flag	True (T) if package is used
13	<code>file, const, ivar, flag</code>	Darcy velocity in x: if <code>flag=0</code> → <code>qx=const</code> , else if → <code>flag=1</code> use <code>file</code> of format GSLIB where <code>ivar</code> is the column to read and the read values are multiplied with <code>const</code> , else if → <code>flag=2</code> use MODFLOW2000 binary output <code>file</code> (specification of <code>qy</code> and <code>qz</code> is not necessary for this case)
14	<code>file, const, ivar, flag</code>	Darcy velocity in y: if <code>flag=0</code> → <code>qy=const</code> , else if → <code>flag=1</code> use <code>file</code> of format GSLIB where <code>ivar</code> is the column to read and the read values are multiplied with <code>const</code>
15	<code>file, const, ivar, flag</code>	Darcy velocity in z: if <code>flag=0</code> → <code>qz=const</code> , else if → <code>flag=1</code> use <code>file</code> of format GSLIB where <code>ivar</code> is the column to read and the read values are multiplied with <code>const</code>

- continues on the following page -

Line	Variable	Description
16	file,const,ivar,flag	Porosity: if flag=0→ qx=const, else if → flag=1 use file of format GSLIB where ivar is the column to read and the read values are multiplied with const
17	<i>Text</i>	
18	Logical Flag	True (T) if package is used
19	file,const,ivar,flag	longitudinal dispersivity: if flag=0→ α_L =const, else if → flag=1 use file of format GSLIB where ivar is the column to read and the read values are multiplied with const
20	file,const,ivar,flag	transverse horizontal dispersivity: if flag=0→ α_{TH} =const, else if → flag=1 use file of format GSLIB where ivar is the column to read and the read values are multiplied with const
21	file,const,ivar,flag	transverse vertical dispersivity: if flag=0→ α_{TV} =const, else if → flag=1 use file of format GSLIB where ivar is the column to read and the read values are multiplied with const
22	Dm	Molecular Diffusion
23	<i>Text</i>	
24	Logical Flag	True (T) if package is used
25	Bd	Bulk Density
26	f	Fraction of sorption sites in contact with mobile zone
27	file,const,ivar,flag	Distribution coefficient K_d : if flag=0→ K_d =const, else if → flag=1 use file of format GSLIB where ivar is the column to read and the read values are multiplied with const
28	<i>Text</i>	
29	Logical Flag, mtype, nseries	True (T) if package is used, if mtype=0→ first-order mass transfer, else if → mtype=1 spherical diffusion with a total of nseries compartments used by the multirate mass transfer
30	file,const,ivar,flag	Mass Transfer Rate: if flag=0→ α =const, else if → flag=1 use file of format PMWIN

- continues on the following page -

Line	Variable	Description
31	<code>file, const, ivar, flag</code>	Immobile Domain Porosity: if <code>flag=0</code> → $\theta_{im} = \text{const}$, else if → <code>flag=1</code> use <code>file</code> of format GSLIB where <code>ivar</code> is the column to read and the read values are multiplied with <code>const</code>
32	<i>Text</i>	
33	<code>Cu</code>	Courant Number
34	<code>tlen, ntstep, tmult</code> (Only for snapshot times)	Total length of time, number of steps, expansion factor
35	<code>Xr0, Yr0</code> (Only for radial spatial moments)	X, Y origin coordinates for radial spatial moments
36	<code>ngrid, inc, ifker, ifbw, bw</code>	Variables for histogram and cumulative frequency of particle arrival times: The program uses kernel densities to calculate the histogram (breakthrough curve) and needs the following parameters: <code>ngrid</code> = number support points for histogram, <code>ifker</code> = type of kernel density function (<code>ifker</code> = 0 → Box, <code>ifker</code> = 1 → Triangle, <code>ifker</code> = 2 → Gaussian), <code>ifbw</code> = bandwidth kernel density (<code>ifbw</code> = 0 → Specified by the user with <code>bw</code> , <code>ifbw</code> = 0 → optimal <code>bw</code> for Gaussian shape), the cumulative frequency distribution of arrival times only needs: <code>inc</code> = Number of skip points for plotting <code>iwcbtc</code>
37	<i>Text</i>	
38	<code>Nwell</code>	Number of wells
	For each well:	
39	<code>xwell, ywell, rwell, flag</code>	X, Y well coordinates, well radius, if <code>flag=1</code> remove particles
40	<code>Nplane</code>	Number of control planes
	For each control plane:	
41	<code>xdist, type, flag</code>	Distance control plane, type of plane, if <code>flag=1</code> remove particles
42	<i>Text</i>	
43	<code>np, totmass</code>	Number of particles, total mass injected
44	<code>ninj</code>	Number of injections
	For each injection:	

- continues on the following page -

Line	Variable	Description
45	Type (string)	Type of injections: <i>Point injection</i> Type = point; <i>Vertical line injection, randomly distributed</i> Type = line; <i>Block injection, uniformly distributed</i> Type = block; <i>Circle injection, randomly distributed</i> Type = circle; <i>Radial injection, uniformly distributed</i> Type = radial; <i>Plane injection, uniformly distributed, perpendicular to x</i> Type = plane; <i>Plane injection, randomly distributed</i> Type = plane_random; <i>Line injection by points, uniformly distributed</i> Type = line_by_points; <i>User defined distribution</i> Type = user.
46	Parameters depending on the type of injection	<i>Point injection</i> : xinj, yinj, zinj = x,y,z point coordinates; <i>Vertical line injection</i> : xinj, yinj, zbot, ztop, xinj, yinj = x,y coordinates vertical line, zbot = z line bottom, vertical position ztop = z line top vertical position; <i>Block injection</i> : idwn, jdown, kdown, iup, jup, kup, lower left and upper right cell number in x,y,z direction; <i>Circle injection</i> : x0, y0, zbot, ztop, rcy, x0, y0 = coordinates origin cylinder, zbot = z bottom position cylinder, ztop = z top position cylinder, rcy = cylinder radius; <i>Radial injection</i> : xinj, yinj, zbot, ztop, rcp, definition see <i>Circle injection</i> ; <i>Plane injection</i> : xdist, width, height, xdist = x position of the vertical plane, width = width of the plane in the y direction, height = height of the plane in the z direction; <i>Plane injection random</i> : xdist, width, height definition see <i>Plane injection</i> ; <i>Line injection by points</i> : x1, y1, z1, x2, y2, z2, x, y, z coordinates of the first and second point; <i>User defined injection</i> : filename (string).

The following articles have been published using RW3D for the numerical solute transport simulations:

- Cassiraga, E. F., D. Fernàndez-Garcia, and J. J. Gómez-Hernández (2005) Performance assessment of solute transport upscaling methods in the context of nuclear waste disposal, *International Journal of Rock Mechanics and Mining Sciences*, 42(5-6), 756-764.
- Fernàndez-Garcia, D., T. H. Illangasekare, and H. Rajaram (2004) Conservative and sorptive forced-gradient and uniform flow tracer tests in a three-dimensional laboratory test aquifer, *Water Resources Research*, 40(10), doi: 10.1029/2004WR003112.
- Fernàndez-Garcia, D., T. H. Illangasekare, and H. Rajaram (2005a), Differences in the scale dependence of dispersivity and retardation factors estimated from forced-gradient and uniform flow tracer tests in three-dimensional physically and chemically heterogeneous porous media, *Water Resources Research*, 41(3), doi: 10.1029/2004WR003523.
- Fernàndez-Garcia, D., T. H. Illangasekare, and H. Rajaram (2005b), Differences in the scale dependence of dispersivity estimated from temporal and spatial moments in chemically and physically heterogeneous porous media, *Advances in Water Resources*, 28(7), 745-759.
- Fernàndez-Garcia, D., and J. J. Gómez-Hernández (2006), Impact of upscaling on solute transport: travel times, scale-dependence of dispersivity and propagation of uncertainty, *Water Resources Research*, accepted for publication.
- Fernàndez-Garcia, D., H. Rajaram, and T. H. Illangasekare (2005) Assessment of the predictive capabilities of stochastic theories in a three-dimensional laboratory test aquifer: Effective hydraulic conductivity and temporal moments of breakthrough curves, *Water Resources Research*, 41(4), W04002 10.1029/2004WR003523
- Salamon, P., D. Fernàndez-Garcia, and J. J. Gómez-Hernández (2006), A review and numerical assessment of the random walk particle tracking method, *Journal of Contaminant Hydrology*, in press.
- Salamon, P., D. Fernàndez-Garcia, and J. J. Gómez-Hernández (2006), Modeling Mass Transfer Processes Using Random Walk Particle Tracking, *Water Resources Research*, in press.
- Salamon, P., D. Fernàndez-Garcia, and J. J. Gómez-Hernández (2006), Modeling Tracer Transport at the Macrodispersion Experiment (MADE) site: Only a problem of scales?, submitted to *Water Resources Research*.

